DESIGN AND IMPLEMENTATION OF AN INCREMENTAL SHEET FORMING PROCESS FOR BENDING OF HIGH STRENGTH THICK STEEL SHEETS

A THESIS SUBMITTED TO
THE GRADUATE SCHOOL OF NATURAL AND APPLIED SCIENCES
OF
ATILIM UNIVERSITY

BY

BARIŞ ÇETIN

IN PARTIAL FULFILLMENT OF THE REQUIREMENTS
FOR
THE DEGREE OF MASTER OF SCIENCE
IN
MANUFACTURING ENGINEERING

FEBRUARY 2018

Approval of the Graduate School of Natural and Applied Sciences, Atılım University.

_____

Prof. Dr. Ali Kara

Director

I certify that this thesis satisfies all the requirements as a thesis for the degree of Master of Science.

_____

Prof. Dr. S. Engin Kılıç

Head of Department

This is to certify that we have read the thesis "Design and Implementation of an Incremental Sheet Forming Process for Bending of High Strength Thick Steel Sheets" submitted by Barış Çetin and that in our opinion it is fully adequate, in scope and quality, as a thesis for the degree of Master of Science.

_____	_____
Assist. Prof. Dr. Besim Baranoğlu	Assist. Prof. Dr. Eren Billur
Co-Supervisor	Supervisor

Examining Committee Members

Assoc. Prof. Dr. Özgür Aslan	_____
Assoc. Prof. Dr. Hakkı Özgür Ünver	_____
Assist. Prof. Dr. Besim Baranoğlu	_____
Assist. Prof. Dr. Eren Billur	_____
Assist. Prof. Dr. Kemal Davut	_____

Date: 26.01.2018

I hereby declare that all information in this document has been obtained and presented in accordance with academic rules and ethical conduct. I also declare that, as required by these rules and conduct, I have fully cited and referenced all material and results that are not original to this work.

Name, Last Name: BARIŞ ÇETIN

Signature :

ABSTRACT

DESIGN AND IMPLEMENTATION OF AN INCREMENTAL SHEET FORMING PROCESS FOR BENDING OF HIGH STRENGTH THICK STEEL SHEETS

Çetin, Barış
M.S., Manufacturing Engineering
Supervisor : Assist. Prof. Dr. Eren Billur
Co-Supervisor : Assist. Prof. Dr. Besim Baranoğlu

February 2018, 94 pages

As a specific section of armored combat vehichle industry, hull production, for many case, has a production step for bending of ultra high strength steels (UHSS). This bending operation is generally performed by means of high tonnage press brakes in air bending condition. The steels in hull production have very high tensile strengtht values compared to conventional mild steel such as 1250 MPa or even higher. These strength levels absolutely require high bending forces, undoubtfully. On the other hand, incremental sheet forming process has been recently implemented in metal forming industry which is mainly based on the gradual and local excitation of plastic deformation. This new generation technique has some advantages such as increasing the formability, eliminating the complex tool requirements and reducing the forming forces reasonably. In this study, basically the potential of incremental forming

process in force reduction is investigated. A new incremental bending process is proposed, simulated and experimentally verified within the scope of the study. Through the wide range of data obtained from the simulation and experimental efforts, some optimization could also be conducted on the process parameters. Briefly, the results of the incremental bending of UHSS plates are compared with the conventional air bending operation.

Keywords: Incremental sheet metal forming, incremental bending, high strength steels

ÖZ

YÜKSEK MUKAVEMETLİ KALIN ÇELİK PLAKALARIN ADIMSAL BÜKÜLMESİNE YÖNELİK YENİ BİR PROSES TASARIMI VE UYGULAMASI

Çetin, Barış
Yüksek Lisans, İmalat Mühendisliği
Tez Yöneticisi : Yrd. Doç. Dr. Eren Billur
Ortak Tez Yöneticisi : Yrd. Doç. Dr. Besim Baranoğlu

Şubat 2018 , 94 sayfa

Zırhlı muharebe aracı üretiminin önemli bir alt işlemi olan gövde imalatında ultra yüksek mukavemetli çeliklerin (UHSS) bükülmesi önemli bir üretim aşamasıdır. Bu bükme işlemi genellikle havada bükme koşulunda (air bending) yüksek tonajlı abkant preslerde gerçekleştirilmektedir. Gövde üretiminde kullanılan çelikler, 1250 MPa gibi geleneksel yumuşak çeliklere kıyasla çok yüksek kopma mukavemetlerine değerlerine sahip olabilmektedir. Bu mukavemet seviyelerinin doğal bir sonucu olarak yüksek bükme kuvvetlerine ihtiyaç doğmaktadır. Diğer yandan, yeni nesil bir imalat yöntemi olarak adlandırılabilecek olan, plastik şekil değiştirmenin adımsal olarak uygulanmasına dayanan adımsal sac şekillendirme yöntemi, son dönemlerde metal şekillendirme endüstrisinde kullanılmaktadır. Bu yeni teknik, şekillendirilebilirliğin arttı-

rılması, karmaşık kalıp tasarımlarına olan gerekliliğin ortadan kaldırılması ve şekillendirme kuvvetlerinin önemli ölçüde azaltılmasında bazı avantajlara sahiptir. Bu tez çalışmasında temel olarak adımsal şekillendirme prosesinin büküm kuvvetinin azaltılması üzerindeki potansiyeli araştırılmıştır. Tezin kapsamı içerisinde yeni bir adımsal bükme prosesi önerilmiş, proses sonlu elemanlar yöntemi ile benzetilmiş ve deneysel olarak doğrulanmıştır. Benzetimler ve deneysel çalışmalar sonucunda elde edilen datalar üzerinde yapılan çalışmalar sayesinde bazı proses parametreleri de optimize edilmiştir. Bununla birlikte, adımsal bükme işlemi, konvansiyonel havada bükme işlemi de ile karşılaştırılmıştır.

Anahtar Kelimeler: Adımsal sac şekillendirme, adımsal bükme, yüksek mukavemetli çelikler

to my Mother, to my Wife, to my Family...

ACKNOWLEDGMENTS

It was actually a long journey of three years. Chosing the thesis subject, preparing the SAYP project proposal, regular term reportings, finite element analysis based simulations, experimental works and etc. all of these stuff is conducted with the supervision and collaboration of my supervisors. Without their supervision and assistance, I would definitely not be able to accomplish this thesis successfully. Therefore, at the very beginning, I would like to express my deepest regards to my supervisors Dr. Eren Billur and Dr. Besim Baranoğlu by stating that I am really honored to be supervised by them for three years.

To be honest, for a mechanical engineer who has stayed a little bit far away from academia for twelve years after graduation, especially heavy non-linear finite element simulations were sometimes really compelling. There were those moments when I was really stucked up and did not know which technical solution should be followed. For these specific moments, the technical assistance from Metal Forming Center of Excellence team was incredibly valuable and helpful for me. Hence, it would be a big fault of me if I did not acknowledge the support of Dr. Ömer Music, Dr. Caner Şimşir, Dr. Kemal Davut and Dr. Celaleddin Karadoğan.

During my master studies, I have also some regular work in my company as usual. Consequently, I have sometimes been pressed between the academic studies and regular responsibilities of a professional. Fortunately, it was a chance of me to have peers who maintain enthusiasm and encourging comments when needed. For this reason, I would also thank to FNSS Material and Special Process team and Dr. Kıvılcım Ersoy, who is the industrial consultant of the project and finally Dr. Caner Taşan, who is the manager of my department at FNSS.

This laborious M.Sc. study had also some effects on my family life. However the comprehensive and considerate behavior of my wife Mrs. Oya Uslu Çetin toward me, made things relatively easier. I am heavily grateful to her and I would like to apologise for any time which I might have not met her expectations as her husband in that period.

As aforementioned, my thesis is also a SAYP project which is supported by the Undersecreteriat of Defense Industries of Turkey. I am very thankful to the authority for their financial support. As a consequnce of being a SAYP project, there was a big amount of offical paper work needed to be worked through and followed. The

official requirements of the project have been met by Mr. Ozan Kayadelen, Ms. Selin Satar, Ms. Banu Eski Özdemir, Mr. Fatih Başaran, Ms. Ayşegül Öztürk and Ms. Nebahat Karasu Atabey, who are all my colllegaues at FNSS. I am grateful for their collaboration and assistance.

Within the scope of the project, advanced optics and solutions have to be implemented for the topology measurements of the samples. Thanks to the powerful technical facilities and knowledge of Atılım University Nanoscopy Lab., this task could be fullfilled easily. I felt myself a very privileged person for having the technical assistance of Dr. Göksel Durkaya and Dr. Hüseyin Kurtuldu. I am very thankful to them for all of the contributions they made.

At this moment, I would also like to state the support of my brother Dr. Barbaros Çetin during not only my M.Sc. but also my whole professional life. He is my brother, my colleague and meanwhile my volunteer surpervisor just like a shinning street lamb in the dark which enlights my road and pushes me towards deeper technical issues.

The last but not the least gratitude should be submitted to my mother who passed away in 2014. What I have achieved in my life today, is a result of her struggle which enables me and my brother to have quality education from prestigious schools. I would like to dedicate this thesis which I obtained at the age of 37, firstly to my mother. I am pretty sure that she is watching me and my brother proudly from somewhere in the sky.

TABLE OF CONTENTS

LIST OF TABLES

TABLES

LIST OF FIGURES

FIGURES

LIST OF ABBREVIATIONS

2D	Two Dimensional
3D	Three Dimensional
BDC	Bottom Dead Center
cof	Coefficient of Friction
FEA	Finite Element Analysis
FP	Final Position
IBP	Incremental Bending Process
ISMF	Incremental Sheet Metal Forming
RD	Rolling Direction
RPM	Revolution per Minute
R_e	Yield Strength
SPM	Stroke per Minute
TCMP	Thermo-mechanically Controlled Processing
TD	Transverse Direction
TWIP	Twinning Induced Plasticity
UTS	Ultimate Tensile Strength
YS	Yield Stress
UHSS	Ultra High Strength Steels
$\%$ TE	Percentage Total Elongation
σ	Engineering Stress
σ_{true}	True Stress
e	Engineering Strain
ϵ	True Strain
$\epsilon_{\text{true plastic}}$	True Plastic Strain

CHAPTER 1

INTRODUCTION

In the hull production of armored combat vehicles, there are three main steps of the process chain. These are laser cutting, bending and welding respectively. As a first step, the hull material which is generally supplied as large-sized plates are trimmed buy laser cutting to the desired dimensions. Then, the plates are bent with respect to the technical drawings. For most of the cases, assuring the dimensional tolerances of the design after bending is a challenging task due to the technical difficulties such as high spring-back tendency which often necessitates some trial and error efforts in prototype production. And finally, the bent plates are transfered to welding workshop in order to obtain the hull assembly. Unlike the automotive or heavy-duty machinery industry, the materials used in armoed combat vehicles have larger thicknesses and dimensions. The thicknesses of the UHSS plates may reach up to $25\,mm$ in certain cases. Moreover, the length of the plates to be bent can also exceed 8 meters. As it could be easily predicted in bending of such thick and long UHSS plates, high pres tonnages are compulsory. The example designs of a hull assembly and a bottom plate are illustrated in Fig.1.1.

As an aforementioned fact, assuring the desired dimensional tolerances which are de-

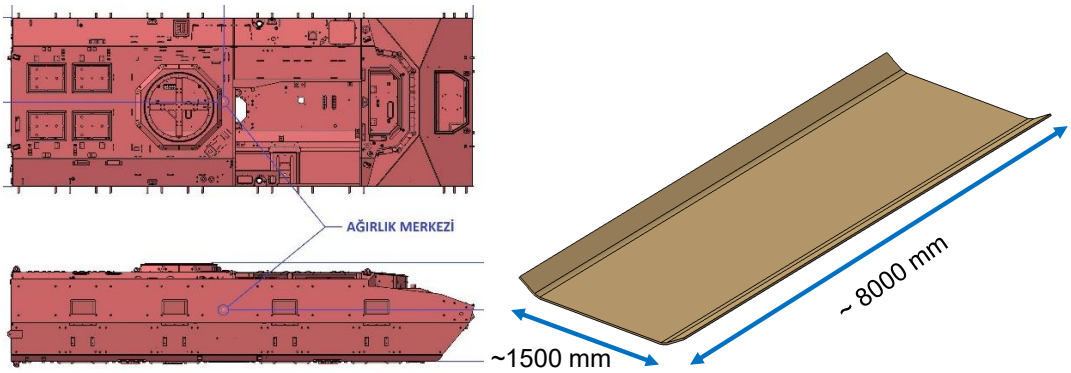

(a) (b)

Figure 1.1: **(a)** An example of hull design **(b)** An example of bottom plate design

fined in the technical drawings is a compelling task in general (see Fig.1.3). The first challenge is the high spring-back tendency of UHSS. The characteristic of UHSS is high R_e and UTS which means to be capable of exciting more elastic strain compared to mild steels. Since the whole elastic strain will be recovered when the loading diminishes, high strength levels cause higher spring-backs (see Fig.1.2). This tendency is also a wide research field in forming of AHSS on which many scientific groups are focused [3, 4, 5].

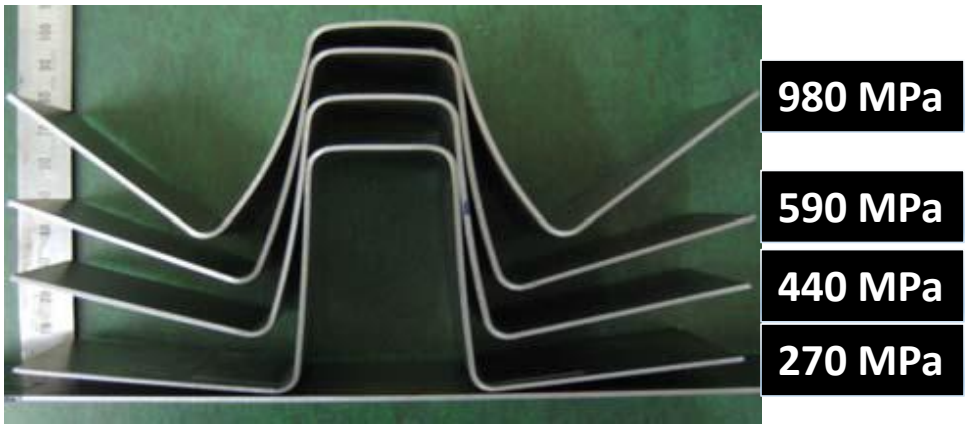

Figure 1.2: Increase in spring-back phenomena by the increase of strength

As could be seen in Fig.1.1 and Fig.1.3 the bending axis is often a straight line for plates to be bent. Therefore, bending in general is a simple one stroke operation. This simplicity of the bending operation enables the usage of press brakes instead

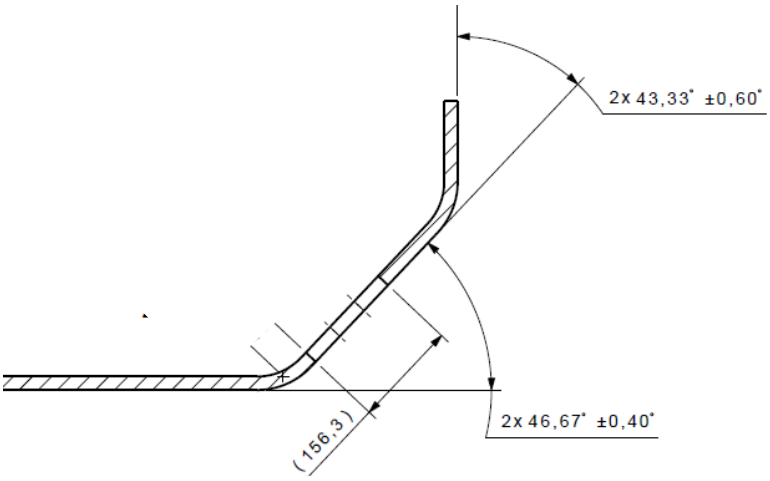

Figure 1.3: An example angle tolerance of a bent UHSS plate

of more complex machinery such as conventional hydraulic or mechanical presses. On the other hand, as shown in Fig.1.1, the length of bending axis could reach up to $8\,meters$ which introduces an important constraint for the operations. In a more detailed manner, in case of bending with press brakes, the bending axis is perpendicular to the uprights of the press. As a consequence, the all length of the plate to be bent should be located between the uprights of the press a priori to the operation. Therefore, for bending operations of hull production, not only high tonnage but also large table dimensions are needed for the desired operations (see Fig.1.4). Thus, a novel bending operation which is an alternative to decrease the bending force and table dimensions is needed to provide enormous benefits for industrial applications of UHSS bending for hull production.

1.1 Aim and Scope of the Study

As mentioned before, one or multi-axes bending is one of the basic operations in the production of armored combat vehicles. This process cannot be performed unless there is high tonnage and large-sized press which in general leads to high investment

Figure 1.4: A $2500\,ton$ capacity press brake with $9100\,mm$ table length

costs. For most of the cases, it is also very difficult to find sub-contractors which has such high tonnage capabilities even this bending operation is outsourced. Therefore, any effort which aims to decrease the bending force may create an alternative to use conventional press brakes whose tonnages are nearly $250\,tons$ in defense industry. On the other hand, regrading the general tendency in hull design, it is very likely to have thicker plates in short term. This fact obviously results in higher and higher bending forces. It could be possible in near the future that $2500\,Ton$ capacity press brakes will not be sufficient enough in bending of UHSS plate to be used in hull production. For that purpose, it is found to be important to investigate whether it is necessary to design an alternative and novel bending method which will enable UHSS bending operation with lower tonnage preses. The novel bending method could also easily be implemented to the subcontractors since low tonnage press brakes can fairly be found in many small-scale companies unlike high tonnage, large-sized press brakes.

More particularly, it is crucial to be able to perform all critical production operations in-house for defense industry. Even if the cycle times would be fairly longer, any

service which is purchased from outside have more risks compared to in-house production. These risks can be related to confidentiality policy, requirements of end user certification or even some critical quality issues. As a result, it could be stated that the presence of an alternative production method which could decrease the bending force of UHSS plates has definitely some strategical advantages.

Furthermore, the incremental sheet metal forming process (ISMF) emerges as a more flexible and cost-effective manufacturing alternative, especially for low volume production. The incremental sheet metal forming method is based on the principle of applying force locally and gradually in the sheet metal and changing the excitation point over time to achieve the desired permanent plastic deformation (see Fig.1.5). ISMF produces significantly less die / tool costs than the conventional forming methods, and it also decreases the pay-load needed for the operations. In other words, low tonnage presses or machines could be used in ISMF for specific applications.

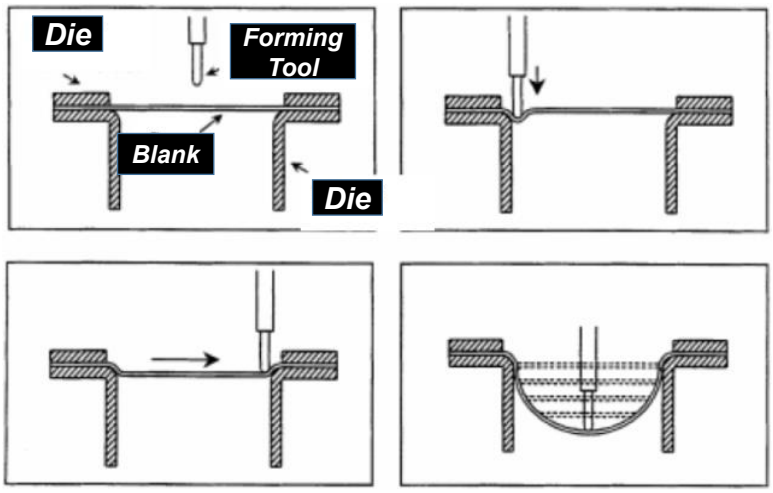

Figure 1.5: A representative of dieless incremental sheet metal forming process

The main purpose of this project is to re-design the bending operation so that the process can be carried out with a lower tonnage press (preferred press brakes like 230 tons capacity), using alternative sheet metal forming principles, as an alternative

to the double-sided bending process for hull production of armored vehicles. A descriptive information is illustrated in Fig.1.6 For this purpose, the dies for press brake application are re-designed to try to develop a manufacturing system in which plate bending can be carried out perpendicular to the conventional bending axis of the press brake (see Fig.1.6).

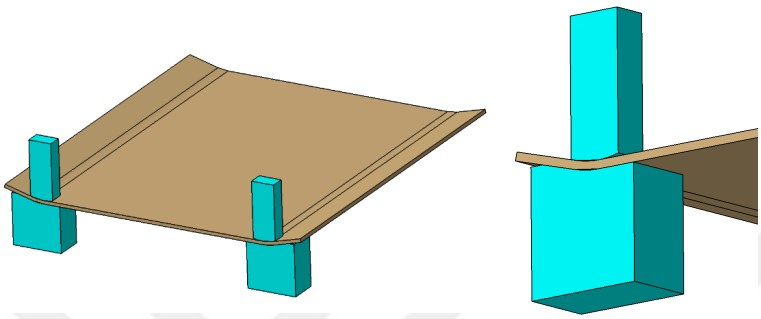

Figure 1.6: A representative of incremental bending process in press brake

ISMF processes are also quite flexible compared to conventional methods, regrading to the changes in dimensions, bending angles and axes, and etc. All of these modifications which could be the case in any time of the design or even during service life of the vehicles may require the renewal of the whole bending dies which is a time-consuming process. On the other hand, in the case of ISMF, the desired results may only be obtained by altering the process parameters in bending process.

Finally, similar to the recent trend of automotive industry, the quantity of variants have also been increasing for armored combat vehicles. For a specific project, there may exist armored vehicles with remarkably different designs, i.e. materials, dimensions, bending angles. It is expected that the result of this thesis study will provide a much more practical method to be used in hull production for different projects easily. Besides, the proposed new incremental bending process will be a method which can be easily put into operation on low tonnage press brakes with less die investment

instead of high tonnage ones. In that sense, it is also expected that an advantageous method will be realized in terms of process simplicity and applicability.

1.2 Introduction to the Theory of Bending

Bending of plates as previously mentioned is a vital process in manufacturing industry. From a general point-of-view, bending of plates is the plastic deformation of the work piece over a bending axis, aiming to create the desired final geometry. For pure bending case, where the bending moment is constant (without any dependence on the location) bending may produce a very small change in sheet thickness.

Bending operation may differ from the other metal forming processes in such a way that the bent materials have always both tension and compression zones within the material. And generally, these two specific zones are separated by the neutral axis which means the axis where no deformation is occurred [1]. In other words, the length of the neutral axis remains the same during the whole bending operation. One side of the neutral axis material is in tension, but the other side of material is in compression. The magnitude of tension or compression increases as the distance from the neutral axis increases. A representative sketch is shown in Fig.1.7, where R is the bending radius, r is the radius of the neutral axis and t is the thickness of the plate.

Bending processes differ in many cases with respect to the deformation mode. The size, the thickness of the bent plate and the design of the dies which are directly dependent on the bend angle and bend radius are important factors. These factors all have a straight forward influence on the plastic strain value exerted on the materials. In other words, they effect the formability or the possible fractures which may occur

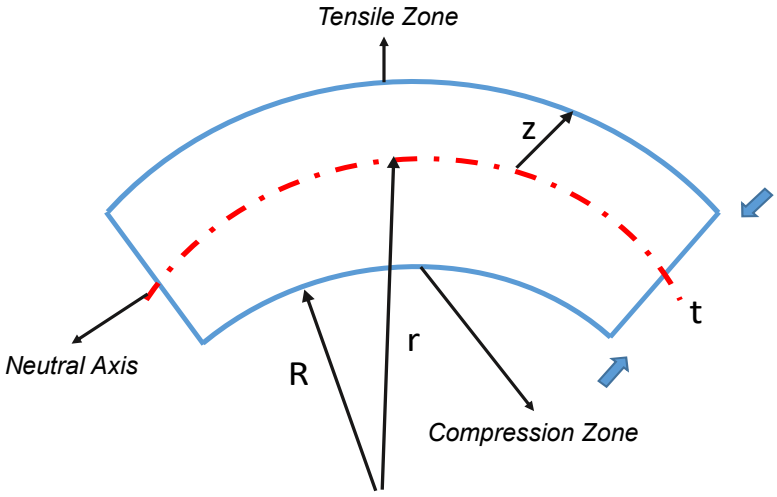

Figure 1.7: A representative of pure bending operation

during the bending process.

The strain values on the plate could be calculated by the following formulas:

$$e_x = \frac{(L - L_0)}{L_0} = \frac{z * \theta}{r * \theta} = \frac{z}{r} \tag{1.1}$$

$$\epsilon_x = ln\left(\frac{L}{L_0}\right) = ln\left(\frac{z}{r} + 1\right) = ln(e_x + 1) \tag{1.2}$$

In many bending operations, especially for the UHSS, the max. strain values that can be reached by the bending operations lies below 0.10. Therefore, for these small plastic strain values, the direct approximation could also be employed for many cases. From plasticity point-of-view, the following approximations can be used for small strain regime whereas this approach would not be a good assumption anymore for moderate strain zone.

$$\epsilon_x \approx e_x \tag{1.3}$$

$$\epsilon_x \approx \frac{z}{r} \tag{1.4}$$

To simplify the calculations, the neutral axis is accepted as the mid-plane of the plate.

Actually this assumption is not entirely correct since the neutral axis slightly moves toward the compression zone. The basic factors which cause this shift are (i) the elements are thickened in the compression zone, (ii) the true compressive strains are greater than the tensile ones. However, for the specific cases where the bending angles are not so much narrow, i.e. the strains are relatively low, this mid-plane assumption is reasonable. Then, the formulation of the true strain can be simplified as follows:

$$\epsilon_x = \frac{t}{2 * R - t} \tag{1.5}$$

This basic formula is often used for the estimation of the bendability. Most of the steelmakers gives sufficient information about the bendability of their products by indicating the R/t values in the technical data sheets. Nevertheless there also exists a general formula which couples the percentage total elongation of the steel to the max. strain occurred in the bending operation. Thus, Eq.1.6 could be presented as follows:

$$\frac{R}{t} = \frac{1}{2 * TE} - \frac{1}{2} \tag{1.6}$$

As a graphical representation, the following figure is proposed by Hosford and Cadell which uses the aforementioned principles:

1.3 Introduction to the Theory of ISMF

The idea of incrementally forming sheet metal with a single point tool, called 'dieless forming', was patented by Leszak [6] well before it was technically feasible. There have been many studies, which have lead to the present situation [7, 8, 9, 10]. In

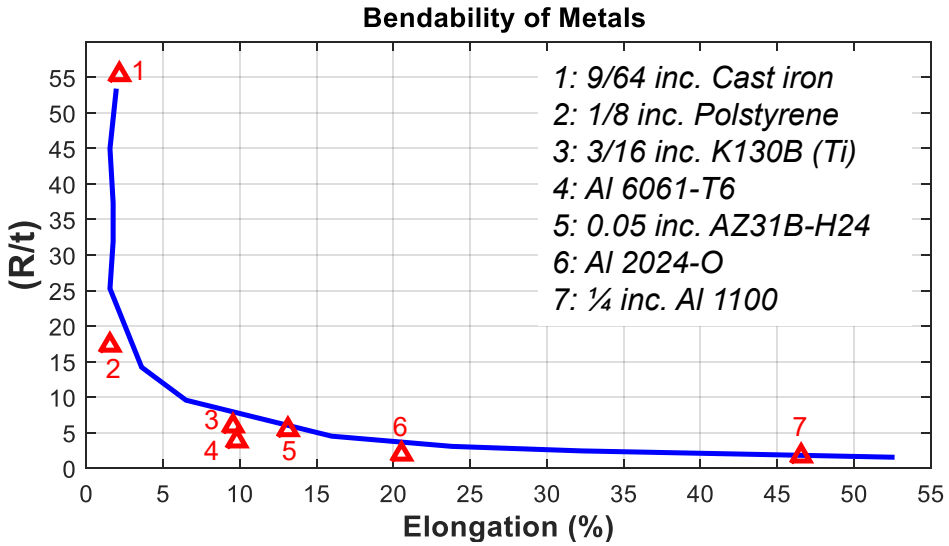

Figure 1.8: Bendability of metals(recreated after[1])

these researches, it is commonly observed that incremental sheet metal forming that allows manufacturing components without development of complex tools in comparison with stamping process, improves the formability due to the shear-dominant characteristics of the process and finally decreases the forming forces [11]. Related to the necessary forming forces, Azauzi et al. [12] showed that tool geometry and tool path design are significantly dominant on the forming forces. Furthermore, forming forces are slightly lower than the experimental values, but results are reasonably satisfying [13]. In other words, the predicted forming forces correspond well with the experimental values in incremental sheet metal forming [14]. It should also be taken into account that ISMF is not a conventional sheet metal forming where the plane stress assumption is valid. An example experimental set-up of ISMF operation is displayed in Fig.1.9.

In other words, 3D stress state exits in ISMF which is similar to the proposed incremental bending process. Like ISMF, the proposed incremental bending operation in this thesis study, is a process that must be evaluated differently from a sheet metal

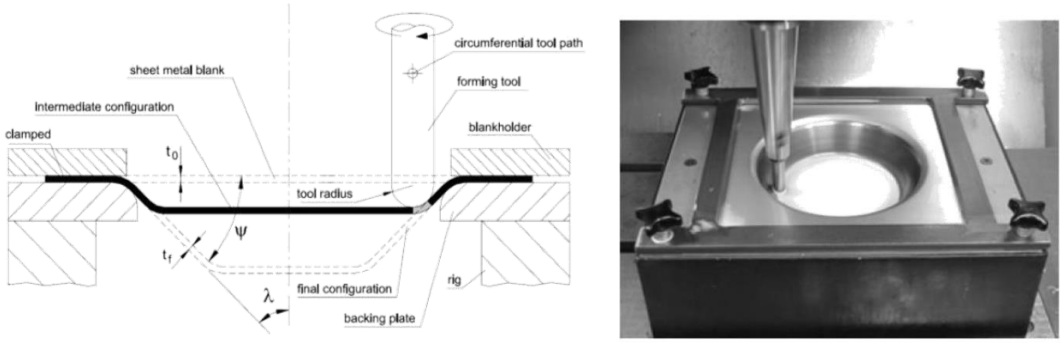

Figure 1.9: An experimental set-up of ISMF

bending process. For sheet metal forming, it is assumed that the stress state is two-dimensional (plane stress case). Actually this assumption loses its accuracy if the thickness is high ($3\,mm$ or more) while, plane stress assumption is significantly close to the reality when sheet thickness is low ($1\,mm$ or less). However, in such a specific case of incremental bending, a 3D stress state is valid which leads to bulk forming conditions rather than sheet metal forming. For that reason, the process proposed in the project, which is envisaged as the sheet bending process, is actually a plate bending-like bulk forming process. It has been shown in many studies that incremental sheet metal forming process includes a 3D stress and strain state characteristics and the forming limits are considerably higher than sheet metal forming processes [10, 15]. From the proposed bending method to be designed within the project, the expectation is to reduce the bending force without sacrificing the quality requirements on surface topology.

The ISMF process is mostly used in experimental or industrial studies aiming to reduce or eliminate the necessity of complex tool geometries or increase the formability of the materials. In literature, there is not any study dealing with decreasing the force of UHSS plate bending operation by incremental forming/bending process. As in our thesis study, any similar efforts focusing on UHSS bending with implementation of

angular and linear increments cannot be found. However, Maatta et al. have studied the incremental bending of UHSS where the increments are defined only in the angular regime [16]. Their conclusion is that the incremental bending could reduce the min. bending radii, hence increase the formability for certain steel grades [16]. Vaisanen at al. also investigated increasing the bendability of UHSS plates with the use of elastic dies. The study succeeded in minimizing the min. bending radii by utilizing elastic lower dies but the required force is increased by 50% [17].

CHAPTER 2

MATERIAL CHARACTERIZATION STUDIES

In metal forming processes, the mechanical properties of the material to be formed (i.e. flow stress or stress–strain curve) greatly influence the operation, the metal flow and the hardening of the material. Therefore, as a first step, the accurate determination of the flow stress is of paramount importance in process simulation by means of FEM [18, 19]. There are several possible methods or test options for determining the flow curve of the materials. It could be stated that apart from the standard tensile test, the other methods necessitate some more complicated set-ups and computations. Even some digital image correlation (DIC) applications which dominantly increase the cost of the experiment may also be compulsory for some cases. Conventionally, tensile test is used to determine flow stress curves. However, tensile test data is limited to small amount of strain (in general max. 0.25) due to plastic instability [20, 21]. Consequently, for most of the metal forming simulations, the flow curve which is obtained by tensile test is extrapolated because the equivalent strain value generally exceed the instability limit of the tensile test during real operating conditions. This approach (extrapolation of the flow curve) generally introduces certain amount of error into the computational calculations as can be seen in Fig.2.1 [22].

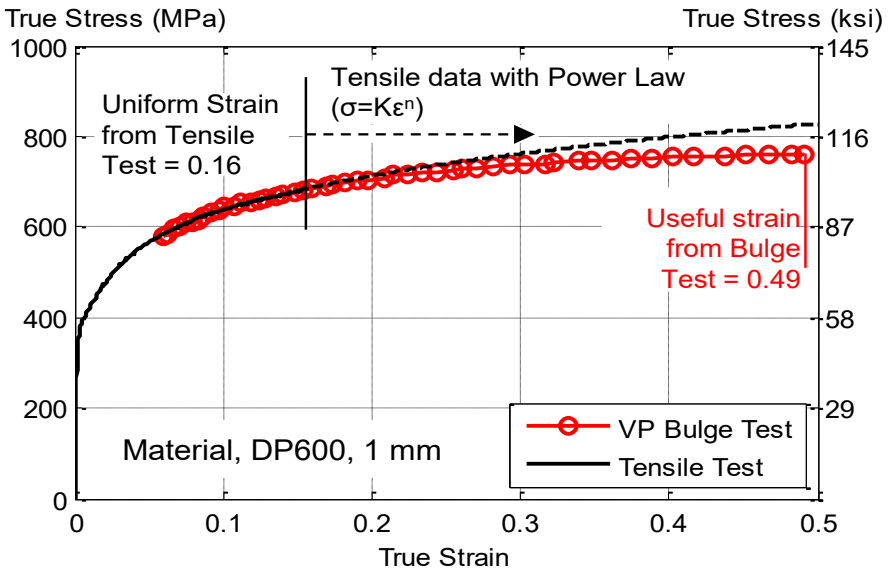

Figure 2.1: A representation of the extrapolation of flow curve in DP600 steel

Despite its limitation on maximum obtainable strain values, standard tensile test is commonly used because of its low cost and ease of accessibility. There is another important point that well-defined testing standards such as EN ISO 6892-1 and technical recommendations exist for many years for standard tensile test. Moreover, even conventional tensile test machine can generate elongation versus force data in any software formats such as $*.csv$, $*.tra$ and etc. Thus, these data may easily be treated by the well-known formulas (Eq. 2.1, 2.2, 2.3, 2.4, 2.5) in order to determine the flow curve of the materials where e is the engineering strain, ϵ is true strain, σ is engineering stress and E is the Young's modulus:

$$e = \frac{(L - L_0)}{L_0} \tag{2.1}$$

$$\epsilon = ln(1 + e) \tag{2.2}$$

$$\sigma = \frac{F}{A_0} \tag{2.3}$$

$$\sigma_{\text{true}} = \sigma * (1 + e) \tag{2.4}$$

$$\epsilon_{\text{true plastic}} = \epsilon - \left(\frac{\sigma_{\text{true}}}{E}\right) \tag{2.5}$$

With the help of these formulations, the flow curve can be computed as the graph of true plastic strain versus true (effective) stress. Just after the determination of the flow curve, necessary curve-fitting operation is straightforwardly applicable to the data so as to calculate the necessary fitting parameters. The graphical explanation of this process is illustrated in Fig.2.2.

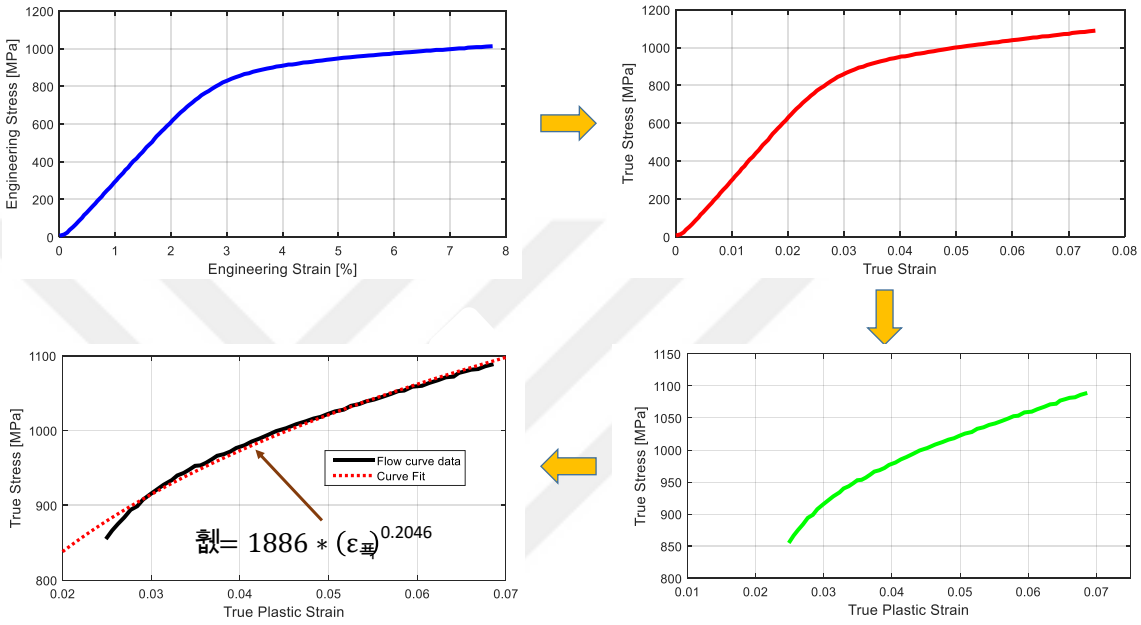

Figure 2.2: Determination of flow curve parameters for ADI material

By means of proper data processing and curve-fitting techniques, it is possible to obtain the flow curves with a reasonable amount of uncertainty. As previously mentioned, the major drawback of this method is the relatively small max. achievable strain of standard tensile test due to the necking. This inhomogeneity phenomena is explained in Table 2.1 and Fig.2.3 .

Nevertheless, this limitation of the standard tensile test could be overcome with the new advances in DIC techniques. In MFCE, there is Aramis GOM system, which is embedded to the Zwick tensile test machine. With the help of this system, the

inhomogeneous strain field could be determined after necking. Then, for the specific area of the max. strain, effective stress could also be computed. The system basically uses the assumption that the most critic region carries the constant percentage of the total load [23]. Therefore, one may easily obtain the flow curve up to the high strain values. Thanks to the Aramis GOM system, the complex DIC algorithms are run by the software automatically and then the result of true strain vs. true stress curve is directly reported for the user.

Table 2.1: Stress and Strain State Comparison Before and After Necking in Tensile Testing

	Stress State	**Strain State**
up to necking	uniform one-dimensional	uniform three-dimensional
during necking	non-uniform three-dimensional	local three-dimensional

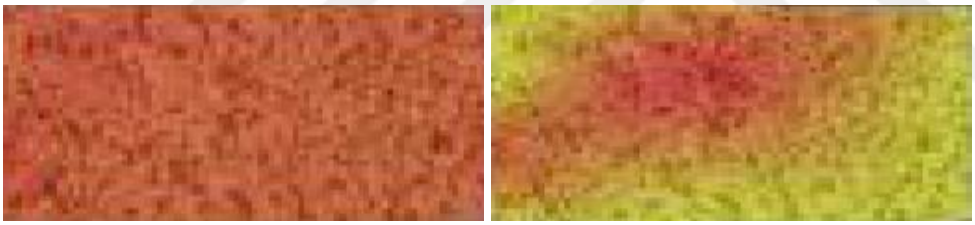

(a) (b)

Figure 2.3: **(a)** DIC image before necking **(b)** DIC image after necking

In this project, the UHSS are characterized firstly by Aramis GOM measurements which enable the determination of the flow curve up to high strain values such as 0.40. Although the max. achievable strain values in plate bending operations is low, it is concluded by the project team that it has always more benefits to have flow curves in wide ranges of strain values (In order to explain this fact in a more detailed manner a comparison is made in Fig.2.4) for TMCP steel. The results of tensile tests will be presented just after Section 2.1.

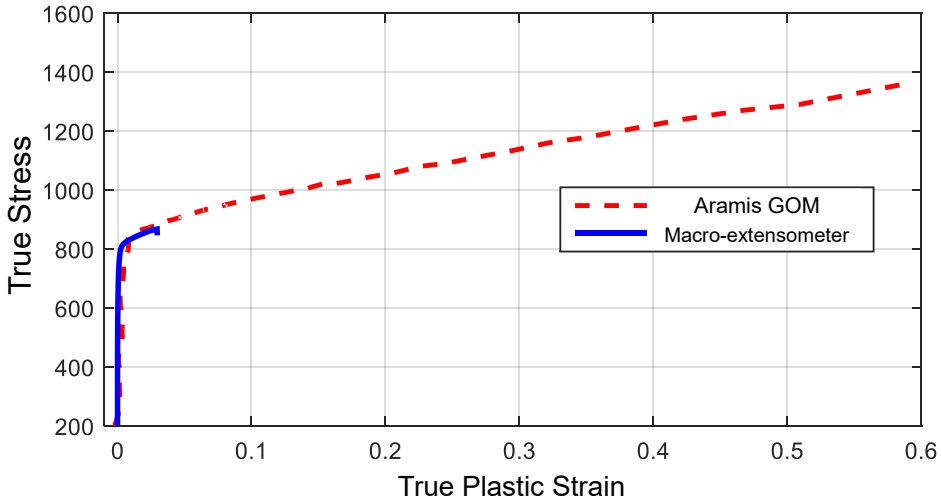

Figure 2.4: A comparison of standard tensile test and DIC with Aramis GOM for Armor Steel-1

2.1 General Information of UHSS Used in Experimental Studies

UHSS steels plates can be classified under two sub-groups. The first group includes the steels which are produced by thermo-mechanically controlled processing (TMCP) such as S700 MC, S800 MC and etc. TMCP steels are produced in accordance with EN 10149 and EN 10025-4 standards. The second group is the quenched and tempered (QT) steel. In general, QT steels are associated with EN 100025-6 standard and moreover, armor steels could be treated as a specific sub-family of QT steels. Their production mostly contains accelerated quenching operations which is engaged to the rolling line after which tempering is also performed with integrated continuous lines. As it could be predicted, armor steels have approximately 100% martensitic micro-structure. Small amount of retained austenite often exists in the micro-structure. Due to this specific micro-structure, UTS of some armor steels can exceed 2000 MPa which is an enormous strength level compared to conventional mild steels. There is also an important issue that the armor steels in general have low-tempering tempera-

Table 2.2: Approximate Mechanical Properties of Studied UHSS

	Approximate YS (MPa)	**Approximate UTS (MPa)**	**Approximate TE**	**Thickness (mm)**
Armor Steel-1	1000	1150	12%	12
Armor Steel-2	1100	1400	10%	20
TMCP Steel-1	700	850	12%	10

tures compared to other heat treated steels like cold work tool steels. Consequently, during any manufacturing process like laser cutting, welding and etc., the heat that will be exposed to the process can lead to a new tempering and hence may reduce the level of strength guaranteed by the producer of the armor steels. For example, in the case of Armox 500T, which is an armor steel conforming to MIL DTL 46100 standard, the manufacturer has stated that the strength values in the product specification may not be available if the material is exposed to temperatures higher than 170 °C [24].

In this project, two armor steels with different thickness values and one TMCP steel have been used for the experimental studies. These UHSS are selected with respect to their common usage in the hull production. In other words, they are widely and commonly used steel materials at FNSS which are subjected to plate bending operations. The brief information on their basic mechanical properties are provided in Table 2.2.

The differences between mechanical properties of Armor Steels and the TMCP Steel, as listed in Table 2.2, is due to the composition and microstructure differences. TMCP steel production involves controlled hot working and micro-alloyed compositions. At the TCMP production route, the initial hot working is carried out at regularly (conventionally) used temperatures (i.e. 170 °C), but the final reduction pass is carried out at temperatures lower than the conventional routes. The final hot working may continue

down to temperatures below the lower critical temperatures Ar_3. This processing route involves plastic deformation at lower temperatures, which promotes grain refinement. Some TMCP grades, cooling after final reduction pass is accelarated by water cooling, to refine grains further. Moreover, this practice also produces fine and evenly dispersed precipitates. Fig.2.5 shows the optical micrograph and Fig.2.6 shows the scanning electron micrograph of the TMCP Steel-1 used in this study. The rolling direction is clearly visible in the optical micrograph. The micrographs were taken from the rolling direction - normal direction (RD-ND) plane. The finer grain structure of the TMCP Steel is more clearly visible in Fig.2.6, which shows that the grains are smaller than $5\,microns$.

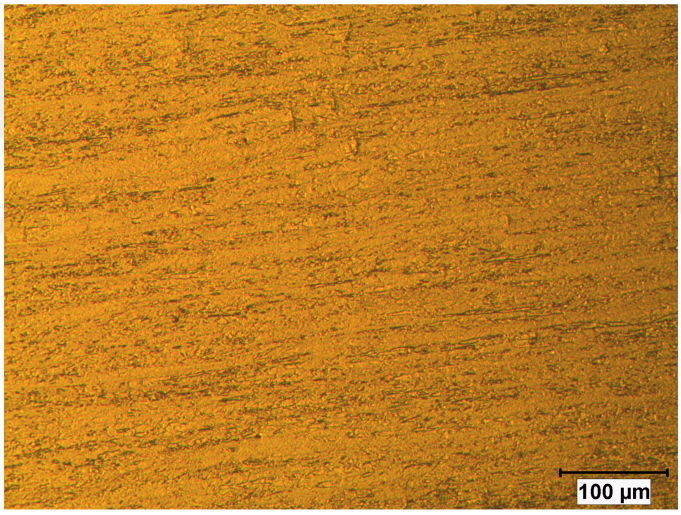

Figure 2.5: Optical micrograph of TCMP Steel-1 (100x)

Armor steels, including the ones used in this study, are produced by quenching and tempering (QT). After hot rolling, those steels are austenitized, quenched and finally tempered between $200 - 600$ °C. During quenching the fastest cooling rates are obtained at the surface of the steel plates; whereas the interior regions cool slower. The composition of the QT plates are selected depending on the section thickness of the plate and the cooling capacity of the lines. The alloying elements that im-

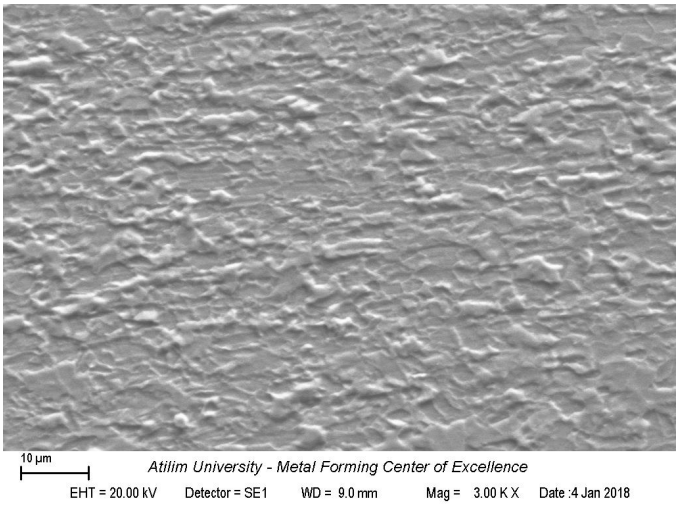

Figure 2.6: SEM micrograph of TCMP Steel-1 (3000x)

prove the hardenability are added to ensure producing martensite even at the slowest cooled core of the plate. The tempering temperature is selected depending on strength and toughness requirements. For armor steels, toughness requirements have priority, therefore higher tempering temperatures are preferred. The QT process produces mainly tempered martensite microstructure, in addition some retained austenite as well as some lower bainite is also acceptable. Fig.2.7 shows the optical micrograph and Fig.2.8 shows the scanning electron micrograph of the Armor Steel-1. The rolling direction is as clear as the TMCP steel; however both micrographs clearly show a refined microstructure. Moreover, the SEM micrograph shows very fine and evenly dispersed carbide precipitates which indicates that the steel has been tempered at a relatively high temperature.

2.2 Tensile Tests of Studied UHSS Plates

As it is explained in the previous sections, the material data is obtained from Aramis GOM system as true stress and true strain curve. The all set of data list could also be extracted as *.cvs file. An example result of the tensile test is shown in Fig.2.10.

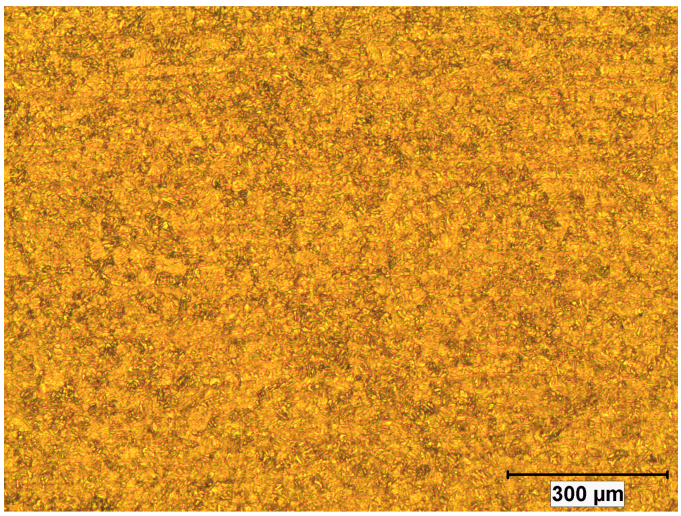

Figure 2.7: Optical micrograph of Armor Steel-1 (100x)

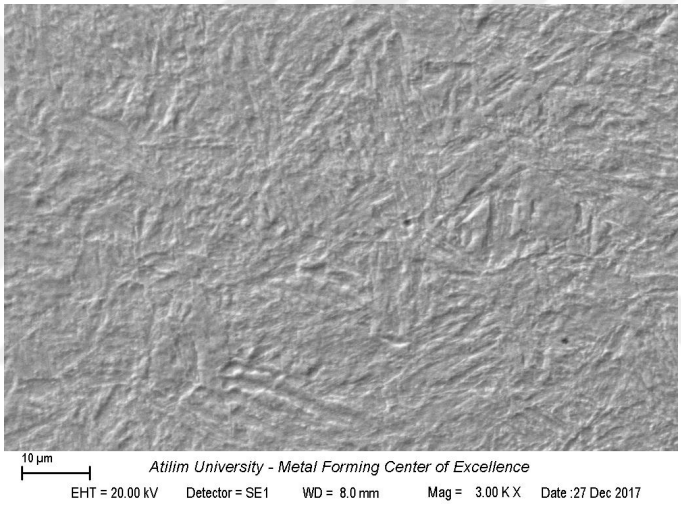

Figure 2.8: SEM micrograph of Armor Steel-1 (3000x)

Then, by using Eq.2.5 and processing true stress and true plastic strain data, the flow curve parameters are determined for TMCP Steel-1. At this point, it is necessary to state that there is sufficient flexibility in defining the flow curve for FEA software. The user can define complex equations or even data point sets for the constitutive behavior. However, the main objective of this study is to define the flow curve as simple as possible (preferably by Hollomon equation) by assuring reasonable success of regression at the same time. More specifically, $R^2 \geq 0.95$ is accepted as the acceptance criteria in $MatLab$ software. The result of the curve-fitting with respect to Hollomon

equation Eq.2.6 is listed in Table2.3. For any case that Hollomon equation is not sufficiently appropriate, other alternatives could also be employed. For instance, Fig.2.9 show another alternative solution.

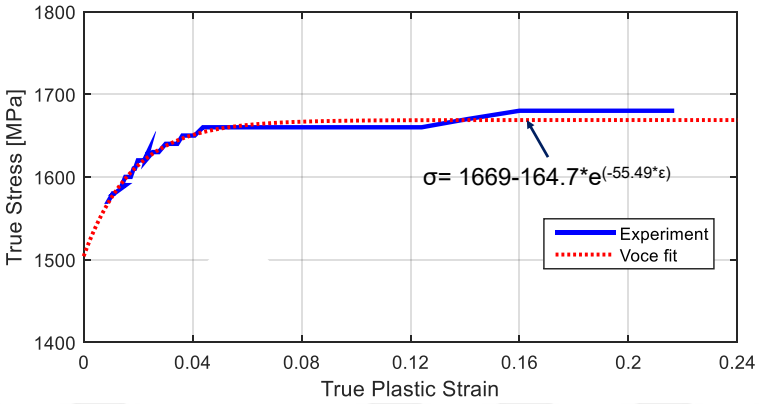

Figure 2.9: Tensile test results of Armor Steel-3

$$\sigma = K * \epsilon^{n} \tag{2.6}$$

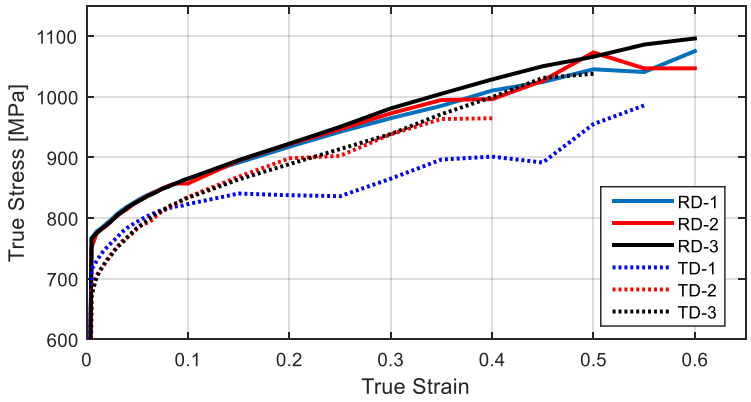

Figure 2.10: Tensile test results of TCMP Steel-1

Regarding the determination of the flow curve parameters for TMCP-1 steel in rolling direction, Fig.2.11 is prepared to explain the computation process. The R^2 value of this curve fitting operations was 0.9589.

Regarding the computation of yield stress, there is always some ambiguity. As it is stated in the literature, the yield strength is not unique in recognition that the plastic

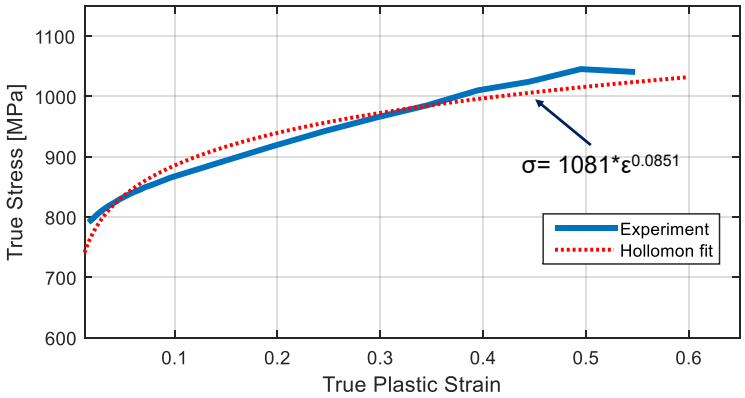

Figure 2.11: Determination of Hollomon equation parameters of TMCP-1 in rolling direction

Table 2.3: Flow Curve Parameters of TMCP-1

TMCP-1	K	n	YS (MPa)
RD-1	1081	0.0851	774.62
RD-2	1093	0.0938	778.68
RD-3	1091	0.0902	770.24
TD-1	959.6	0.0628	736.15
TD-2	1036	0.0897	697.74
TD-3	1091	0.1088	697.82

deformation in metals due to dislocation flow is not a singular event but a diffuse process [25]. In order to avoid ambiguities in determination of the yield strength, the most commonly used convention is to use a pre-defined offset strain of 0.2% ($R_{\text{p0.2}}$ approach). However, in this $R_{\text{p0.2}}$ approach, the data used for the calculation is the elastic strains which are very small values (few microns) and may contain some uncertainty due to the stick/slip effect which may occur on the onset of the loading. Thus, some more sophisticated and precise approaches also exist in sheet metal forming applications in determining the yield stress. For instance, the extrapolations of the flow curve to the zero true plastic strain value [19] can be applied. An example of the extrapolation operation is illustrated in Fig.2.12 and the YS values in Table 2.3 are computed by this extrapolation method. This more specific computation of yield

stress is considered more accurate for determining yield surface.

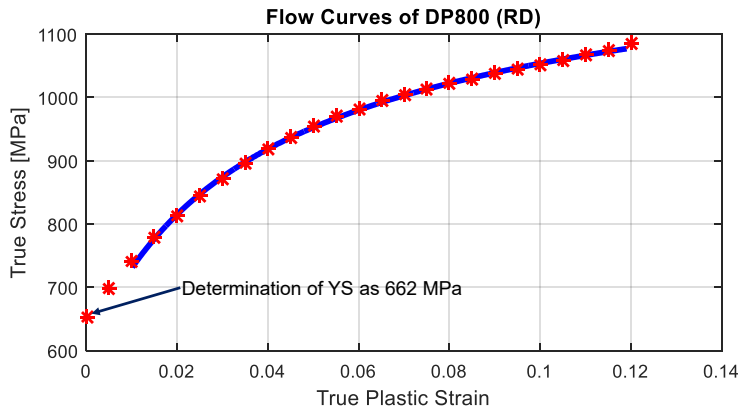

Figure 2.12: Determination of YS by extrapolation of flow curve for DP800 steel

The tensile test results of Armor Steel-1 is also shown in Fig.2.13. As it can easily be seen, the results of rolling direction and transverse direction correspond each other. Therefore, it is decided that the flow curve in rolling direction would be sufficient for the simulation studies. The same methodology is also performed to determine the flow curve parameters of Armor Steel-1. The parameters obtained and the curve-fitting graph is illustrated in Fig.2.14.

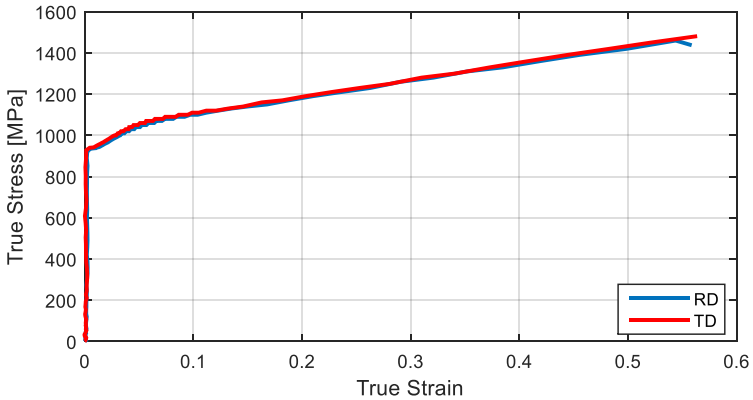

Figure 2.13: Tensile test results of Armor Steel-1 with DIC system

Similary, tensile tests for Armor Steel-2 are also conducted with $Gom\ Aramis$ optical system. The results of these tests are displayed in Fig.2.15. As it can easily be seen, the results fairly correspond with each other. Therefore, it is decided that the flow curve data of RD-2 could be applied for the simulation studies. The flow curve

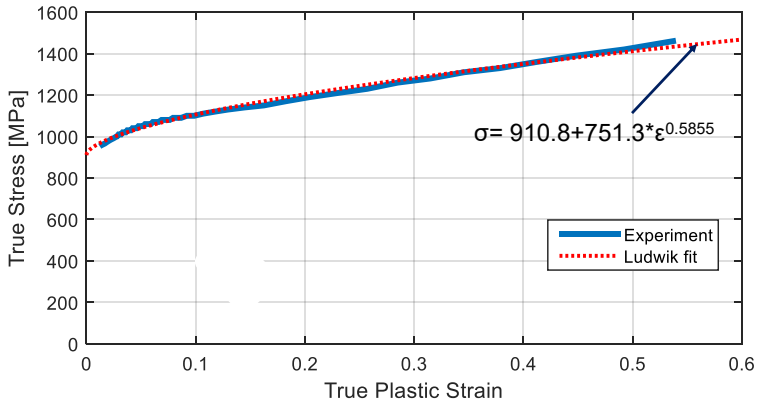

Figure 2.14: Determination of Ludwik equation parameters of Armor Steel-1

Table 2.4: Flow Curve Parameters of UHSS

	Y_0	K	n
TMCP Steel-1	0	1081	0.0851
Armor Steel-1	910.8	751.3	0.5855
Armor Steel-2	1346	1479	0.9891

parameters are obtained by using Ludwik equation fit to the experimental data. The parameters obtained and the curve fitting graph is illustrated in Fig.2.16.

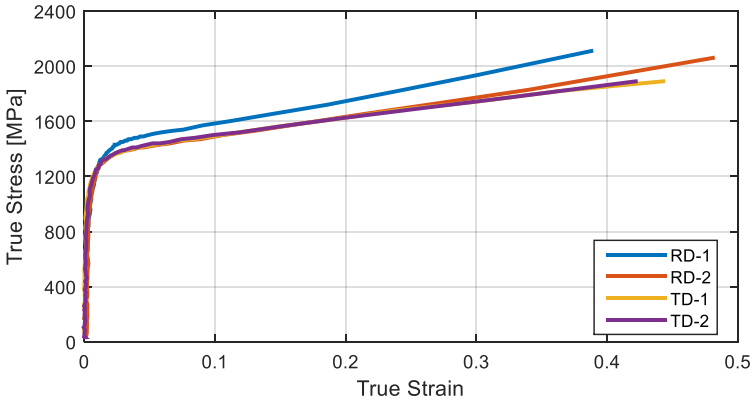

Figure 2.15: Tensile test results of Armor Steel-2

In sum, the computed flow curve parameters of the designated steels are tabulated in Table2.4 where Y_0, K and n are the parameters which are defined in Eq.2.7

$$\sigma = Y_0 + K * \epsilon^n \tag{2.7}$$

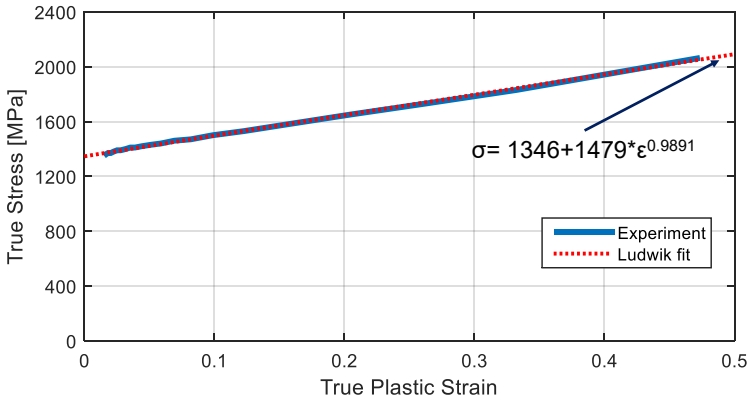

Figure 2.16: Determination of Ludwik equation parameters of Armor Steel-2

2.3 Yield Surface Definition

In tensile testing where the loading is only one-dimensional and more specifically where the stress tensor has only one non-zero value, plastic deformation (yielding) occurs when the uni-axial stress exceeds the yield stress. However, this is actually an idealized case since there is multi-axial stress state nearly for all of the metal forming operations. This more complex yielding condition is treated with phenomenological (approximating the experimental data by analytical functions) theories called yield criteria or yield surface definition [26].

Yield surface definitions can be divided into two groups as isotropic or anisotropic (quadratic, non-quadratic and etc) ones. For bulk metal forming operations, i.e. where the stress state is three-dimensional instead of plane stress condition, it is more proper to assume an isotropic material behavior. In other words, the polycrystalline structures, under the condition that there is sufficient amount of grains that are randomly oriented exhibit isotropic behavior [27, 28]. Regarding this fact, thick UHSS plates are accepted as isotropic materials. Therefore, isotropic Von Mises yield criterion is used during the FEA simulations of plate bending. This criterion can be formulated as follows: material passes through elastic to plastic state when the elastic energy of

distortion reaches a critical value which is independent of the stress state [29, 26]. It is first proposed by R. Von Mises in 1913 [30]. This yield surface could be described with Eq.2.8 in principal stress plane where σ_Y is the uni-axial yielding stess in $1st$ principal direction

$$[(\sigma_1 - \sigma_2)^2 + (\sigma_2 - \sigma_3)^2) + (\sigma_3 - \sigma_1)^2 = 2 * \sigma_Y^2 \tag{2.8}$$

As it can be concluded from Eq.2.8, for plane stress case where the $\sigma_3 = 0$ then Eq. 2.8 converts to Eq.2.9 and Eq.2.10

$$[(\sigma_1 - \sigma_2)^2 + (\sigma_2)^2 + (-\sigma_1)^2 = 2 * \sigma_Y^2 \tag{2.9}$$

$$\sigma_1^2 - \sigma_1 * \sigma_2 + \sigma_2^2 = \sigma_Y^2 \tag{2.10}$$

According to this definition of Von Mise's yield surface, the studied UHSS are processed and for the better understanding of the definition, Fig.2.17 is created for the 2D case. While using Von Mise's equations, the yield stress is calculated as described in Fig.2.12. Then, the material constitutive behavior is accomplished by implementation of the flow curve to the yield surface. It could also be stated that the input of flow curve and Von Mise's yield criteria will be sufficient for FEA to run the non-linear numerical simulation of plate bending operation.

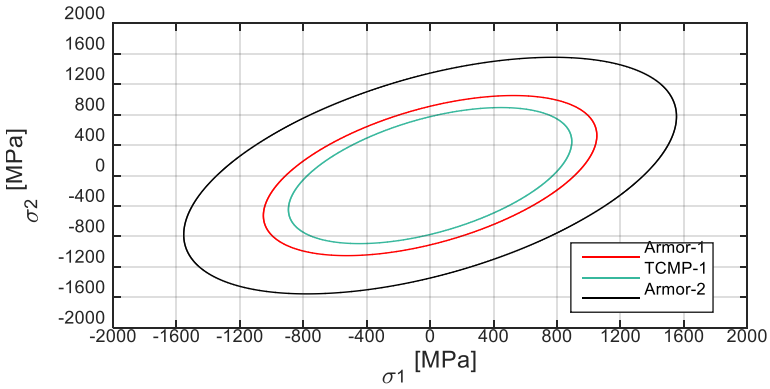

Figure 2.17: Von Mise's yield surface of studied UHSS in 2-D stress state

2.4 Definition of the Hardening Rule

The simplest way to define the hardening of a material is to assume an isotropic hardening case where the yield surface protects its shape without any change but it expands. When this hardening model is applied with Von Mise's yield criteria, the hardening could be defined just with a yield surface and a flow curve as in Fig.2.18. Another important point is that the isotropic hardening assumption relies on the fact that the yield stress does not change in tension and compression directions, which is an acceptable approach for sheet or bulk materials.

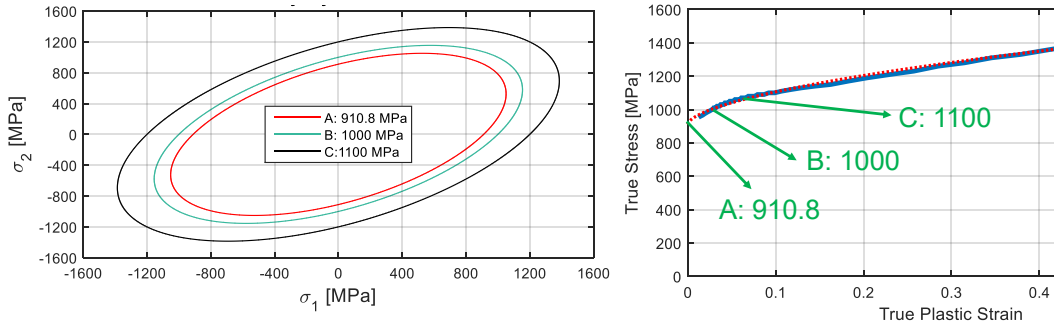

Figure 2.18: Definition of the isotropic hardening case of Armor Steel-1

On the contrary, if the cyclic loading condition is valid, in other words, the stress state changes into tensile to compression or vise versa the estimation of yield stress gets more complicated due to Bauschinger effect. Thus, in such cases, kinematic harden-

ing models are usually engaged for FEA analysis. In other words, the kinematic behavior of the yield surface plays an essential role since it is indispensable to describe the Bauschinger effect, i.e., the material's answer to the multiple tension-compression cycles to which material points are submitted during the forming process[31]. A comparison of isotropic and kinematic hardening is illustrated in Fig.2.19. Especially in the studies regarding the precise prediction of spring-back, kinematic hardening formulations are deeply investigated. Yoshida and Uemori have also performed many researches on the subject and proposed some material models which are currently implemented to some commercial FEA sofware [32, 33, 34, 35].

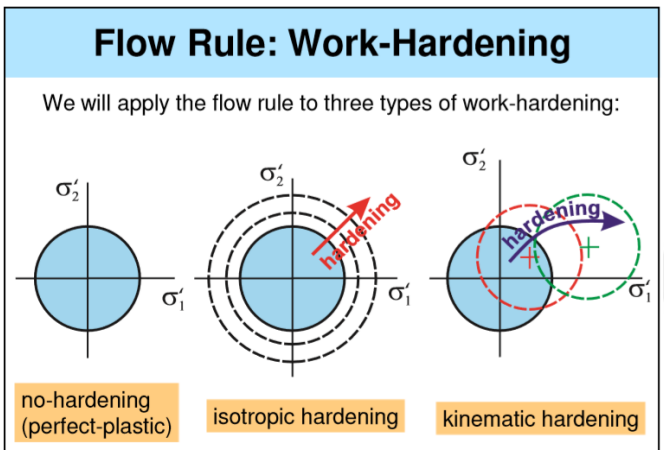

Figure 2.19: Schematic description of isotropic and kinematic hardening [2]

More particularly, the proposed Yoshida–Uemori material model ($YU\ model$) combines the work hardening principles of isotropic hardening and kinematic hardening, enabling it to comprehensively describe the Bauschinger effect and work hardening that occur in metal during cyclic large plastic deformation. Thus, the $YU\ model$ has been incorporated into several simulation software packages, such as the $MAT-125$ material model in LS-DYNA and the Yoshida kinematic hardening model in Pam-Stamp [36].

However, even the isotropic-kinematic hardening may not be effectively enough to

account for more general non-proportional loading [37]. It is possible to define non-proportional loading as the case where the principal stresses do not maintain constant directions and constant ratios. In the experimental researches for non-proportional loading [38, 39, 40, 41, 42], including tension after pre-tension or shear after pre-tension, the cross-effect is often observed. For the description of complex deformation behaviors which can be faced with in non-proportional loading, the association of kinematic hardening and distortional hardening provides further refinement[37]. Furthermore, homogeneous anisotropic hardening (HAH) model is also proposed by Barlat et al. [43, 44, 45]. The HAH model provides a modular frame-work for the description of anisotropy, Bauschinger and latent effects, either independently or combined in an arbitrary manner [46].

To conclude, this complex hardening models are not implemented to numerical analysis since the conventional and incremental bending processes are considered as monotonic loading case. This monotonic loading assumption is investigated in Chapter 3. For the FEA analysis in this study, isotropic hardening approach is used. This decision is made by taking into account that isotropic hardening, in which only the yield surface changes its size, is reasonably effective for monotonic loading cases [37].

CHAPTER 3

FINITE ELEMENT ANALYSIS STUDIES

The plate bending simulations are modeled in MSC Marc software by using the same geometry of the die and punch sets which are used in experimental studies. MSC Marc is a non-linear based FEA software which especially focuses on implicit time integration solutions. There is always the issue of spring-back in the case of bending and especially incremental bending. Therefore, the implicit time integration is thought to be optimum and/or proper method. However, as a general rule of thumb, it could also be suggested that in order to simulate stamping processes, an explicit method, which is conditionally stable, is generally thought to be the most adapted. Such an algorithm presents the advantage of being non-iterative while, the contact configuration evolves rapidly, and the conditional stability is not a disadvantage since time steps must be small enough anyway for an accurate computation. Yet, during the spring-back simulation, an implicit method, which is iterative, presents the advantage of unconditional stability [47]. Still, there is some effort in the literature which deals with combined explicit and implicit time integration coupling with stamping operations in order to benefit from the advantages of the both [47, 48, 49]. However, in the current thesis study, implicit time integration method is preferred as a single alterna-

tive. For that purpose, MSC Marc software is used as implicit solver option (Fig.3.1 and Fig.3.2 is shown to demonstrate the environment of the simulation).

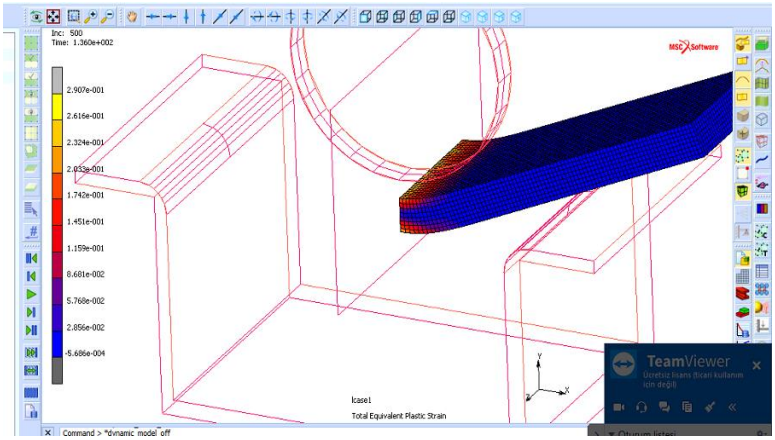

Figure 3.1: Marc simulation, color map of max. plastic strain

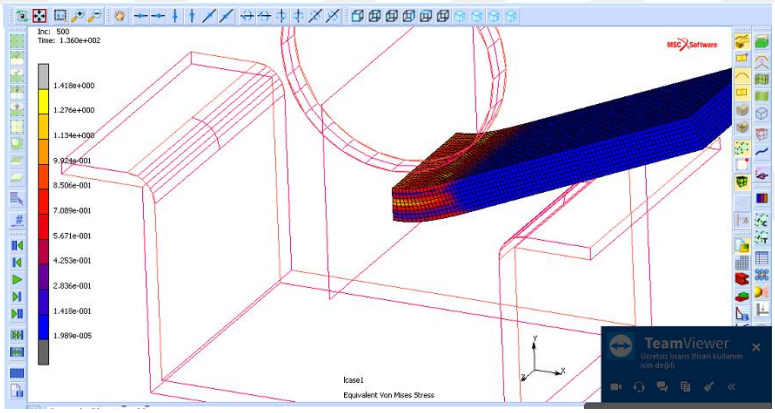

Figure 3.2: Marc simulation, color map of max. equivalent Von Mise's stress

Having made this decision, the following issues are investigated and/or optimized in FEA studies which are significantly dominant on the predicted bending force:

- The type of elements in FEA
- The quantitiy of elements to be used in the direction of thickness
- The success of the symmetrical modeling

In the following sections these issues will be discussed respectively.

3.1 Element Type in FEA

Thanks to the simple geometry of plates to be bent, the mesh structure could all be created by brick elements which have several advantages in numeric computations. Brick elements are actually hexahedron shaped elements. More specifically, a hexahedron is a polyhedron with six faces, eight corners and twelve edges or sides. It is topologically equivalent to a cube or a prizm. Hexahedral elements, as a general rule of thumb, can be accepted as assuring high precision compared to tetrahedrons. Besides being more accurate, the hexahedral element presents other advantages. Meshes consisting of hexahedrons are easier to visualize than meshes consisting of tetrahedrons. In addition, the reaction of hexahedral elements to the application of body loads corresponds more precisely to loads under real-world conditions. The eight-node hexahedral elements are therefore superior to tetrahedral elements for finite element analysis [50].

For the p-q convergence optimization, a benchmark study is accomplished for three hexahedral elements which are defined in Marc software. The bending simulation of Armor Steel-1 is modeled in the software and the predicted bending force is determined for $Hex-8$ (Element type 7), $Hex-20$ (Element type 21) and $Hex-8$ reduced integration elements (Element type 117) respectively. The result of this benchmark study is designated in Fig.3.3.

Furthermore, the three different type of elements are compared with respect to the relative error each time increment by computing the average relative error as well. The result of this analysis is shown in Fig.3.4. When the huge amount of computational cost of quadratic elements $(Hex-20)$ is taken into account concurrently with

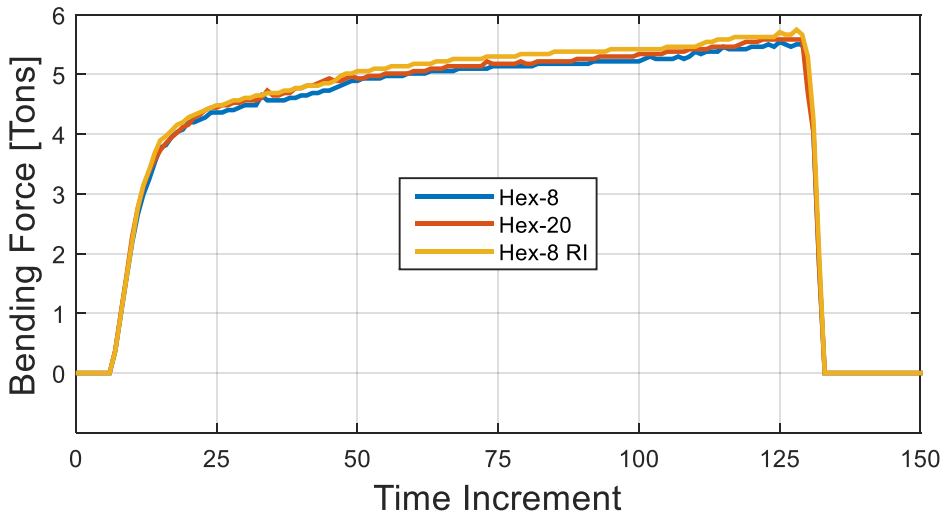

Figure 3.3: Prediction of bending force wrt three different element types of Marc software

approximately 2% relative error, the concluding decision is made as modeling with $Hex-8$ elements. While resulting in this decision, it is also observed that there is not so much computing time difference between $Hex-8$ and $Hex-8$ reduced integration elements.

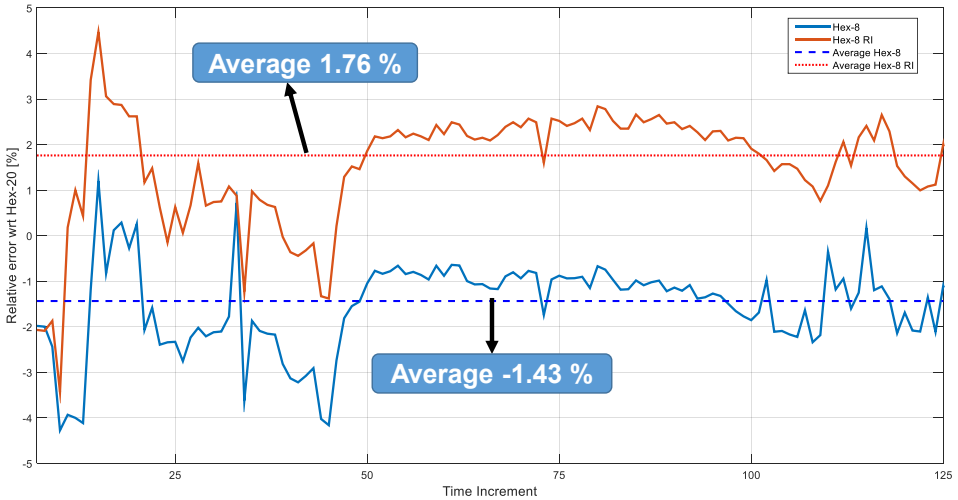

Figure 3.4: Relative error of elements in bending force prediction

3.2 Quantity of Elements in Thickness Direction

One of the most important parameters in the bending simulations of thick UHSS plates, which is actually a bulk forming process, is the number of elements to be used in the direction of thickness [51, 52]. Simulation trials are carried out to determine the number of elements in the thickness direction. The bending force is calculated by using different quantity of elements in thickness directions and this effort is concluded in the decision that eight (8) elements in thickness direction is the optimum solution (precision and computational cost) for the problem. Therefore, the further simulations are performed according to this finding which corresponds well with the industrial applications with respect to the optimum point for precision and calculation time. The following graphs shows the examples of comparison:

$$\%RelativeError = \frac{1}{m} * \sum_{i=1}^{m} (\frac{F(i) - F^{16}(i)}{F^{16}(i)} * 100) \tag{3.1}$$

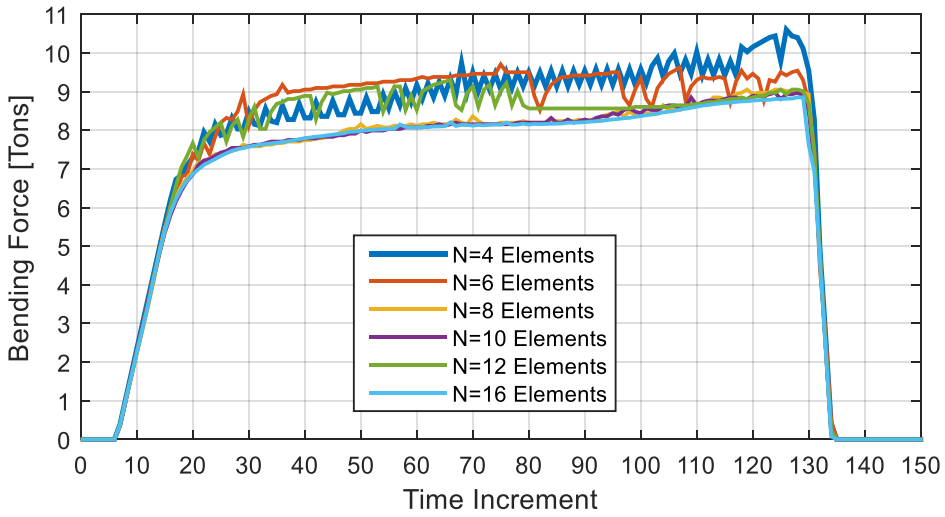

Figure 3.5: Comparison of bending force wrt different mesh structures

The results of this specific optimization study are illustrated in Fig.3.5, Fig.3.6 and Fig.3.7. The $(\%)$ relative error in bending force is computed with Eq.3.1 where m is

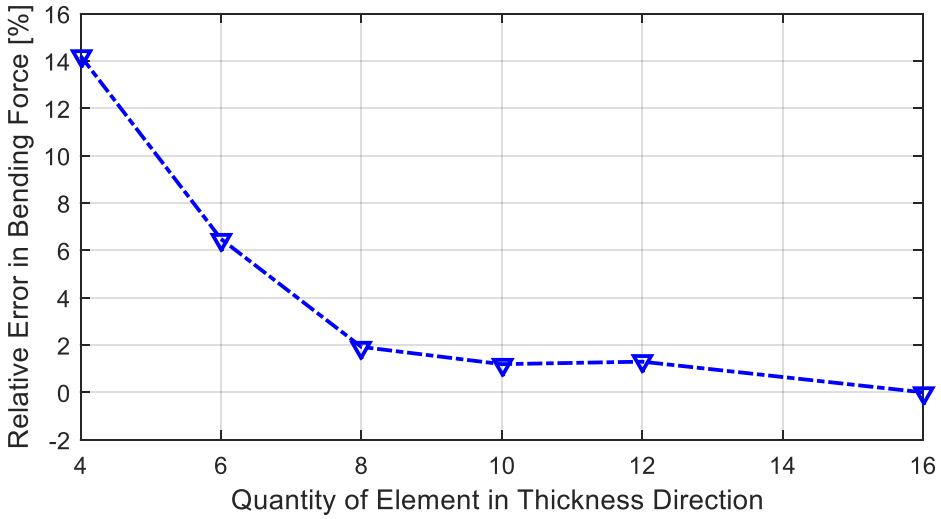

Figure 3.6: Convergence of bending force wrt different mesh structures

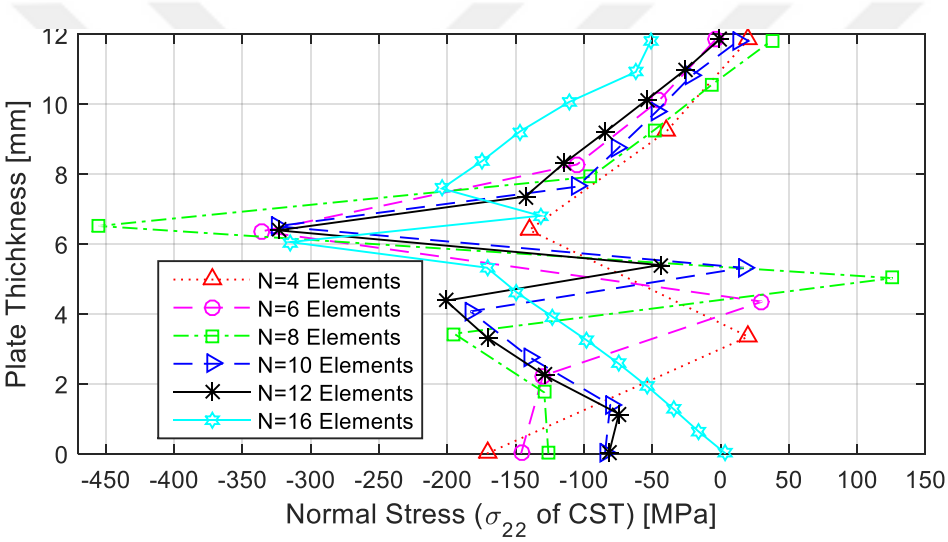

Figure 3.7: Convergence of normal stress wrt different mesh structures

the total quantity of the time increments and $F(i)$ is the bending force at the i^{th} increment of the operation and $F^{16}(i)$ is the bending force of the same time increment of model which has 16 elements in thickness direction respectively. As it is obvious in previous graphs, eight elements in thickness direction showed sufficient performance in numerical analysis. With respect to Fig.3.6, it could be concluded that the model with 8 elements in thickness direction, is nearly the onset of the asymptotic behavior and it has approximately a relative error of 2%. On the other hand, it has huge advantage in computational cost. For this reason, use of eight elements in thickness

direction with equivalent aspect ratios is decided to implement in FEA models.

3.3 Verification of Symmetry Conditions

When plate bending operation is considered, it is reasonably stated that the process is symmetrical. Therefore, $1/4$ model approach is found to be optimum solution in FEA studies. However, in order to investigate the possible effects of symmetrical modeling, a comparison study is performed. In order to designate the symmetric planes and full model data in FEA model, Fig.3.8 and Fig.3.9 are prepared.

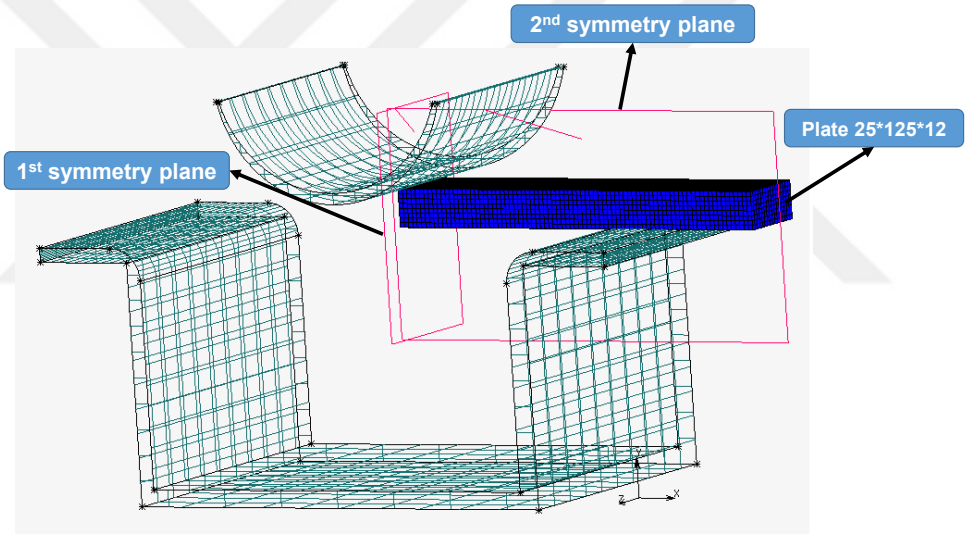

Figure 3.8: Symmterical modelling approach in MSC Marc

In the beginning of the FEA efforts, a full model and a $1/4$ model are compared with respect to predicted bending forces. The comparison is shown in Fig.3.10.

Like the element type comparison, a relative error graph is also created for symmetrical modeling. The average error is determined as 7.51% as seen in Fig.3.11 which is found to be reasonable by taking into account the computational advantages of symmetrical modeling.

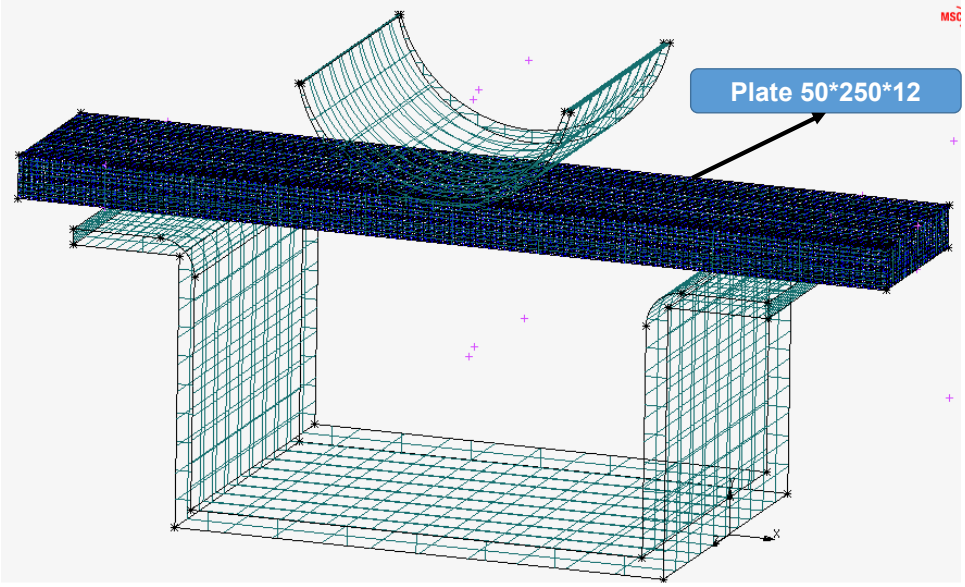

Figure 3.9: Full modelling approach in MSC Marc

In conclusion, regarding the Sections 3.1, 3.2 and 3.3, it is concluded that 1/4 model symmetrical approach with 8-node hexahedral elements is proper for the purpose of the project. Moreover, eight elements in the thickness direction is also sufficient to assure necessary precision amount. For further FEA analysis, this modeling strategy is used for simulation efforts. By determining these main parameters with preliminary FEA analysis, the final FEA models are prepared to provide the simulation data to compare with experimental studies. In that step, some fine-tuning is also performed to improve the simulation models. These were explained in the followings:

- Minimization of the noise in predicted force data. For this goal, two actions are taken: (i) the die and punch sets are modeled in Marc software instead of importing the $*.igs$ data (ii) $segment-to-segment$ contact approach is used instead of node-to-segment contact type. Fig.3.12 is created for the comparison of the results.

- Some benchmark study is done for the friction model used in numerical analysis

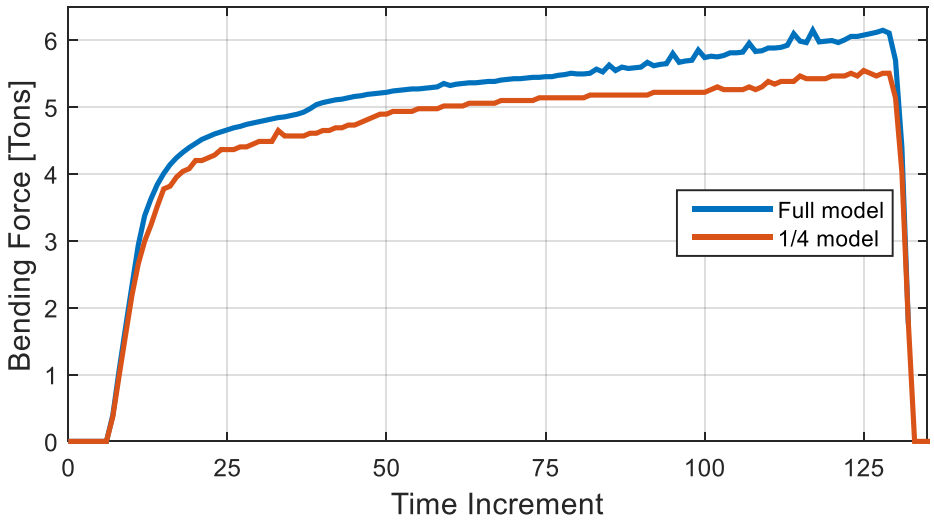

Figure 3.10: Bending force comparison in symmetrical modeling

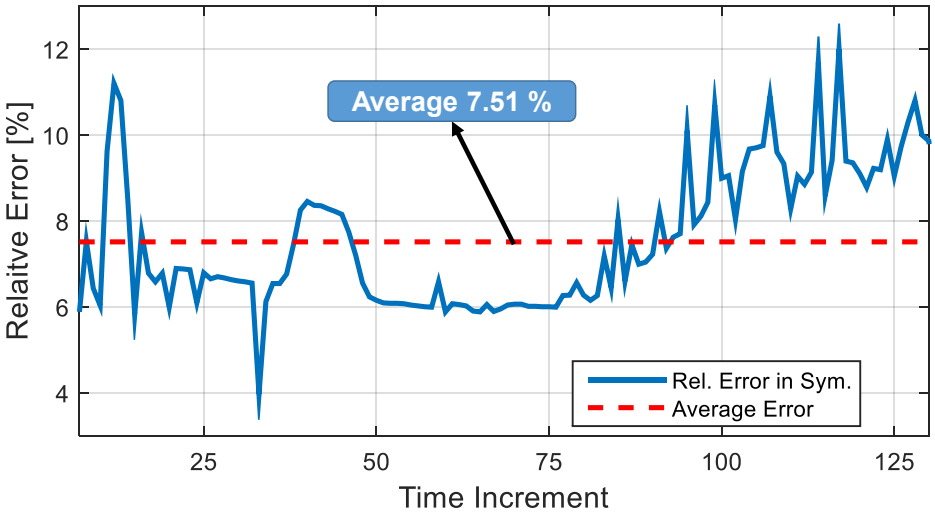

Figure 3.11: Relative error of bending force in symmetrical modeling

and moreover, the effect of friction coefficient is investigated.

As explained previously, symmetry boundary conditions are engaged for FEA models . Furthermore, gravity load is defined for all of the nodes as another boundary condition. And finally, the displacement of the punch is defined as y-position vs. time data into the Marc software. The punch and die sets are assumed to be rigid body in simulations. In other words, only the plates are modeled as deformable bodies in FEA models.

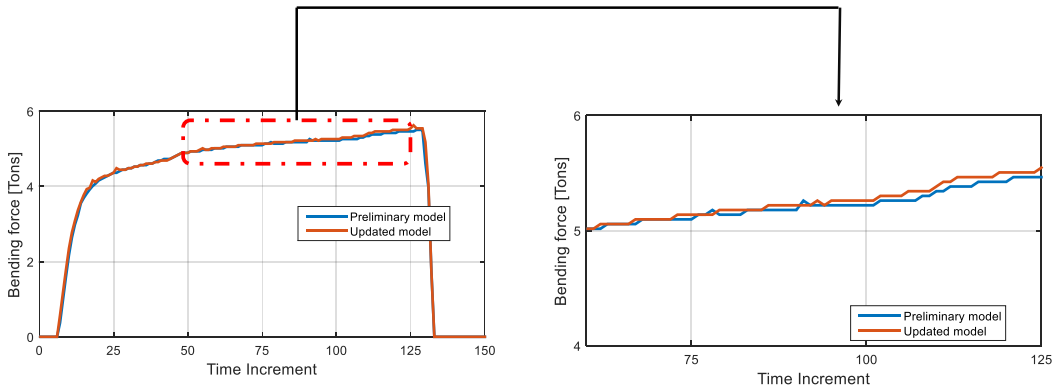

Figure 3.12: Updated FEA models vs. preliminary model

By means of this advanced FEA models, UHSS plate bending operations could be simulated. Fig.3.13 and Fig.3.14 are prepared to illustrate the experimental set-up and FEA model concurrently.

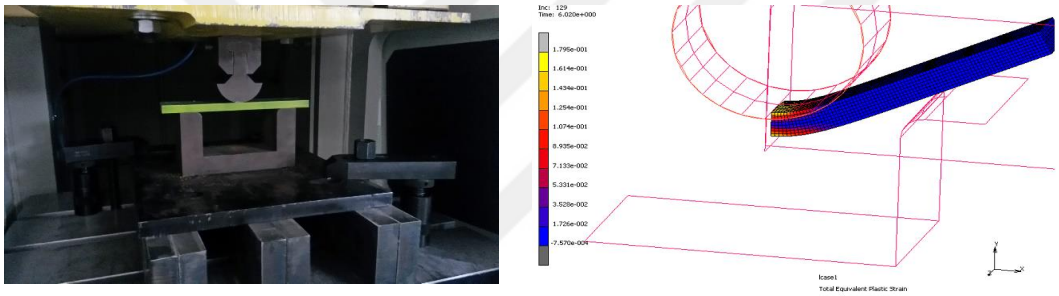

Figure 3.13: Experimental set-up and FEA model of Armor Steel-1

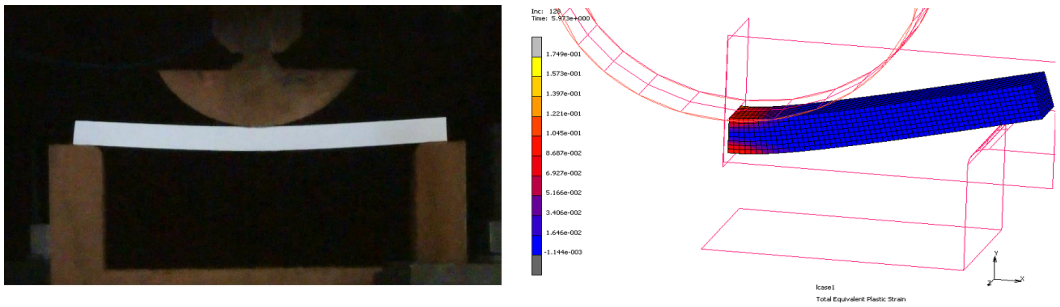

Figure 3.14: Experimental set-up anf FEA model of Armor Steel-2

By means of this FEA models, bending forces are also predicted for the whole stroke profile. The predicted bending forces with respect to the time increments are shown in Fig.3.15. As previously discussed, this result is the prediction of the fine-tuned FEA models. Thus, mathematical models of dies are engaged and surface to surface

contact modeling is valid. Furthermore, this bending operations is performed for a total of $30\,mm$ stroke.

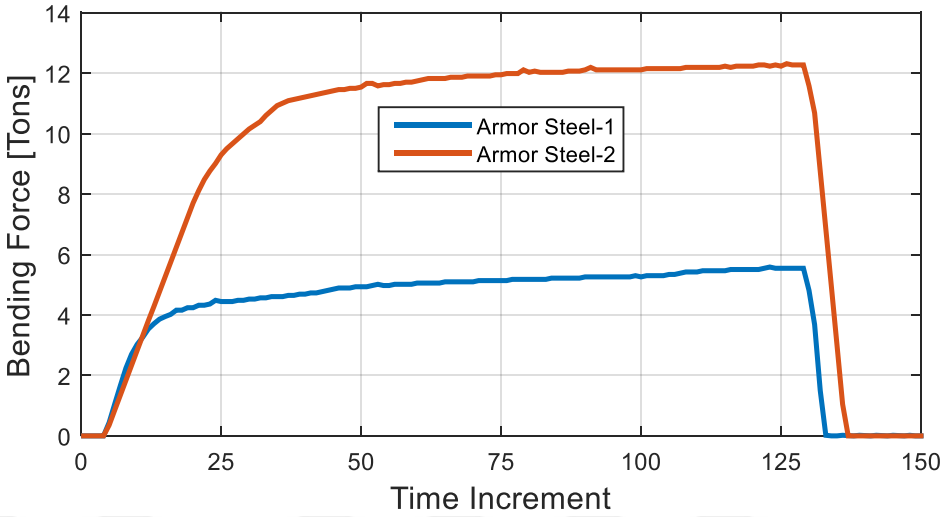

Figure 3.15: Predicted bending force for Armor Steel-1 and Armor Steel-2

Armor Steel-1 has $12\,mm$ thickness whereas Armor Steel-2 has a $20\,mm$ thickness. The average mechanical properties of these steels are listed in Table2.2 previously. When the higher yield stress and thickness of Armor Steel-2 are taken into account, the difference between the predicted bending forces are found to be reasonable.

In this step, a benchmark study is also performed for the coefficient of friction (cof). Predicted bending force are re-computed according to different cof starting from 0.10, 0.15 and 0.20 respectively. The results are designated in Fig3.16. By implementing different cof and friction models into FEA, bending force is changed max 4.5% which is found to be negligible. However, at this point, it could be stated that the Coulomb bilinear friction model predicts higher bending forces than that of shear bilinear model. This finding is reasonable since in the contact zones of the dies (radius zones), the contact pressure may reach high values which can lead to prediction of high fictitious friction forces. Nevertheless, this over-assumption resulted in max of 4.5% bending force. Then, to be more conservative, it would be proper to use

Coulomb friction model by taking into account that the high contact pressure can only be achieved in a very specific zone for the whole FEA model. By means of these assumptions, Coulomb bilinear friction model was decided to be used with a cof of 0.15 for the further analysis.

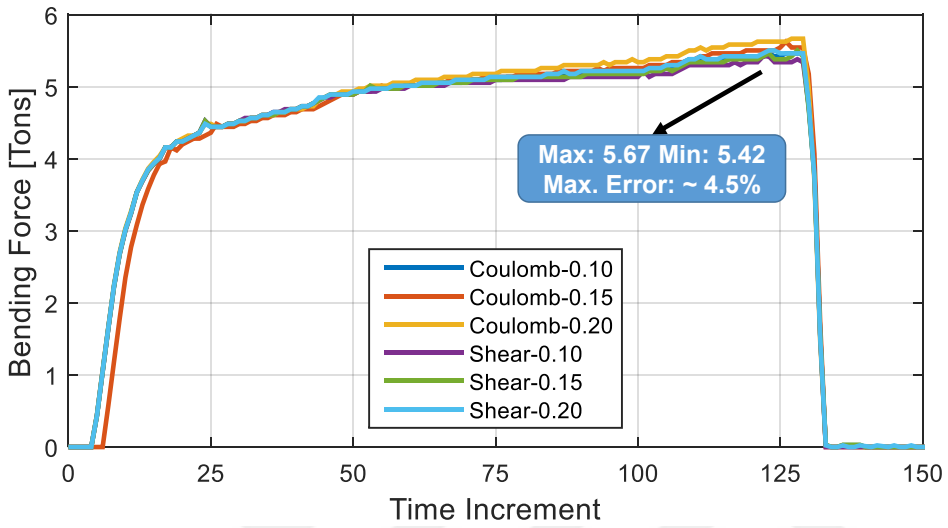

Figure 3.16: A comparison of cof and friction modeling wrt predicted bending force

Thanks to the flexible structure of Marc software, punch position or velocity data can be altered very easily so that some incremental bending simulations is quickly performed with different theoretical stroke profiles (see Fig.3.17).

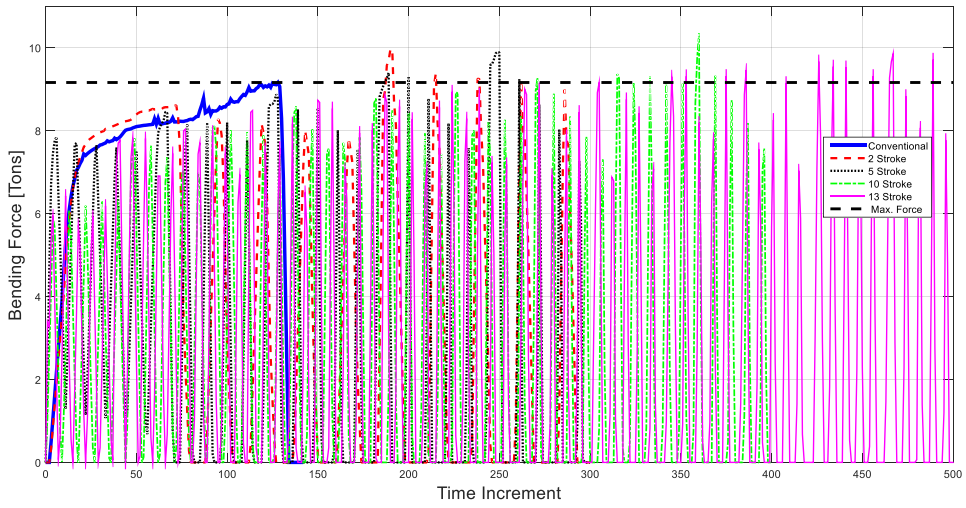

Figure 3.17: A comparison for different increments in bending force of Armor Steel-1

These efforts exhibit important results regarding the tool-path design strategy. Some

geometry changes in punch orientation are also studied in Marc software. An example from these efforts is shown in Fig.3.18 and Fig.3.19.

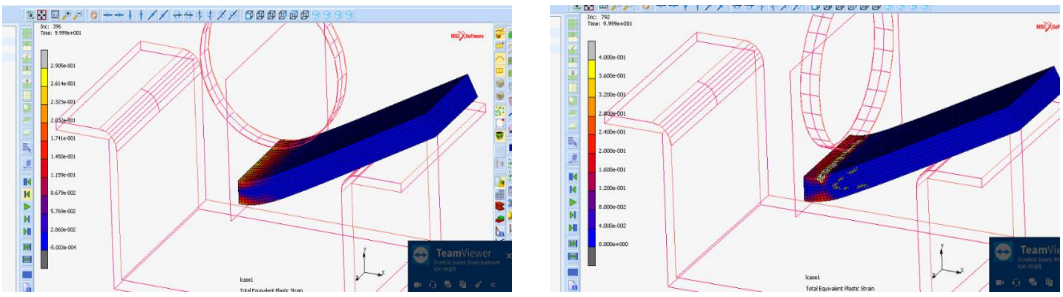

Figure 3.18: Marc models of different punch orientations

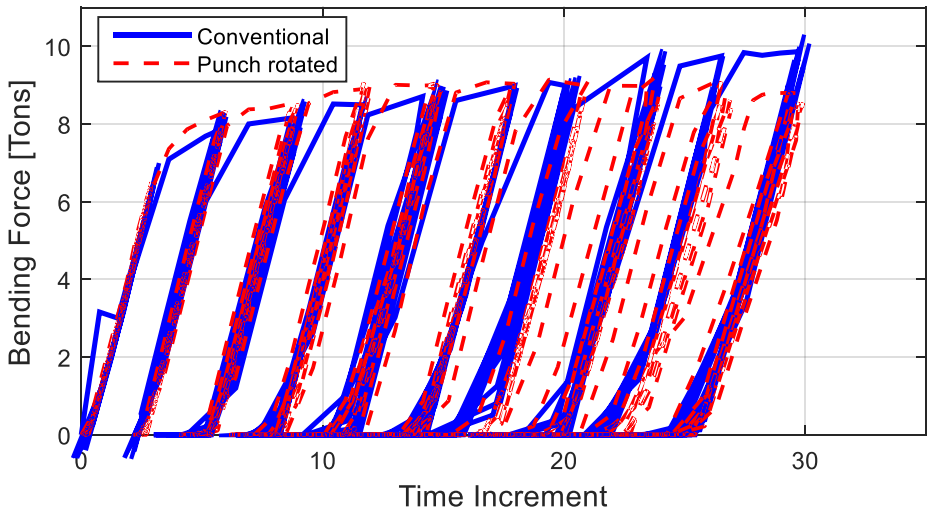

Figure 3.19: A comparison for punch orientation in bending force of Armor Steel-1

As a last step, in order to verify the monotonic loading condition, a specific analysis is performed. To do this observation, the nodes which are designated in Fig5.24 are analyzed during the bending operation.The first component (σ_{11}) of Cauchy stress tensor (CST) is plotted versus the time increment. As expected, the stresses are occurred in a constant tensile and compressive trend which implies that the monotonic loading is the case for the modeled plate bending operation. The detailed plot is illustrated in Fig.3.21. When the global coordinate system is investigated, it can be realized that σ_x is the major direction where the tensile and compressive strains are present.

Thus, the approach which is described in Chapter 2 is proved to be an optimum and

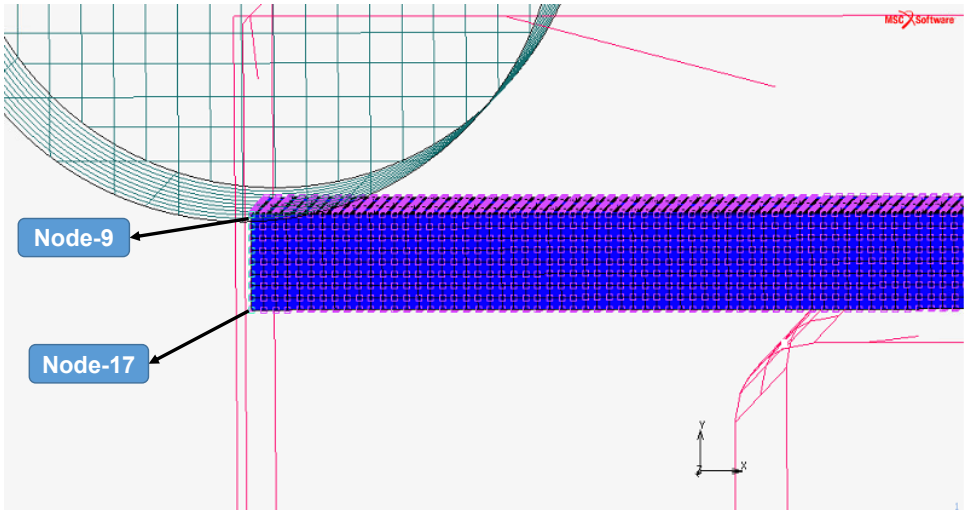

Figure 3.20: Designation of the nomination of nodes in the next figure

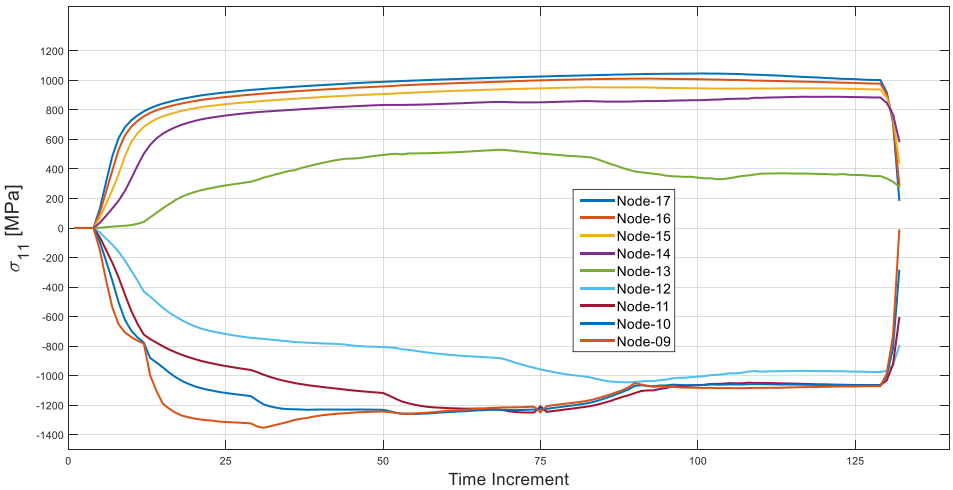

Figure 3.21: Evolution of 1st component of CST during bending for the designated nodes

proper assumption. In other words, since the plate bending operations is a deeply monotonic loading case, the isotropic hardening behavior approach is a reasonable assumption for this specific operation.

3.4 Determination of Spring-back from FEA Results

The bending force is computed through Marc software straight-forwardly. The sofware can compute the force on the punch in y-axis so that this data could easily be plotted

with respect to any scalar value like time increment, position of the punch and etc. However the calculation of the spring-back from FEA data needs some more complicated methods. For that purpose, a special $MatLab$ script is created. This script imports the coordinates of the nodes and makes necessary filtering and curve-fitting operations to determine the angles. The benefit of the code is that when the BDC (bottom dead center) data is imported, the spring-back can be calculated with respect to the actual case. For better explanation of the $MatLab$ script, Fig.3.22 is created by defining the synoptics of the calculation process.

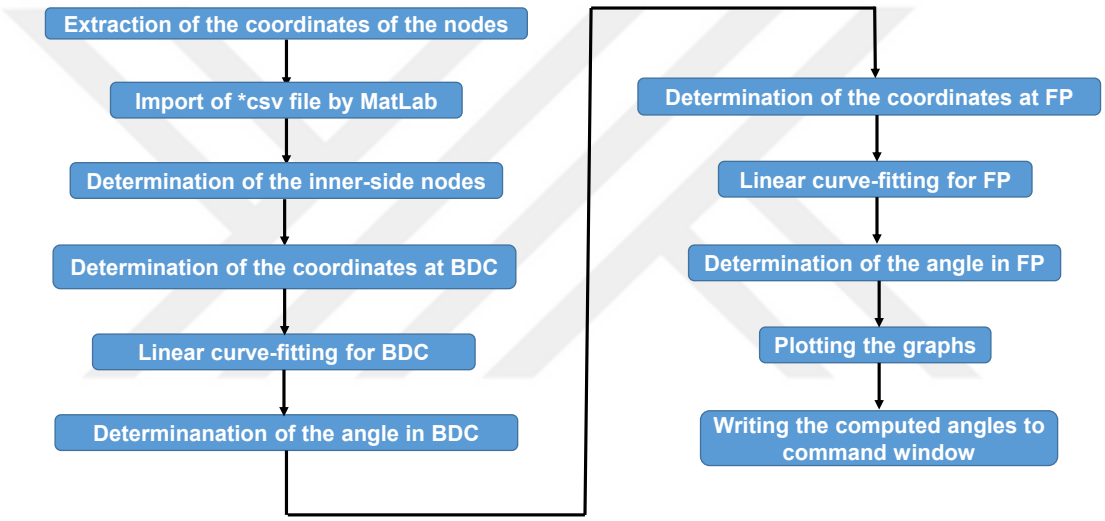

Figure 3.22: Synoptics of the $MatLab$ script which is created for spring-back calculation

The import of the script is the node data list which is extracted from Marc software. More specifically, the coordinates of the nodes in pre-determined time increments are extracted from the software. As a first step of the process, the scripts detects the inner-side of the nodes by evaluating the y-coordinates. For that operation, a threshold value is defined by the user so that the nodes which have y-coordinates higher than the threshold value are pre-selected. An example analysis of the script is shown in Fig.3.23. In this analysis, the angles are calculated with line fitting operation

in $MatLab$ as previously explained.

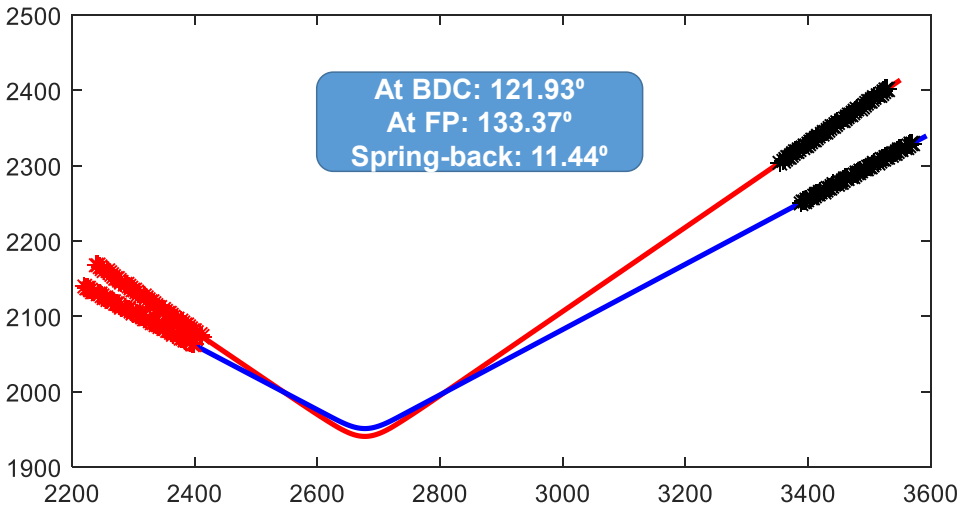

Figure 3.23: Output of the $MatLab$ script which is created for spring-back calculation

CHAPTER 4

EXPERIMENTAL STUDIES

First lot bending experiments are performed at 80 Ton servo-press which is located at MFCE. Within the first lot bending experiments, UHSS plates are bent with respect to the conventional (one-stroke) and incremental bending conditions. Data of the experiments are collected by the acquisition system of the servo-press and the operations are recorded by digital camera. The description of the experimental set-up for the servo-press is shown in Fig.4.1. Before proceeding any further, some information will be given in the following section regarding servo-presses.

(a) (b)

Figure 4.1: **(a)** Experimental die set **(b)** Set-up for image record

4.1 Brief Information on Servo-presses

Servo motors have been used in machine tools since 1950's. However, they were not powerful enough to generate forces required in a forming press. Today, a servo press can be built in 5 different ways:

- A servo-hydraulic press may have conventional motor and the motion can be controlled using a set of proportional (servo-hydraulic) valves.

- Another way to build a servo-hydraulic press uses at least two servo motors (for descending and return motions) and simple gear pumps.

- The first servo-mechanical press was built by Komatsu in 1997 and had a ball screw drive powered by a low torque high rpm servo motor [53]. These presses are available up to $1000\,ton$ force.

- With the improvements in servo motor technology, low rpm high torque motors have become available. The fourth method is to use crank, eccentric or knuckle joint mechanisms without a flywheel but a high torque servo motor. This is the most common servo press type. Since its inception, more than 1000 of these presses are built. Currently, servo-presses over $2500\,ton$ presses are available [54].

- The last method is to use linear motors. These are currently used in tensile test machines and micro forming operations. Servo-presses up to 10 ton forces are available since 2014 [55, 24].

4.2 Experimental Set-up of Bending of UHSS Plates

In this study, a Komatsu H1F-80 OS type servo press is used. The press has a knuckle joint like mechanism with nearly $135\,mm$ stroke. At full speed, it was possible to achieve $37.5\,spm$ (stroke per minute), however, the bending experiments are done in low speed profile as the case of industrial operations. The press is equipped with a linear displacement sensor on the slide, a digital encoder on the crank and two load cells located on two uprights. The maximum capacity of the press is $80\,tons$. Notwithstanding, if either of the uprights is loaded over $440\,kN$, the overload protection will be activated. Data acquisition was carried out by using Komatsu's Visual Inspection System v2.2.2.0. By means of this specific system, the data of the experiments are recorded by $*.csv$ file. The $*.csv$ files contain the data of force, crank position, crank angle, speed, slide position and etc. An example of a result file is shown in Fig.4.2.

No.	Shaft Angle	Crank Angle	Left Load	Right Load	Total Load	Slide Position
	(degree)	(degree)	(kN)	(kN)	(kN)	mm
1	323	0.4	0	0	0	132.562
2	323	0.4	0	0	0	132.562
3	323	0.4	0	0	0	132.562
4	323	0.4	0	0	0	132.562
5	323	0.4	0	0	0	132.562
6	323	0.4	0	0	0	132.562
7	323	0.4	0	0	0	132.562
8	323	0.4	0	0	0	132.562
9	323	0.4	0	0	0	132.562

Figure 4.2: An example of recorded files of the servo-press

This file is processed to obtain the force versus stroke profile of the specific experiments. An example of the experimental force versus stroke profile of Armor Steel-1 (RD) is shown in Fig.4.3.

This data is crucial since it provides an extremely powerful tool for the comparison

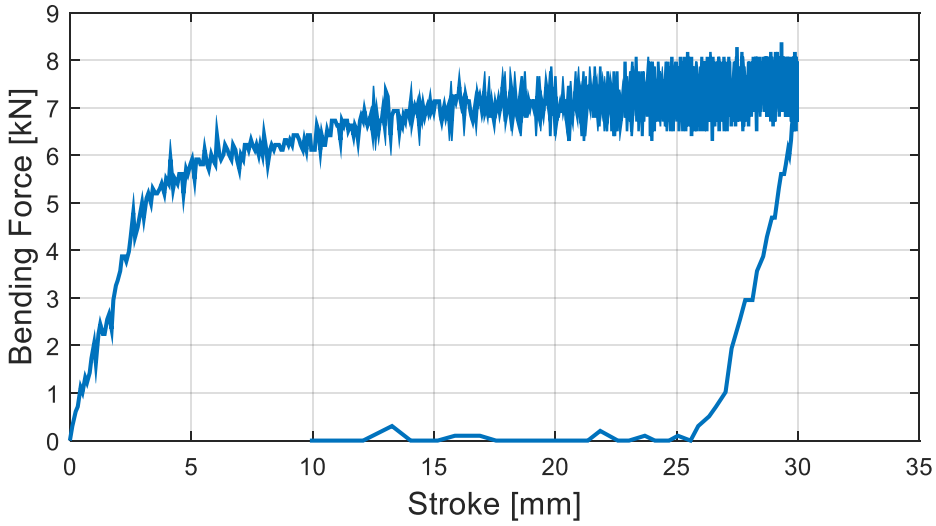

Figure 4.3: Experimental stoke vs. bending force graph of Armor Steel-1 (RD)

of FEA models and experiments. Hence, it serves as a powerful calibration tool.

For the experimental studies, several die and punch sets are designed and manufactured as can be seen in Fig.4.4. When the tools are designed, the real manufacturing conditions are taken into account so as to provide a set-up which is similar to the real workshop application.

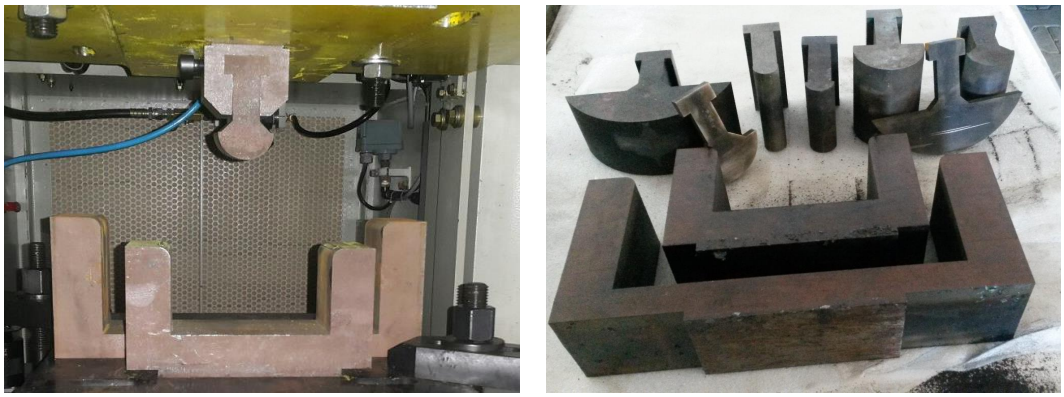
Figure 4.4: Die and punch sets designed and manufactured for the experimental studies

Thanks to the CNC infrastructure of the servo-press, the stroke increments can be adjusted with a high precision level. For each onset of the angular step, the stroke is changed as intended with the help of the control panel. And finally, the linear step is

Table 4.1: Experimental Design of the UHSS bending operations

	Plate Dimensions (mm)	Total Stroke (mm)	Total Feed (mm)	Increments in Stroke	Increments in Feed
Conventional Bending					
TMCP-1 Steel	$10 * 50 * 250$	60.8	-	-	-
Armor Steel-1	$12 * 50 * 250$	30	-	-	-
Armor Steel-2	$20 * 50 * 350$	30	-	-	-
1st Lot Incr. Bending					
Armor Steel-1	$12 * 50 * 250$	30	50	14	5
Armor Steel-2	$20 * 50 * 350$	30	50	14	5
2nd Lot Incr. Bending					
Armor Steel-1	$12 * 350 * 350$	21	160	3	9
Armor Steel-1	$12 * 350 * 350$	21	160	5	9

assured by the use of a digital caliper. The displacement of UHSS plates are applied manually with a digital caliper.

However, for the second lot incremental bending experiments, where UHSS Plates with dimensional size $12 * 350 * 350\,mm$ are bent, the displacements are performed with the help of a tape measure. Fig.4.5 is created to describe the methodology.

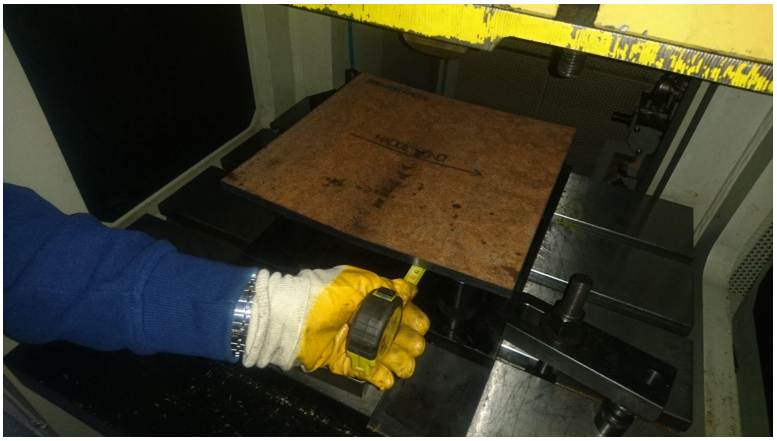

Figure 4.5: Adjustment of the linear feed in 2nd lot incremental bending experiments

To sum up, Table4.1 is constructed in order to describe the experimental design for each UHSS plate respectively.

4.3 Optical Scanning Studies

The bent plates are investigated by optical scanning techniques in order to detect any possible difference between conventional (RD and TD) and incremental bending processes (RD Inc. and TD Inc.). This investigation is carried out for RD and TD samples aiming to provide a topological data. The set-up of the optical scanning system is illustrated in Fig.4.6.

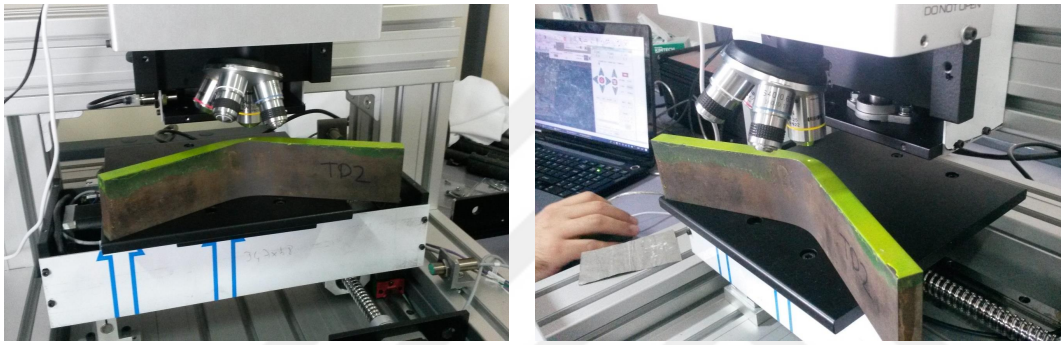

Figure 4.6: Optical scanning set-up of bent specimens

More particularly, surface profile measurements were made with the PSARON 1000 metallurgical microscope analysis system. Pre-determined areas are raster-scanned to obtain three-dimensional surface profiles. Depth measurement accuracy is $0.2\,micrometer$ and height differences up to $100\,mm$ can be optically measured with this system, in which the microscope objective is precisely moved in the axial direction (1 micron movement accuracy) at a specified surface point. And the depth corresponding to the best focus plane is determined by examining the image data acquired by the microscope camera.

On each of the plates (TD, TD Inc., RD, and RD Inc.), $8 * 10\,mm$ square areas are determined in the same region of the plates, and raster scanning is performed by a $1mm$ lateral movement (in x-y direction) to obtain the depth profile. Fig.4.7 shows

the surface profiles of the TD and TD Inc , while Fig.4.8 shows the surface profiles of the RD and RD Inc. specimens.

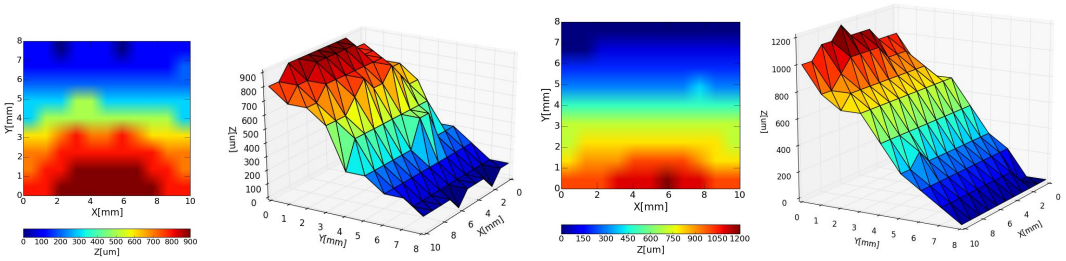

(a) (b)

Figure 4.7: **(a)** Optical scanning result of TD sample **(b)** Optical scanning result of TD Inc. samples

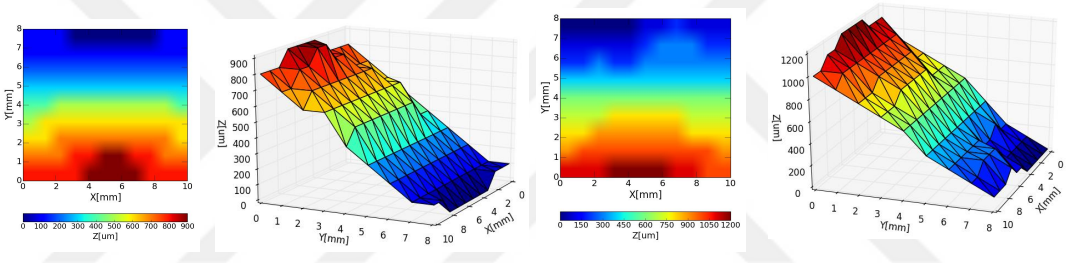

(a) (b)

Figure 4.8: **(a)** Optical scanning result of RD sample **(b)** Optical scanning result of RD Inc. samples

The profiles are shown both in two dimensions with the color-coded depth and in 3D. For each plate, the depth values (z) were averaged over the x-direction. The depth as a function of the distance y is delineated. The result of this analysis is displayed in Fig.4.9 in order to explain the depth profile difference between conventionally and incrementally bent specimens more clearly. When Fig.4.9 is investigated, it could be stated that the incrementally bent specimens show a similar behavior in RD and TD direction such that the z component of the strain tensor is bigger than that of conventionally bent specimens. However, this specific region where the equivalent

strain is bigger, is limited to the upper-most section. And the Δz value converges to zero along to symmetry axis through the transition to compression compression zone to tension zone.

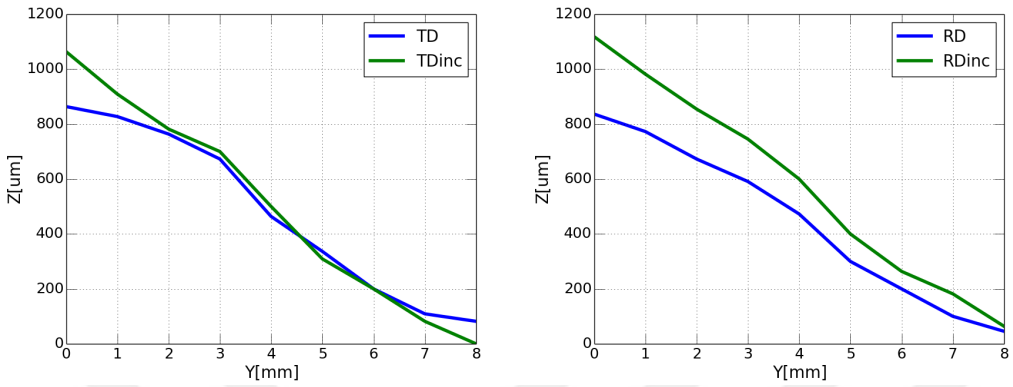

Figure 4.9: Averaged depth evaluation in y direction of the bent specimens

CHAPTER 5

RESULTS AND DISCUSSION

5.1 Analysis of the Prediction of Bending Forces in Conventional Bending Process

As described in Chapter 4, the experimental studies are conducted in 80T Komatsu servo-press by means of which the bending forces can be recorded. Initially, the conventional bending operations are analyzed, i.e. the experimental values are compared with the prediction of the FEA models. The first analysis regarding the TCMP Steel-1 is given in Fig.5.1.

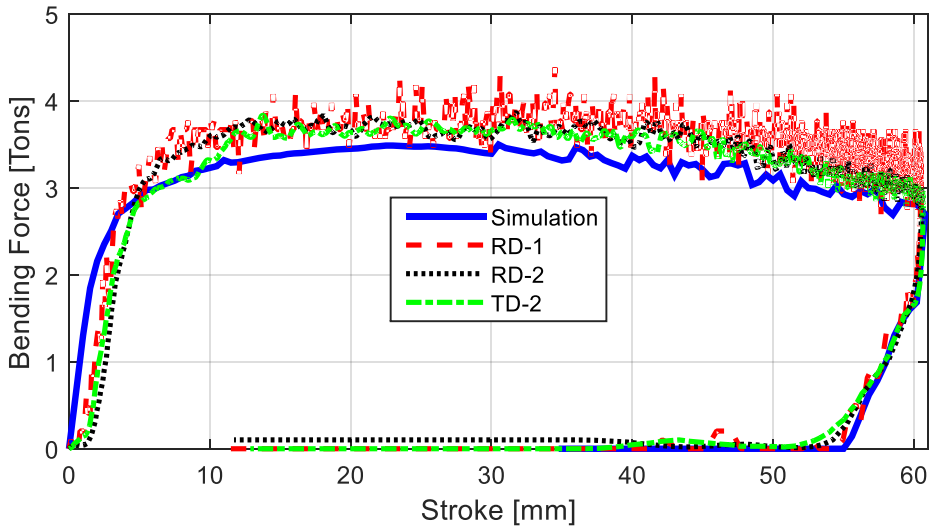

Figure 5.1: Comparison of experimental and simulation data for TCMP Steel-1

In this figure one can detect two problems:

- Firstly, there is relatively high noise in experimental data. This could be a result of the very low tonnage compared to the full capacity of the servo-press. As expected, the data resolution of servo-press decreases when the force in significantly low ($\leq \%10$ nominal capacity).
- Secondly, there is also some noise in experimental data which may be caused by the high stroke value applied in the operation. For bending of TCMP Steel-1, a stroke of $60\,mm$ is applied where the contact conditions are fairly forced. For this reason, it is found to be reasonable

For the solution of these problem, data filtering is applied in $MatLab$ software. The resulting graph exists in Fig.5.2.

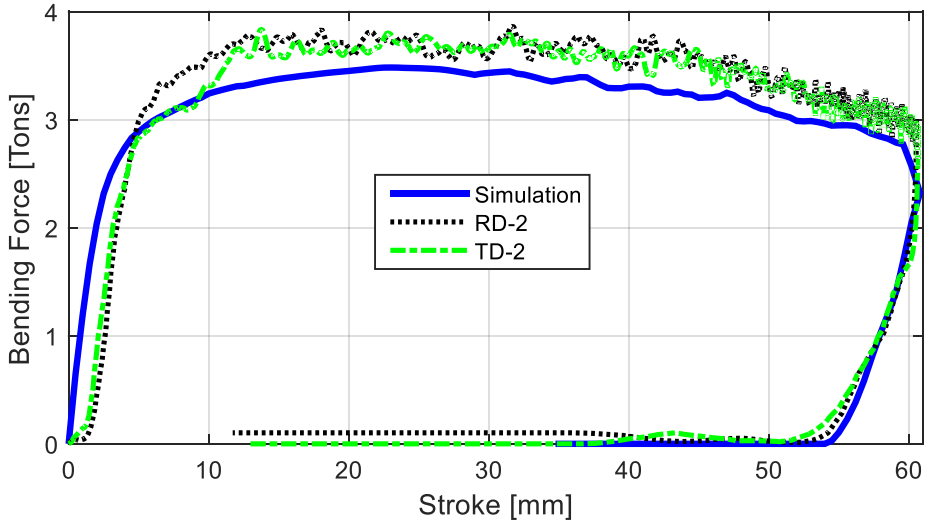

Figure 5.2: Filtered data for bending of TCMP Steel-1

As it can be observed from Fig.5.2, the Marc simulation under-estimated the bending force with respect to the experimental data. However, it is also observed that the predicted force has a precision which is under 10% relative error as designated in Fig.5.3.

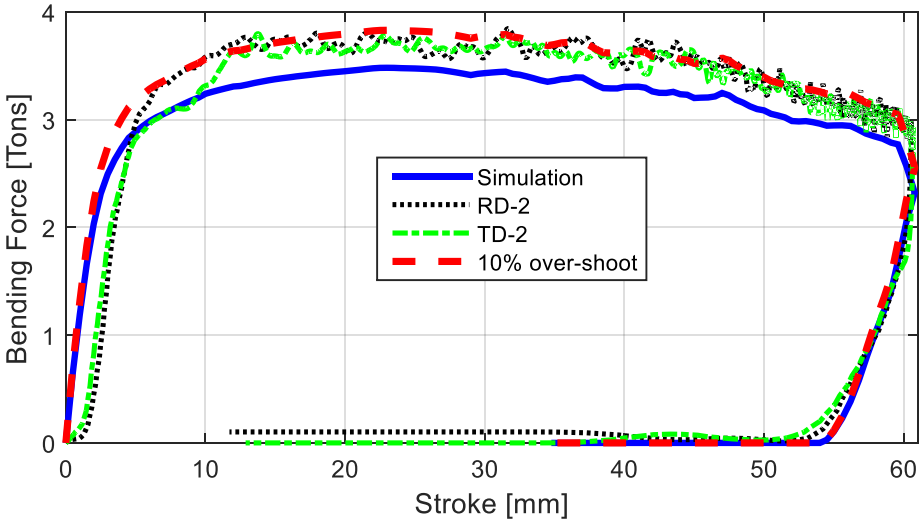

Figure 5.3: Comparison of experimental, simulation and over-shoot data for TCMP Steel-1

The same analysis is performed for Armor Steel-1. The comparison of the experimental and FEA results are illustrated in Fig.5.4.

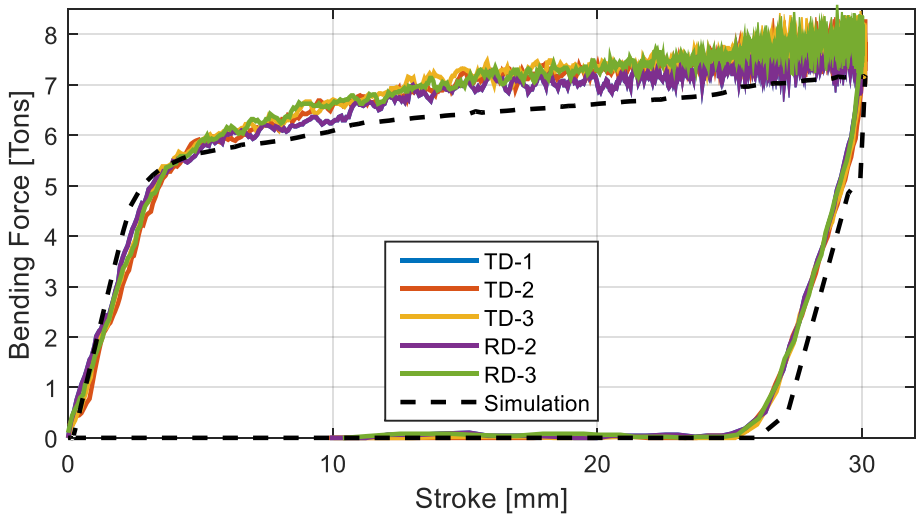

Figure 5.4: Comparison of experimental and simulation data for Armor Steel-1

As in the case for TCMP Steel-1, the FEA analysis made a prediction of bending force which is lower than the experimental data. For further analysis, 10% over-shoot data of the FEA result is plotted to observe the relative difference between the experimental and numeric data. This plot is illustrated in Fig.5.5.

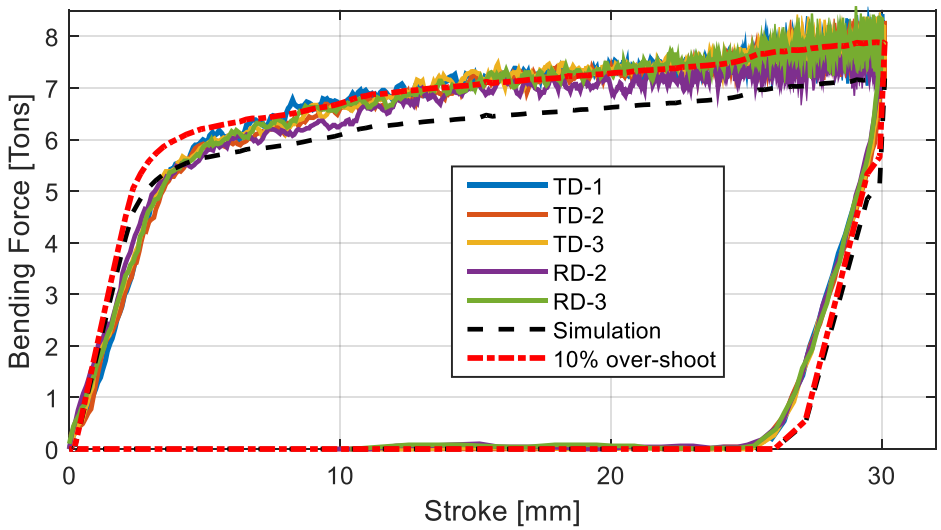

Figure 5.5: Comparison of experimental, simulation and over-shoot data for Armor Steel-1

Following the conventional bending analysis of Armor Steel-1, equivalent comparison is made for Armor Steel-2. The prediction of FEA and the experimental bending forces are plotted in Fig.5.6.

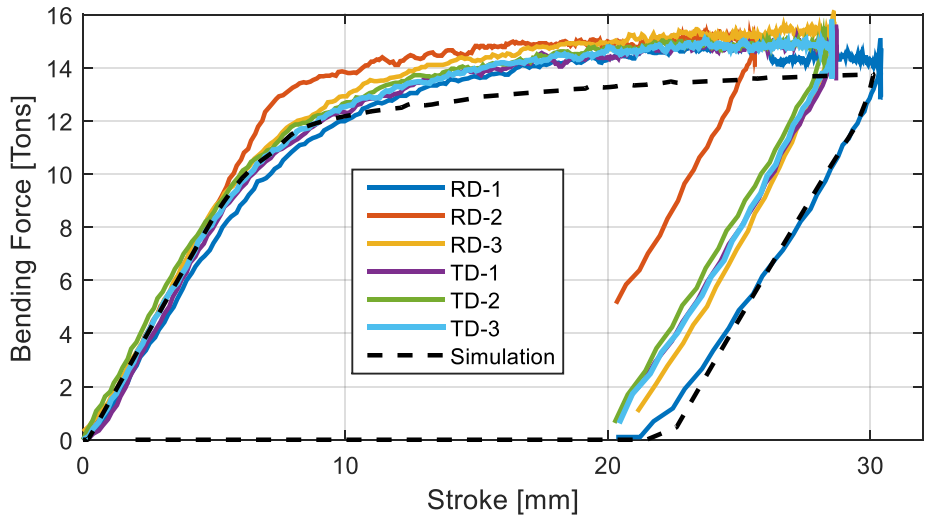

Figure 5.6: Comparison of experimental and simulation data for Armor Steel-2

As in the case for other UHSS plates, the FEA model performed an under-estimation of the bending force compared to the experimental data. For better understanding of the precision level, 10% over-shoot data of the prediction is constructed for Armor

Steel-2 in Fig.5.7.

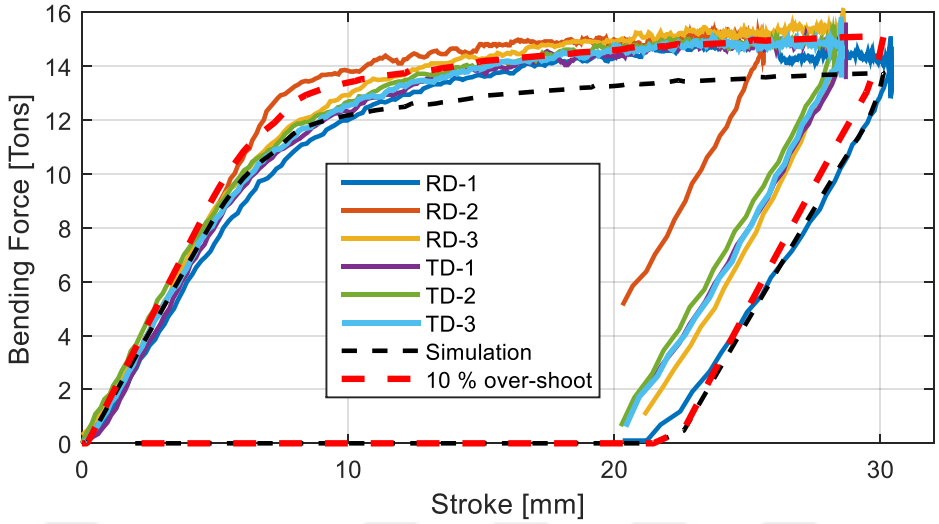

Figure 5.7: Comparison of experimental, simulation and over-shoot data for Armor Steel-2

By means of these efforts, the conventional bending operations of UHSS plates are studied by means of predicting the bending forces. The outputs obtained from this task could be stated as follows:

- For all three types of UHSS plates, the bending forces are under-predicted by Marc software compared to the experimental force data which are obtained from the servo-press.
- It is found to be interesting that for all of the cases, the precision of the numeric results (the amount of the under-estimation) is approximately 10% of the predicted bending force.
- When the uncertainty in the material data, the general assumptions used in contact/friction modeling and the yield surface definition and finally the possible numerical error of the non-linear analysis are considered concurrently, a global error of 10% is accepted as reasonable. It should also be taken into account

that there may also exist some error in the data acquisition system of the servo-press. It should also be noted that the bending force formulation proposed by the steelmaker is declared to have a precision of 20%. Therefore, the conducted FEA models in this project would definitely increase the technical capabilities in the prediction of the necessary forces regarding the bending of UHSS plates.

- Despite the fact that there is an error in the prediction of the bending force, the overall trend of the stroke vs. force data can be caught well enough as explained in 5.8.

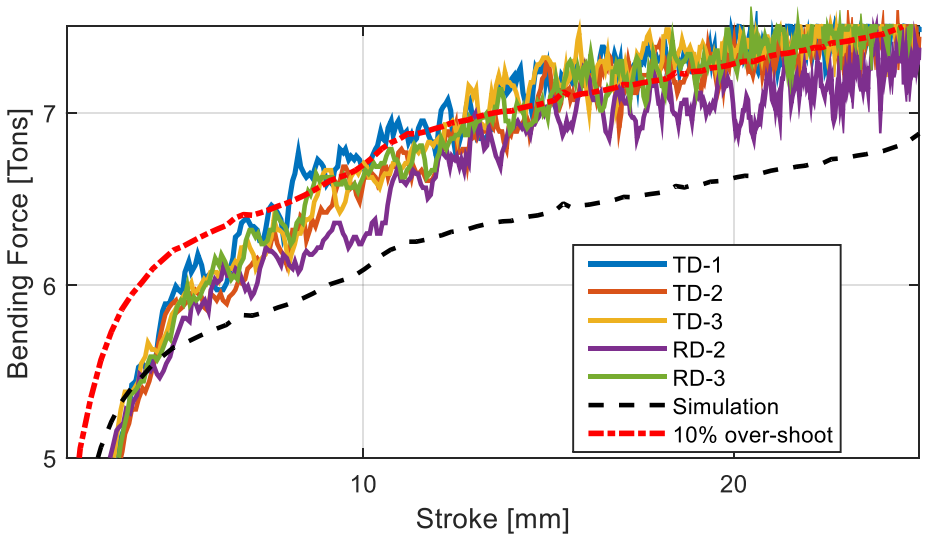

Figure 5.8: Stoke vs. force data of experimental and FEA analysis for Armor Steel-1

5.2 Analysis of the Prediction of Bending Forces in Incremental Bending Process

The incremental bending process is also analyzed with respect to the measured and predicted bending forces. For that purpose, the data acquisition system is all engaged for each incremental bending operation and each data is recorded as a separate $*.csv$ file. For the case of the Armor Steel-2, total 60 bending steps are applied as described

in the Chapter 4. The result is given in Fig.5.9,

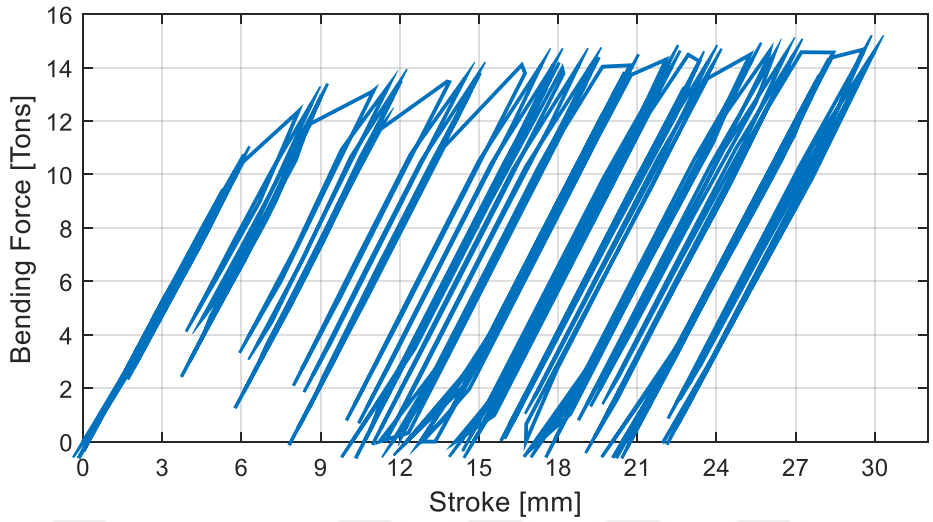

Figure 5.9: Predicted stroke vs. force data for incremental bending of Armor Steel-2

In Fig.5.9, The result of the FEA analysis is designated for the incremental bending of Armor Steel-2. This graph is created for the designation of the stroke vs. bending force data. However, it is observed that the data point set cannot present the extreme points of the stoke profile (tool path) due to the optimum number of time increments. Therefore, it is decided to construct the time increment vs. bending force graph for this numerical analysis aiming to provide a better understanding of the issue as shown in Fig.5.10.

The experimental data is obtained by data processing of the whole set of $*.csv$ file (see Fig.5.11). Regarding this task, a methodology is proposed in such a way that all the max. bending forces are determined for each of the deformation step. By this methodology, the plots which are given in Fig.5.12, Fig.5.13 are created.

In Fig.5.12, the max. bending forces recorded for two specific specimens are designated with the stoke increment data in a more detailed manner. On the other hand, Fig.5.13 is also exposed to assure the better description of the tendency in recorded

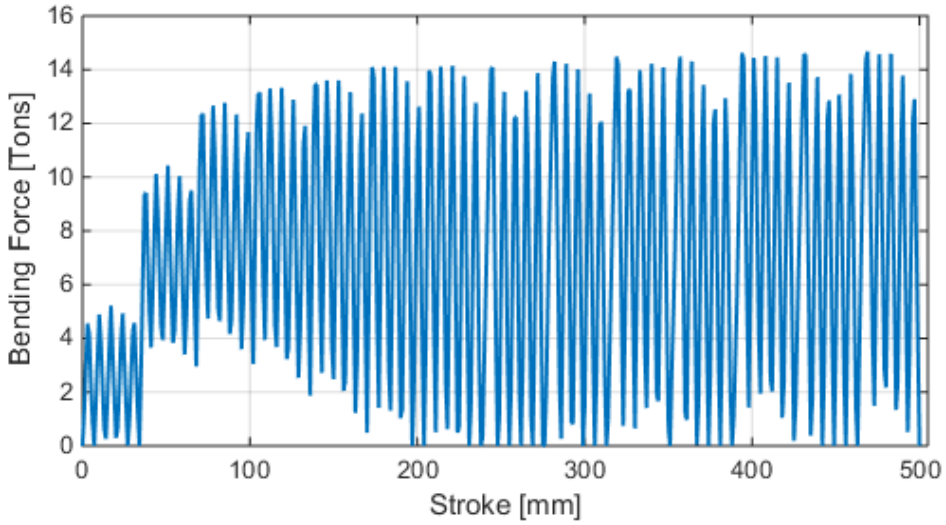

Figure 5.10: Predicted stroke vs. force data for incremental bending of Armor Steel-2

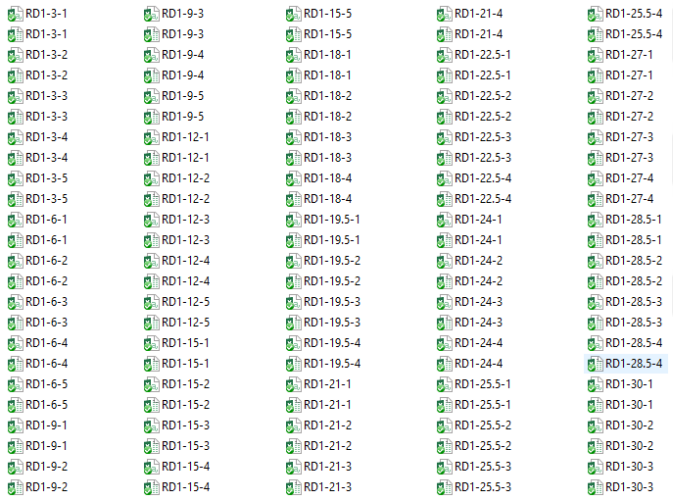

Figure 5.11: File set provided by the servo-press in incremental bending of Armor Steel-2

bending forces. This tendency in the increase of bending force will be analyzed with that of in the conventional bending process in following sections.

As a next step study, the experimental data is directly compared to the FEA results. Related to this comparison, Fig.5.14 is created in a way that the max. experimental bending forces are plotted on the FEA results. Like the cases in the conventional bending analysis, the numerical results made an under-estimation.

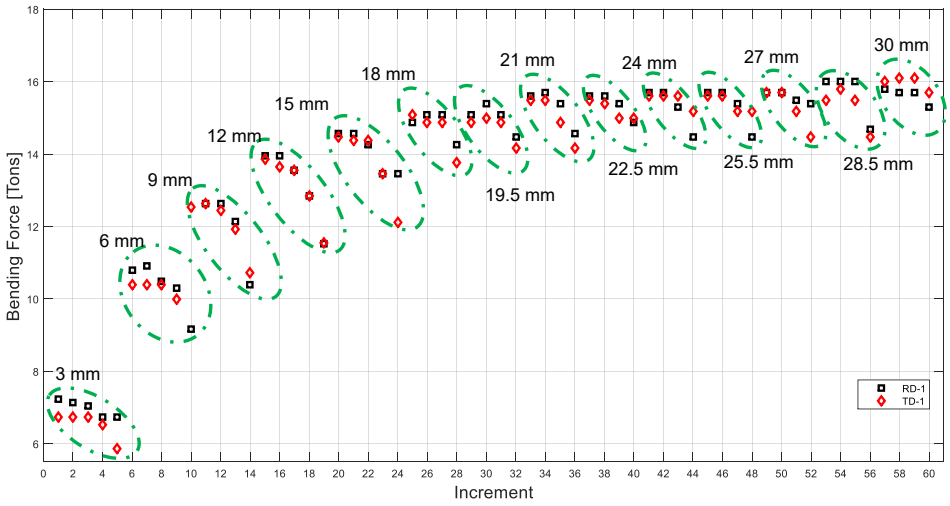

Figure 5.12: Experimental max. bending forces in incremental bending of Armor Steel-2

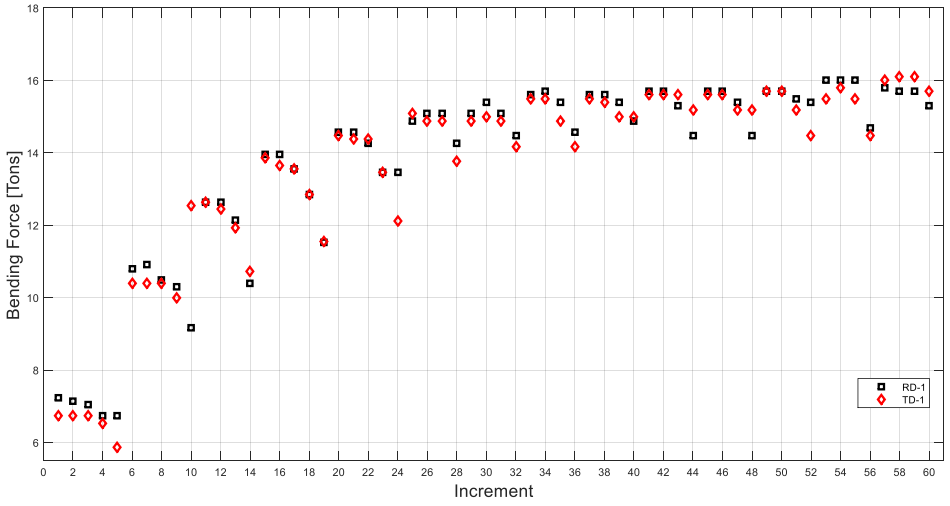

Figure 5.13: Experimental max. bending forces in incremental bending of Armor Steel-2

Therefore, a 10% over-shoot curve is also plotted in Fig.5.15 in order to perform a judgment on the amount of the relative error. Similar to the conventional bending analysis, the incremental bending numeric model showed an under-prediction which is nearly 10% of the numerical estimation.

As an important benchmark between the conventional and the incremental bending of Armor Steel-2, Fig.5.16 is plotted. In this figure, both experimentally obtained

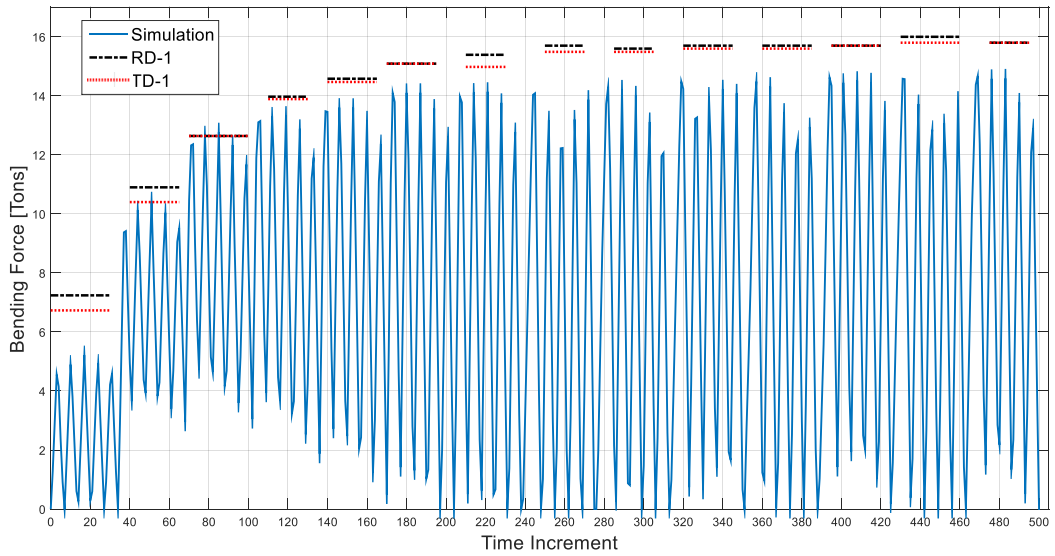

Figure 5.14: Comparison of FEA and experimental data in incremental bending of Armor Steel-2

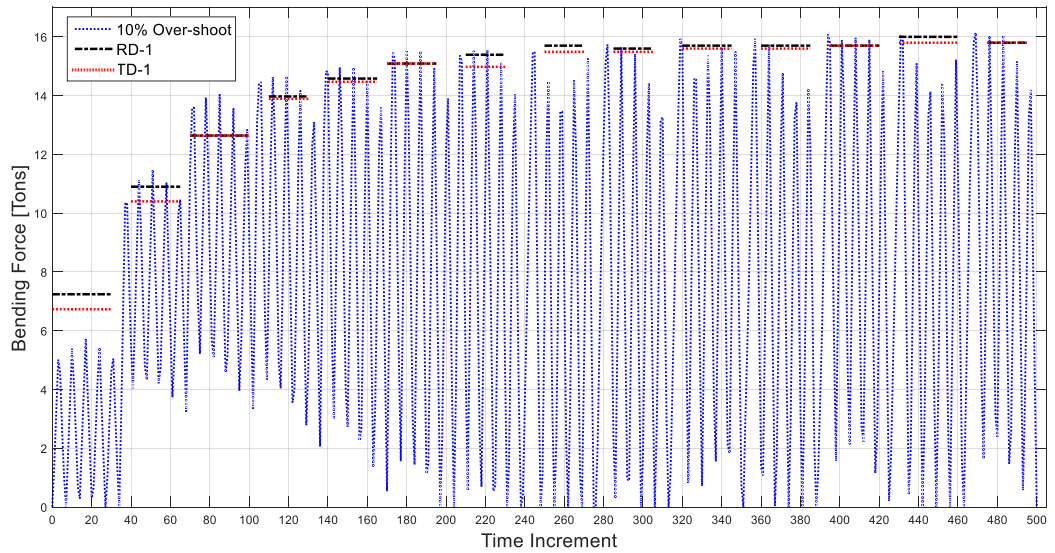

Figure 5.15: Comparison of over-shoot data and experimental data in incremental bending of Armor Steel-2

bending forces could be easily seen and compared.

The outputs obtained from the analysis of the incremental bending process could be stated as follows:

- The bending force for each step (deformation increment) could be predicted

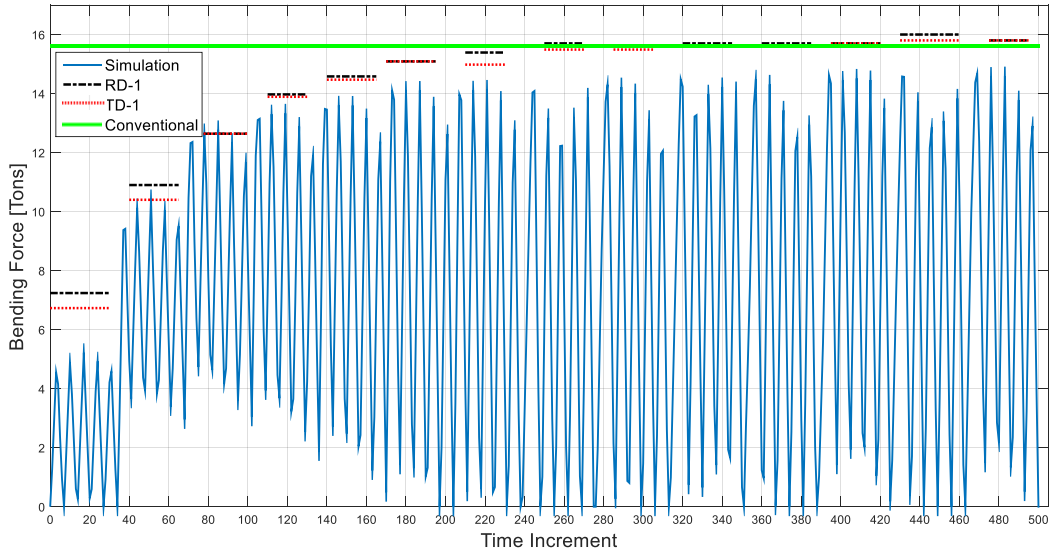

Figure 5.16: Comparison of the conventional and incremental bending in for Armor Steel-2

with nearly 10% relative error. As the case for the conventional bending efforts, this accuracy level can be accepted as reasonable when all of the uncertainty sources are taken into account simultaneously.

- The crucial observation regarding the first lot of incremental bending experiments is that the bending force cannot be decreased for the novel method. On the contrary, the bending force needs to be increased a little bit.

- The basic reason regarding the failure in decreasing the bending force is determined as the insufficient localization of the deformation. From the general point-of-view of incremental forming, the forming force could be decreased if the plastic deformation localized into the vicinity of the contact zone. However, during the first lot of incremental bending experiments, it is observed that the punch which has a length of $10\,mm$ deformed nearly all of the UHSS plate whose length is $50\,mm$ for each increment. Fig.5.17 is created for the description of this specific problem. Normally, this phenomena gives rise to higher

bending forces instead of lowering the necessary tonnage.

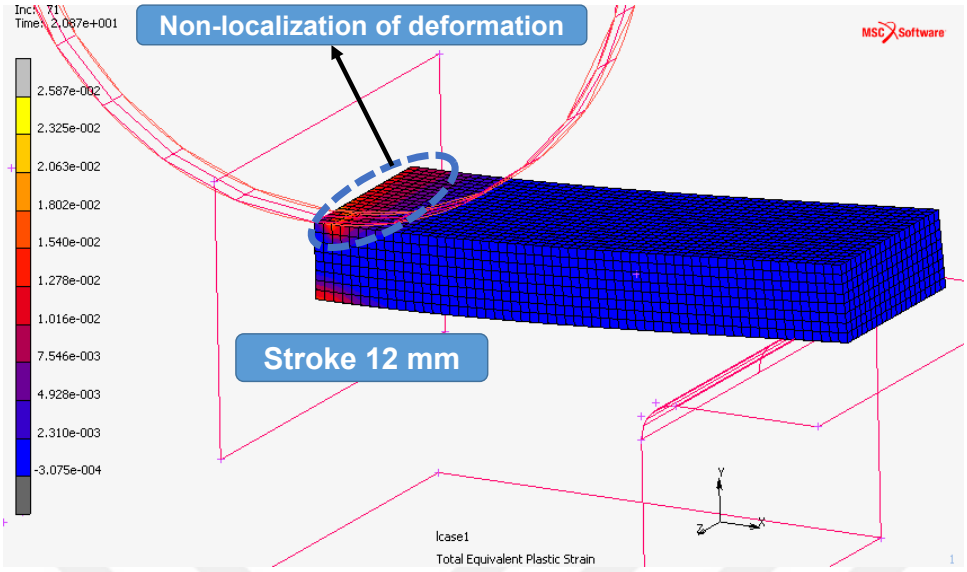

Figure 5.17: Non-localization of the plastic deformation at $12\,mm$ stoke, first increment

- The contact algorithms showed a more problematic behavior compared to conventional bending simulations as accepted. For solution, the time increments are decreased and/or the contact modeling is switched to $node-to-segment$ contact model.

With the guidance of these findings, it is concluded that it is compulsory to localize the deformation in order to yield the benefits of incremental forming process in decreasing the bending force. The possible two ways to satisfy that condition is to (i) decrease the angular step (linear step of the stroke) or (ii) to minimize the punch contact zone. The first solution is not that applicable since the stroke increment is already relatively low in the first lot incremental bending experiments. And any attempt to decrease the stroke increment to values like $0.50\,mm$ is a theoretic approach instead of an industrial one. Thus, it is decided to apply the second solution which is minimizing the contact zone of the punch. However, in this task, the dimensional size

of the UHSS plates are enlarged instead of minimizing the punch dimensions. It is also not an applicable solution to use very small punches in bending operations with presses due to the assembly constraints. Consequently, for the second lot incremental bending operations, a punch with a length of $10\,mm$ is used to process UHSS plates whose dimensions were $350 * 350\,mm$. By means of this strategy, $10/350$ value is assured in deformation zone to overall length ratio which is sufficient in localization of the deformation. This result is proved in first trials with this type of set-up as indicated in Fig.5.18.

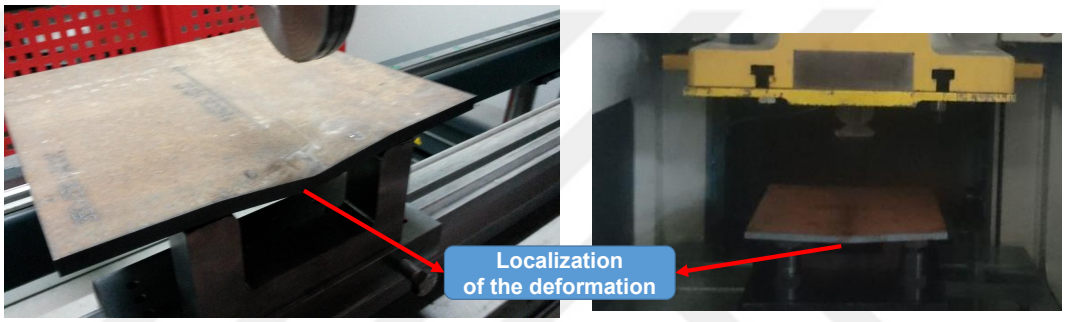

Figure 5.18: Localization of the deformation with new proposed set-up

After the localization of deformations phenomena is detected by preliminary efforts, second lot incremental bending experiment is conducted with Armor Steel-2. Fig.5.19 shows the experimental set-up and FEA model of this specific experiment.

For this bending process, a conventional bending simulation is performed and the max. bending force is computed as 55.56 tons as in Fig.5.20. Concurrently, the data of the second lot incremental bending of Armor Steel-1 is processed and Fig.5.21 is constructed.

Fig.5.22 explains the bending forces provided by the incremental bending experiment. As could be seen, the required bending force is decreased approximately 19% by the incremental bending process which is a promising result. For the direct comparison of

(a) (b)

Figure 5.19: **(a)** Set-up of second lot incremental bending experiment **(b)** FEA analysis model of the equivalent conventional bending process

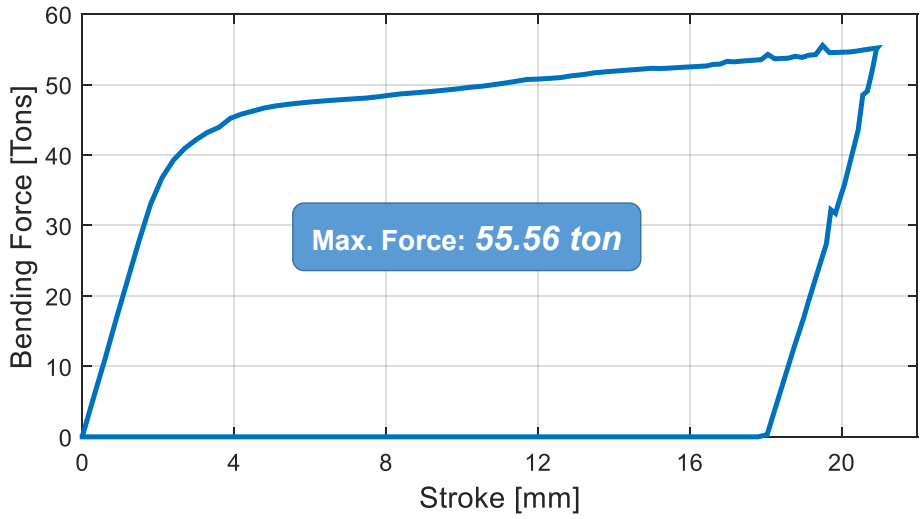

Figure 5.20: Localization of the deformation with the new proposed set-up

the conventional and incremental bending of Armor Steel-1, Fig.5.22 is also created.

As a further step, a new incremental bending experiment is designed and performed for Armor Steel-1. For this experiment, the quantity of the increments is increased to 5 from 3. In a more detailed manner, in the first trial of 2nd lot incremental bending experiment, the stroke values are 9, 15 and 21 mm. However, for the second trial, they are arranged as 9, 12, 15, 18 and 21 mm. By means of this effort, the localization of the plastic deformation was tried to be enhanced. Thus, it is investigated to obtain

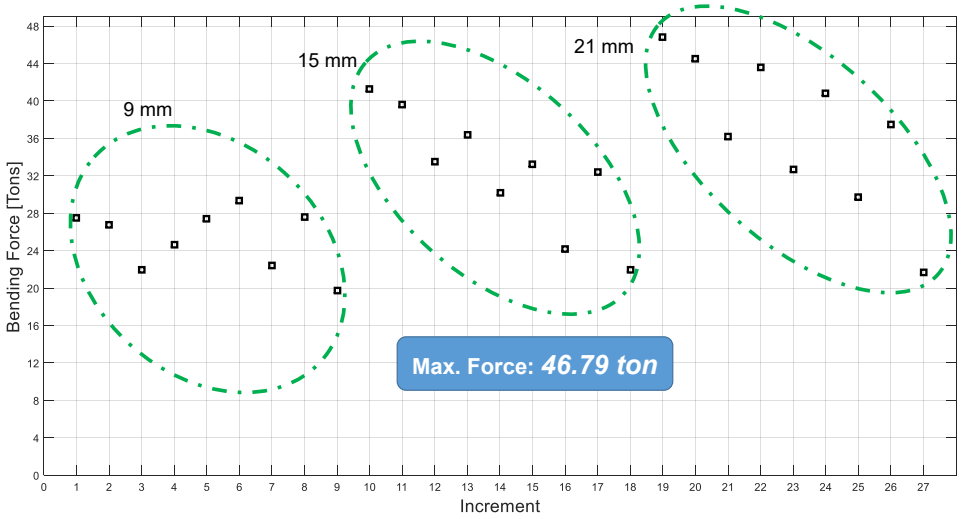

Figure 5.21: Bending force prediction of the conventional bending of the second lot incremental bending operation

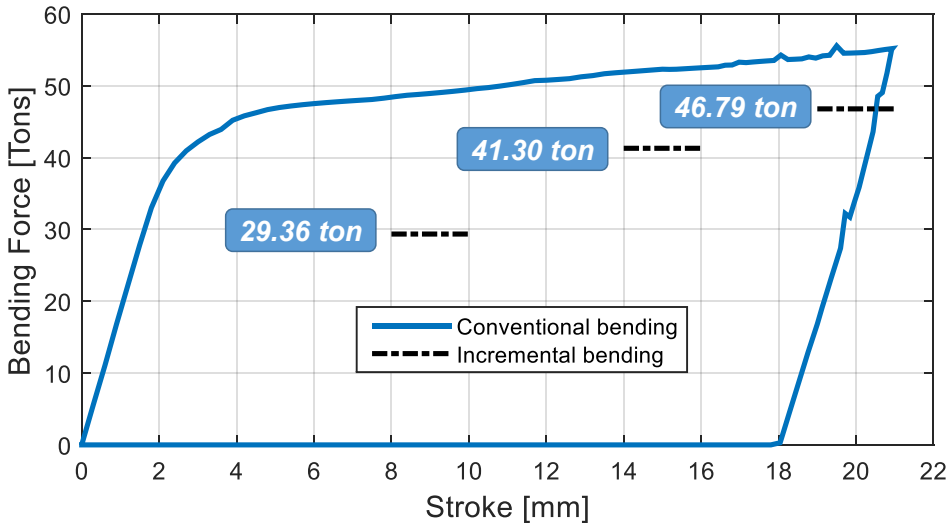

Figure 5.22: Comparison of the second lot incremental bending experiment with the theoretical conventional bending

a bigger reduction in bending force. The results are shown in Fig.5.23. Certainly, Fig.5.23 reveals that the bending force could be decreased much more with smaller increments or more localized deformations. The incremental bending with 5 angular steps produce nearly 26% reduction in bending force. For the conventional bending case, the bending force was $55.56\,tons$ whereas it was $40.97\,tons$ for the final-5 step incremental bending experiment .

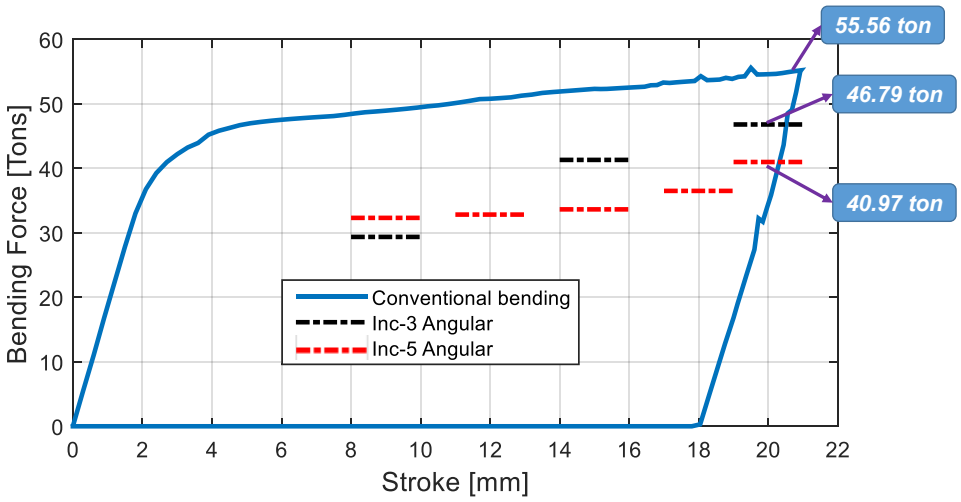

Figure 5.23: Comparison of the all second lot incremental bending experiments with the theoretical conventional bending.

The outputs obtained from the analysis of the second lot incremental bending process could be specified as follows:

- The bending force could be decreased by the localization of the plastic deformation as expected.
- The localization of deformation can be achieved by minimizing the angular step (which is generated by the increment of the stroke profile) or the linear step (which is generated by the feed of UHSS plate). However, the minimization of the contact area of punch or increasing the dimensional sizes of UHSS plates by keeping the same punch geometry can also be other alternatives.
- The forces which occur during the incremental bending operations could be predicted with a reasonable precision level. This achievement enables the design alternative process according to the max. bending force available with the present machine park of a workshop.
- With the help of new FEA models, the bending force could be tuned and more-

over one can optimize the bending force and cycle time of the operation by means of benchmarking among proposed simulations.

- The FEA models also enables the break-even point for incremental bending process. In other words, the max. achievable decrease of the studied bending operation may be determined by simulation efforts.

5.3 Anaylsis of the Prediction of Bending Angles

As explained in the Chapter 3, the bending angles at BDC and the final position are calculated by a specifically created $MatLab$ code. The main input of this code is the node coordinates which are extracted from Marc software. By means of this method, the angles are computed for Armor Steel-1 and Armor Steel-2 which are bent with conventional and incremental bending processes. In order to provide a schematic description, Fig..5.24, Fig.5.25 and Fig.5.27 are constructed.

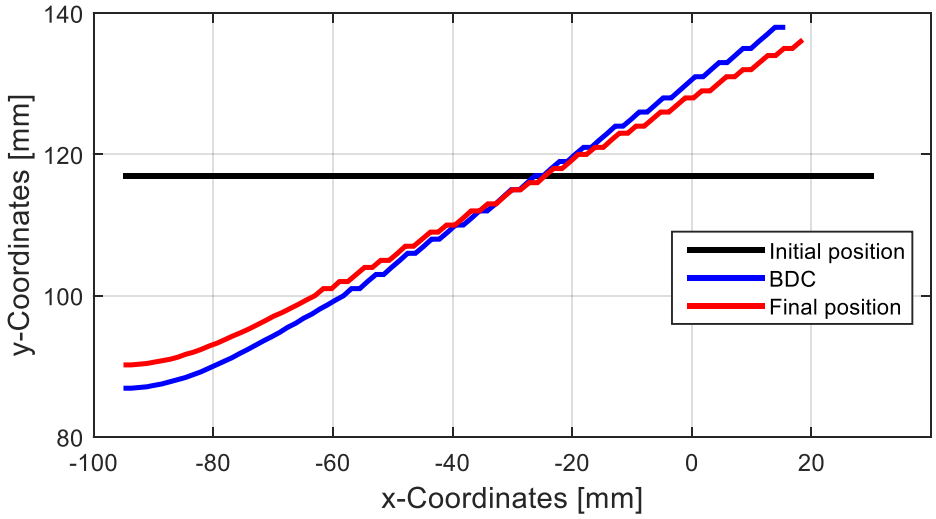

Figure 5.24: The predicted edge line of Armor Steel-1 in conventional bending

Regarding conventional and incremental bending simulations of Armor Steel-1, the final angle of the plate shows a small difference which is an expected outcome. How-

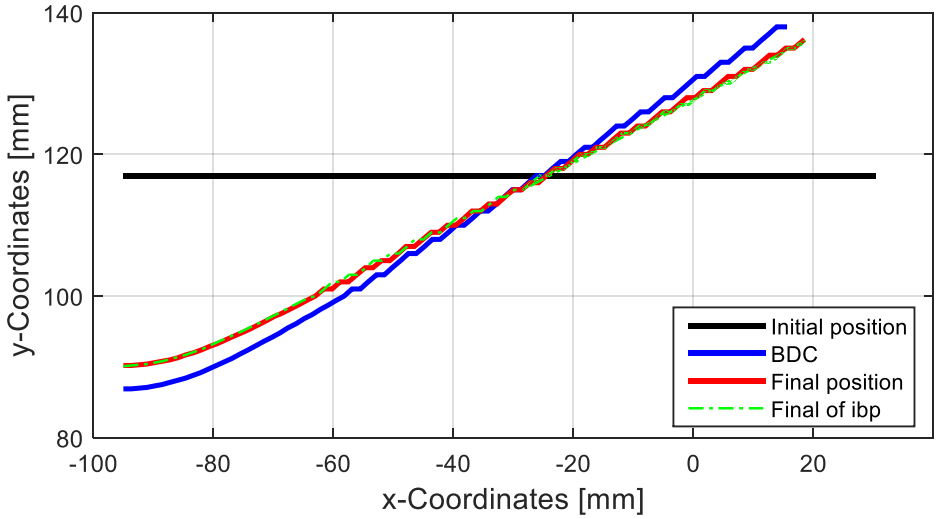

Figure 5.25: The comparison of conventional and incremental bending of Armor Steel-1 wrt angles

ever, in order to observe that there is still a difference regardless of its magnitude, the focused view of Fig.5.25 is illustrated in Fig.5.26.

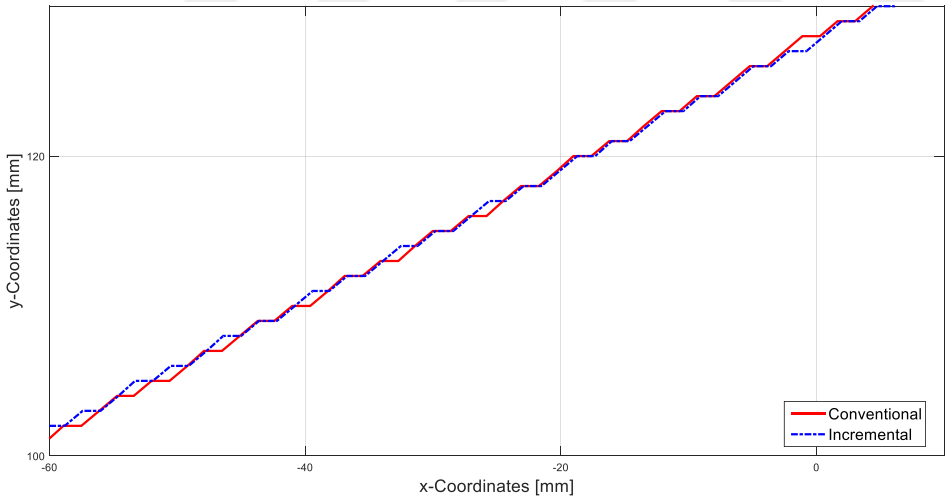

Figure 5.26: The comparison of conventional and incremental bending of Armor Steel-1 (focused version)

Similar behavior is also observed for Armor Steel-2. Between the conventional and incremental bending operations, the resulting bending angles were very close to each other with respect to FEA analysis as indicated in Fig.5.27.

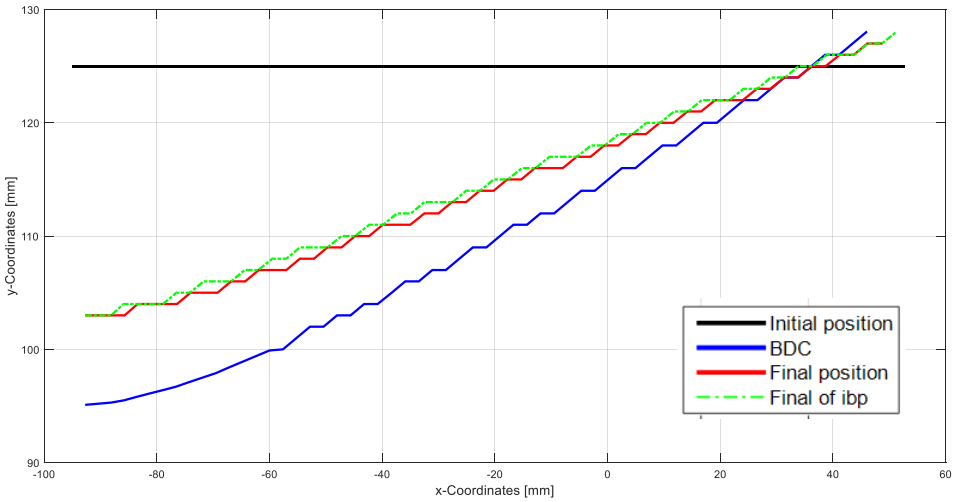

Figure 5.27: The comparison of conventional and incremental bending of Armor Steel-2 wrt angles

Having finished the determination of edges in FEA analysis, a simple linear curve fitting operation is performed to compute the final bending angles. For that operation, the curved zone of the edge is eliminated. Than, the slope of the fitted line is determined after which the angle can be directly computed with the $arctangent$ formulation. The aforementioned methodology is shown in Fig.5.28.

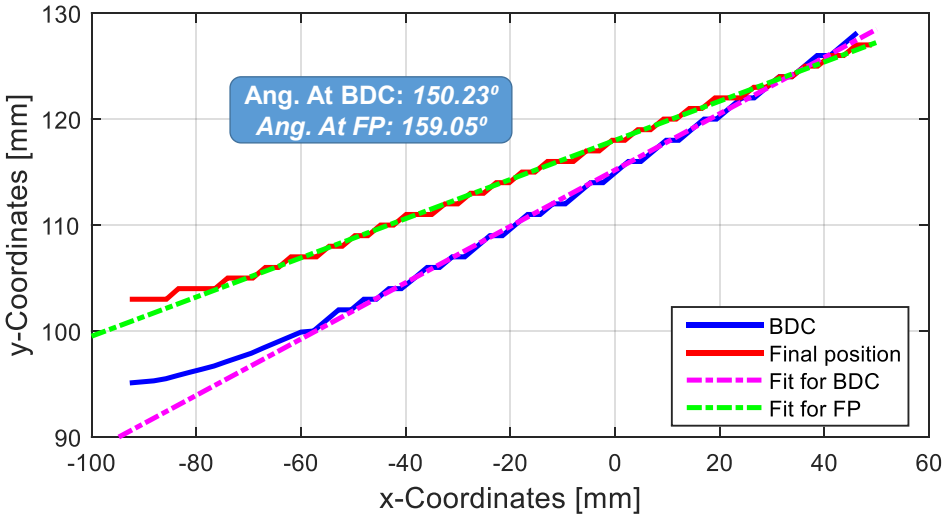

Figure 5.28: Computation of the bending angle of Armor Steel-2 wrt FEA

On the other hand, the bending angles which came out from experiments are determined by digital image analysis techniques. For that purpose, a specific $MatLab$

code is prepared which uses auto-thresholding approach to make a discrimination in pixel scale. As the experimental specimens are painted, it is not so much hard to separate the pixels of the specimen from background. Then, the bending angles are computed with simple line fitting operation as like in the previous $MatLab$ code. An example of the line fitting operation with respect to the auto-thresholdig is displayed in Fig.5.29.

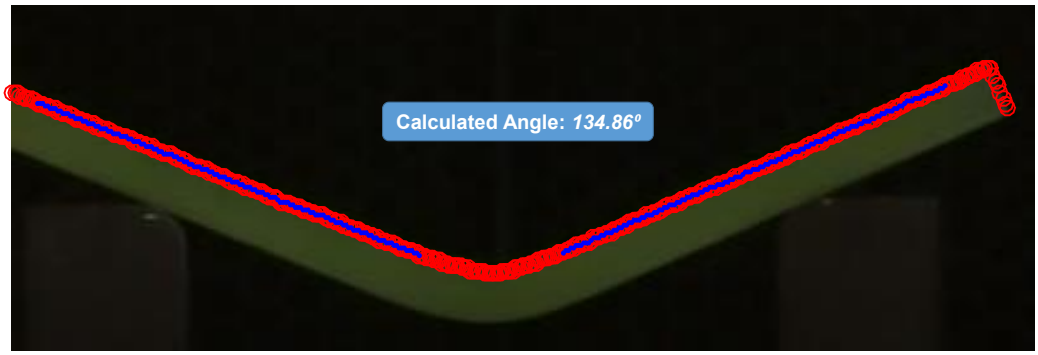

Figure 5.29: Computation of the experimental bending angle of Armor Steel-1 (conventional bending)

The same methodology is followed in computing the angles at BDC and final position for conventionally and incrementally bent experimental specimens. And finally, all the angles are determined which can be compared by the results of FEA analysis. Some examples of image analysis are also shown in Fig.5.30.

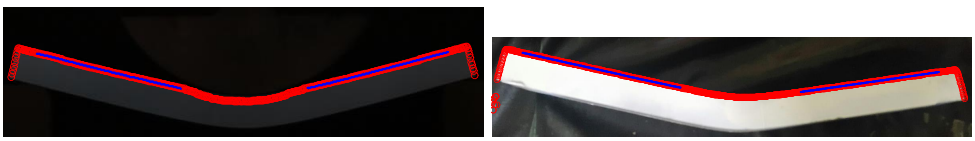

(a) (b)

Figure 5.30: **(a)**Armor Steel-2 at BDC **(b)** Armor Steel-2 at final position

In order to evaluate all the predicted and measured angles of the numerical and experimental studies, Fig.5.31 is created. The spring-back values which are calculated by subtracting the angles at final position from the angles at BDC are also displayed

in Fig.5.31. For the incremental bending experiments, only the final angles are calculated since it does not make any sense to compute the angle at BDC for that specific application. Since it is observed that the results of RD and TD samples are very similar in Fig.5.31, only the results of one RD and one TD specimens are shown with FEA predictions. For better explanation of the results, Fig.5.32 is also displayed as a focused version.

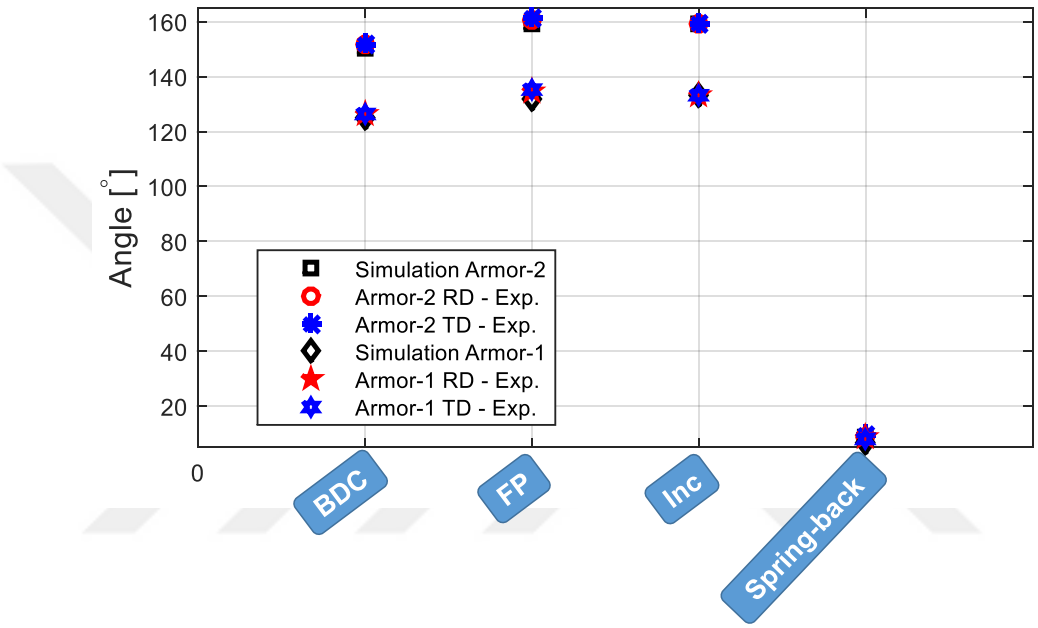

Figure 5.31: Comparison of the measured and predicted bending angles of Armor Steel-1 and Armor Steel-2

As concluding remarks the followings could be stated:

- As expected, the FEA analysis made smaller predictions compared to the experimental results. However, the under-estimation of the spring-back is nearly 3.4% for Armor Steel-2 and 18% for Armor Steel-1. As the bending angle increases, the amount of under-prediction also increases, which is a reasonable outcome from apparent modulus point-of-view. Anyway, the precision of the prediction is accepted as tolerablef for industrial applications.

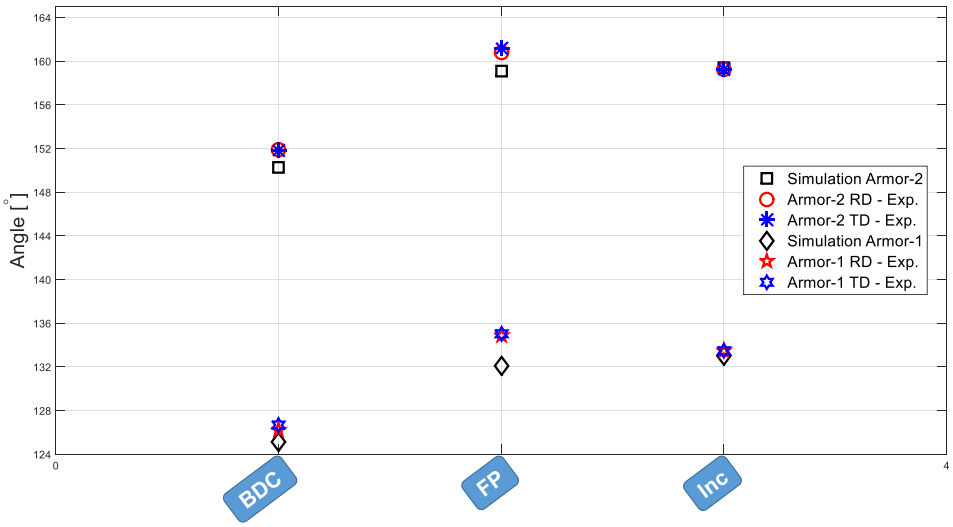

Figure 5.32: Comparison of the measured and predicted bending angles (focused version)

- The prediction of the bending angle of incremental bending is worse than that of conventional bending. FEA analysis predicts a bigger spring-back compared to conventional bending whereas the experimental findings show the opposite behavior. The spring-back decreases With the incremental bending process. At this point, it is concluded that further investigations should be performed on FEA models since it is expectable to have minor spring-back as in the experiments.

5.4 Anaylsis of Optical Scanning Studies

As discussed in the Chapter 4, the bent specimens are processed with raster scanning techniques in optical measurement system. The system has a CNC controlled table, so that the scanning operation can be performed automatically and straightforwardly. After having completed the scanning task, the 3D topological maps are constructed for each specimen. Then, the data of the conventionally and incremen-

tally bent specimens are analyzed concurrently. For that analysis, the mathematical models of both specimens are subtracted from each other in order to provide a more descriptive and visual data. The resulting figures of Armor Steel-1 are shown in Fig.5.33 and Fig.5.34.

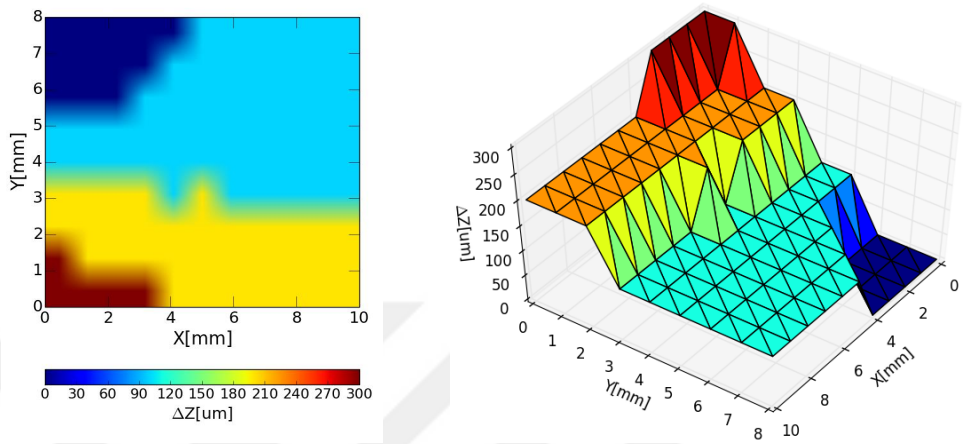

Figure 5.33: Comparison of the optical scanning data of Armor Steel-1 (conventional and incremental bending)

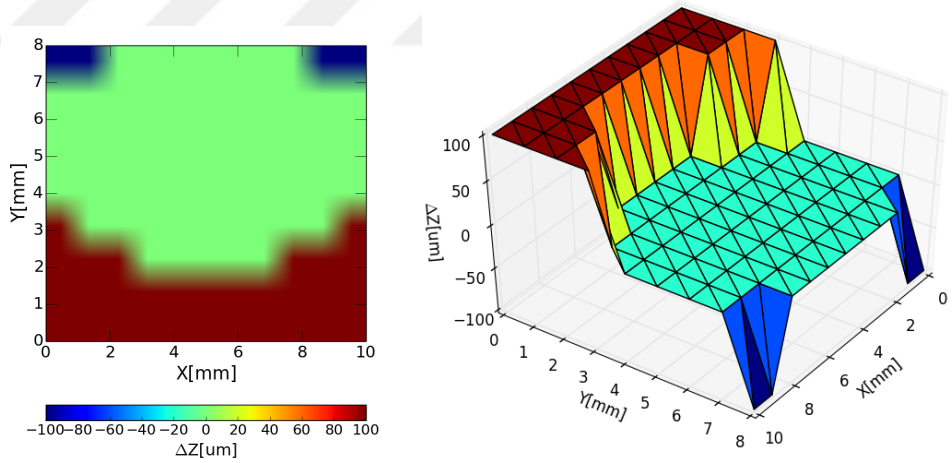

Figure 5.34: Comparison of the optical scanning data of Armor Steel-1 in TD (conventional and incremental bending)

Fig.5.33 implies that for the incremental bending operations the deformation can be localized which actually explains the decrease of the tendency in spring-back. This finding in optical scanning studies correspond with the experimental bending angle

measurements. To make some quantitative comments, it could be concluded that in TD specimens there is max. of $100\,micrometer$ difference in z direction whereas this value is found as $100\,micrometer$ in RD specimens . Moreover, the overall tendency of RD and TD specimens are quite similar. The Δz value is max on the mid-zone and then converges to zero. However, it is certain that the incrementally bent specimens showed more spreading behavior in the most critical region (mid-plane) where the strain is at max.

CHAPTER 6

CONCLUSION AND FUTURE WORK

Within the scope of this thesis study, three different UHSS grades are processed by conventional and incremental bending processes. The results are compared between each other and finally with the simulations studies. The following statements could be made as concluding remarks:

- The forces in conventional and incremental bending processes are predicted by non-linear FEA analysis and the prediction of the simulations are compared with the experimental data. The results reveal that the FEA models can perform predictions with a precision of 10%, i.e. the experimental data is in the range of $+10\%$ of the predictions. This precision level is found to be sufficient for the industrial applications when all of the uncertainties and numerical errors are evaluated concurrently.

- It is possible to decrease the required bending forces with the new proposed incremental bending process. This decrease could be tuned by altering the increment steps in angular and linear components. However, any minimization of increments definitely causes an increase in the cycle time. Therefore, a priori to the real bending operation, it would be useful to make some optimization on

the cycle time and the decrease of the bending force.

- The benchmarks between the conventional and incremental processes brought out that the degradation of the final topology in incremental bending approach is in the range of negligible scale which did not cause any quality problems.

- During the experimental studies, the linear increments are made with manual operations which could not be the case for industrial applications. In order to transfer the proposed incremental bending operation to macro-scale production, it is compulsory to design a specific feeder system which should be embedded to the press brake. It would be possible to control the feeder equipment with the existing CNC infrastructure of a press brake.

- The plane strain assumptions with a L/t ratio > 10 work quite well in bending force prediction. This assumption extremely decreases not only the computational cost of the FEA analysis but also the time for the preparation of the simulation model. From this point-of-view, in hull production where the L/t ratios are significantly high, there is no need for 3D FEA modeling for UHSS plate bending operation. The trial simulations showed that a plane strain assumption of Armor-Steel-1 with a L/t ratio $= 10$ results in an average relative error of nearly 2.30% as can be seen in Fig.6.1.

- The tensile tests with optical extensometer ($Armais\,Gom\,system$) provide true strain vs. true stress data up to high strains such as 0.70 that is away over the max. achievable strain values in standard tensile testings of UHSS. With this new method, the flow curves of the studied UHSS plates could be obtained for a large strain range which actually enlarges the present material data library of FNSS.

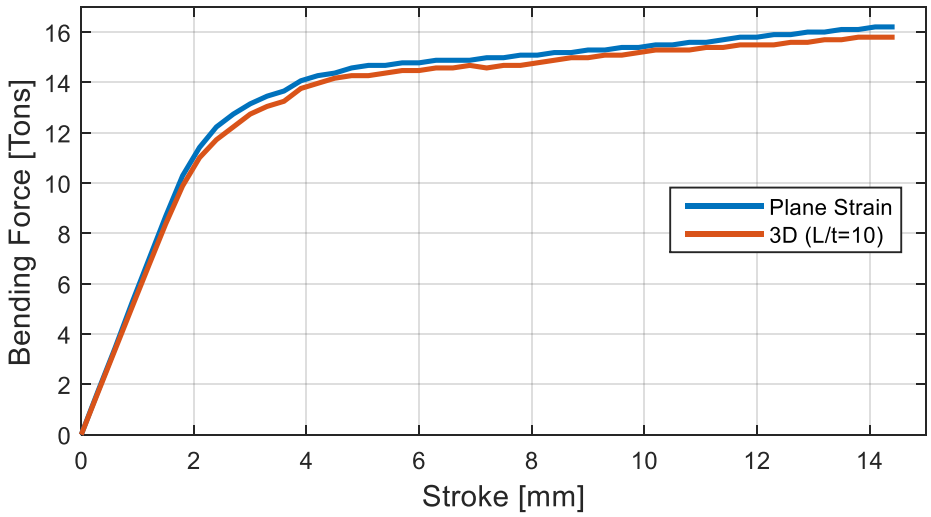

Figure 6.1: Verification of the plane strain assumption for Armor Steel-1 (L/t=10)

- The FEA models perform sufficiently well with $Hex-8$ element which is a linear element whereas the quadratic element ($Hex-20$) results in a very small difference with Hex-8 but causing a huge increase in the computation time. The computaton time is 8 times bigger for quadratic elements $Hex-20$. Therefore, $Hex-8$ element and a quantity of eight elements in thickness direction is decided to be a proper meshing strategy for the simulation of UHSS plate bending for industrial applications.

- The cof values are not so much dominant on the bending forces as expected. Therefore, implementation of generic values like 0.15 or 0.20 to the FEA models would be sufficient for industrial applications.

- As the studies in the literature, FEA software cannot compute the spring-back very precisely and one of the major drawback in this result is the apparent moduli phenomena [56, 57, 4]. Generally, in FEA analysis, the elastic modulus is set to a constant value. However, during real forming conditions, the apparent modulus decreases as the material exhibits plastic deformation. As an example of decreasing loading and unloading apparent moduli of TWIP-980 steel,

Fig.6.2 is displayed [58].

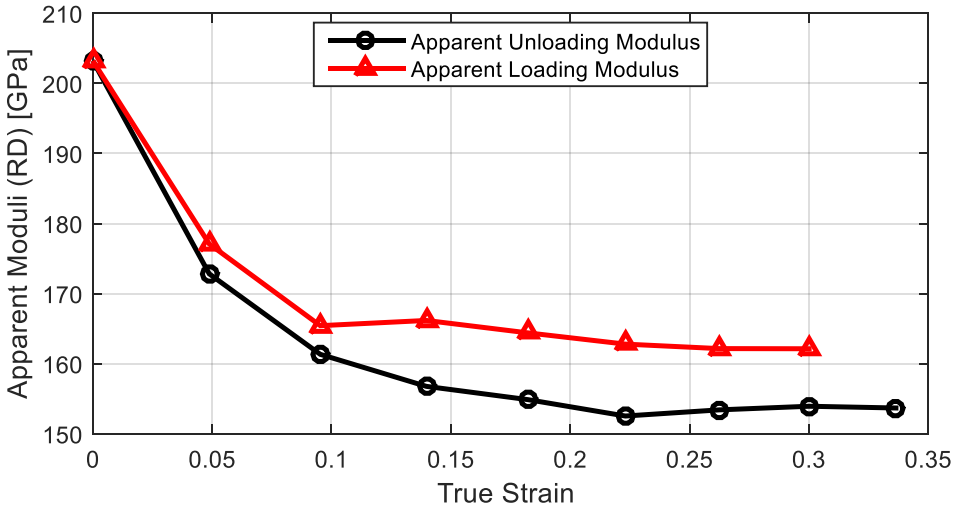

Figure 6.2: Apparent moduli of TWIP-980 steel wrt increasing true strain

As a consequence of constant elastic modulus assumption, the spring-back is often under-estimated by numerical analysis. Therefore, it is concluded that the prediction of the spring-back in UHSS plates with non-constant apparent moduli approach would be a beneficial study which can generate significant scientific contribution. This task is planned as a future work by the project team.

- Related to MSC Marc software, the detection of the contact with $segment - to - segment$ method yields a smooth force versus stroke data. In other words, $node - to - segment$ contact method produce a noisy data than that of $segment - to - segment$ method.

REFERENCES

[1] W. F. Hosford and R. M. Caddell, *Metal forming mechanincs and metallurgy*. Cambridge University Press, 2007.

[2] A. E. Tekkaya, "Lecture notes: A review on theory of plasticity.".

[3] M. Zhang, J. Zhang, Y. X. Ning, T. Wang, and Z. Wan, "Springback behavior of advanced high strength steel (ahss) cp800," in *Metallic Materials and Manufacturing Technology*, vol. 820 of *Advanced Materials Research*, pp. 45–49, Trans Tech Publications, 12 2013.

[4] X. Yang, C. Choi, N. K. Sever, and T. Altan, "Prediction of springback in air-bending of ahss (dp780) considering young's modulus variation and with a piecewise hardening function," *International Journal of Mechanical Sciences*, vol. 105, pp. 266 – 272, 2016.

[5] K.-Y. Seo, J.-H. Kim, H.-S. Lee, J. Kim, and B.-M. Kim, "Effect of constitutive equations on springback prediction accuracy in the trip1180 cold stamping," *Metals*, vol. 8, p. 18, Dec 2017.

[6] E. Leszak, "Apparatus and process for incremental dieless forming," 1967.

[7] H. Müller and H. Enzmann, "Potentials of rapid prototyping techniques for the manufacture of prototype sheet metal forming tools," in *Proc. European Conf. on Rapid Prototyping and Manufacturing, Aachen, 1998*, pp. 337–350, 1998.

[8] D. Müller and H. Müller, "Experiences using rapid prototyping techniques to manufacture sheet metal forming tools," in *Proc. ISATA Conference, Dublin*, p. 9, 200.

[9] T. Nakagawa, "Recent developments in auto body panel forming technology," *CIRP Annals*, vol. 42, no. 2, pp. 717 – 722, 1993.

[10] J. Jeswiet, F. Micari, G. Hirt, A. Bramley, J. Duflou, and J. Allwood, "Asymmetric single point incremental forming of sheet metal," *CIRP Annals*, vol. 54, no. 2, pp. 88 – 114, 2005.

[11] J. Jeswiet, J. R. Duflou, and A. Szekeres, "Forces in single point and two point incremental forming," in *Sheet Metal 2005*, vol. 6 of *Advanced Materials Research*, pp. 449–456, Trans Tech Publications, 5 2005.

[12] M. Azaouzi and N. Lebaal, "Tool path optimization for single point incremental sheet forming using response surface method," *Simulation Modelling Practice and Theory*, vol. 24, pp. 49 – 58, 2012.

[13] I. Cerro, E. Maidagan, J. Arana, A. Rivero, and P. Rodríguez, "Theoretical and experimental analysis of the dieless incremental sheet forming process," *Journal of Materials Processing Technology*, vol. 177, no. 1, pp. 404 – 408, 2006. Proceedings of the 11th International Conference on Metal Forming 2006.

[14] A. Parande, V. Bhalke, D. Kanke, R. Gaikwad, and P. Bhoyar, "Innovative single point incremental forming : A review," *Vishwakarma Journal of Engineering Research*, vol. 1, pp. 221 – 225, 2017.

[15] M. E. Tamer, O. Music, I. Özdemir, B. Baranoğlu, A. Sakin, and I. Durgun, "Simulation for incremental sheet forming process: a comparison of implicit and explicit finite element analysis with experimental data," in *Proceedings of the 7th International Conference and Exhibition on Design and. Production of Machines and Dies/Molds, June 20-23, Antalya, Turkey*, 2013.

[16] A. Määttää, K. Mäntyjärvi, and J. A. Karjalainen, "Incremental bending of ultra high strength steels," *Key Engineering Materials*, vol. 473, pp. 53–60, 2011.

[17] A. Väisänen, K. Mäntyjärvi, and J. A. Karjalainen, "Bendability of ultra-high-strength steel," in *Sheet Metal 2009*, vol. 410 of *Key Engineering Materials*, pp. 611–620, Trans Tech Publications, 10 2009.

[18] G. Gutscher, H.-C. Wu, G. Ngaile, and T. Altan, "Determination of flow stress for sheet metal forming using the viscous pressure bulge (vpb) test," *Journal of Materials Processing Technology*, vol. 146, no. 1, pp. 1 – 7, 2004.

[19] B. Çetin, A. H. Uslu, and M. Kaşıkçı, "Design of a specific matlab code for processing of standard tensile test data for sheet metal forming simulations," *Hittite Journal of Science and Engineering*, vol. 2, pp. 151–157, 2015.

[20] M. Koç, E. Billur, and O. Cora, "An experimental study on the comparative assessment of hydraulic bulge test analysis methods," *Materials and Design*, vol. 32, no. 1, pp. 272 –81, 2011.

[21] E. Billur, Y. Demiralp, A. Groseclose, B. Wadman, and T. Altan, "Factors affecting the accuracy of flow stress determined by the bulge test," *Steel Reserach International*, vol. 2, pp. 50– 62, 2011.

[22] E. Billur and T. Altan, "Determining material properties and batch-to-batch variations with bulge testing," *Stamping Journal*, vol. Sept/Oct 2013, pp. 16–17, 2013.

[23] aramis gom optical measuement systems, *Tensile test evaluation*.

[24] E. Billur, B. Çetin, and M. Gürleyik, "New generation advanced high strength steels: Developments, trends and constraints t," *International Journal of Scientific and Technological Research*, vol. 2, no. 1, pp. 726– 731, 2016.

[25] M. Shetty, *Dislocations and mechanical behaviour of materials*. PHI Learning , US, 2013.

[26] E. Koska, "Numerical and experimental investigation of indentation," Master's thesis, Middle East Technical University, March 2005.

[27] D. Banabic, *Sheet metal forming processes*. Springer, 2010.

[28] M. Iordache, M. Teaca, I. Charpentier, M. Martiny, and G. Ferron, "Identification of sheet metal plastic anisotropy and optimization of initial blank shape in deep drawing," *The Annals of Dunarea de Jos University og Galati*, vol. 5, pp. 149–154, 2009.

[29] D. Banabic, H. Bunge, K. Pöhlandt, and A. Tekkaya, *formability of metallic materials*. Springer, 2000.

[30] R. V. Mises, "Mechanik der festen körper im plastisch deformablen zustand, nachrichten von der königlichen gesellschaft der wissenschaften zu göettingen," *Mathematisch-physikalische Klasse*, pp. 582–592, 1913.

[31] J. L. Alves, S. Bouvier, M. Jomâa, R. Billardon, M. C. Oliveira, and L. F. Menezes, "Kinematic hardening: Characterization, modeling and impact on springback prediction," *AIP Conference Proceedings*, vol. 908, no. 1, pp. 691–698, 2007.

[32] F. Yoshida, T. Uemori, and K. Fujiwara, "Elastic–plastic behavior of steel sheets under in-plane cyclic tension–compression at large strain," *International Journal of Plasticity*, vol. 18, no. 5, pp. 633 – 659, 2002.

[33] F. Yoshida and T. Uemori, "A model of large-strain cyclic plasticity describing the bauschinger effect and workhardening stagnation," *International Journal of Plasticity*, vol. 18, no. 5, pp. 661 – 686, 2002.

[34] F. Yoshida, "A constitutive model of cyclic plasticity," *International Journal of Plasticity*, vol. 16, no. 3, pp. 359 – 380, 2000.

[35] F. Yoshida, T. Uemori, and H. Hamasaki, *Modeling of Large-Strain Cyclic Plasticity Including Description of Anisotropy Evolution for Sheet Metals*, pp. 571–585. Switzerland: Springer Cham, 2015.

[36] C.-Y. Chang, M.-H. Ho, and P.-C. Shen, "Yoshida–uemori material models in cyclic tension–compression tests and shear tests," *Proceedings of the Institution of Mechanical Engineers, Part B: Journal of Engineering Manufacture*, vol. 228, no. 2, pp. 245–254, 2014.

[37] W. He, S. Zhang, and H. Song, "An extended homogenous yield function based anisotropic hardening model for description of anisotropic hardening behavior of materials," *International Journal of Mechanical Sciences*, vol. 77, pp. 343 – 355, 2013.

[38] A. B. Doucet and R. H. Wagoner, "Transient tensile behavior of interstitial-free steel and 70/30 brass following plane-strain deformation," *Metallurgical Transactions A*, vol. 20, pp. 1483–1493, Aug 1989.

[39] M. van Riel and A. van den Boogaard, "Stress–strain responses for continuous orthogonal strain path changes with increasing sharpness," *Scripta Materialia*, vol. 57, no. 5, pp. 381 – 384, 2007.

[40] H. Haddadi, S. Bouvier, M. Banu, C. Maier, and C. Teodosiu, "Towards an accurate description of the anisotropic behaviour of sheet metals under large plastic deformations: Modelling, numerical analysis and identification," *International Journal of Plasticity*, vol. 22, no. 12, pp. 2226 – 2271, 2006.

[41] M. Noman, T. Clausmeyer, C. Barthel, B. Svendsen, J. Huétink, and M. van Riel, "Experimental characterization and modeling of the hardening behavior of the sheet steel lh800," *Materials Science and Engineering: A*, vol. 527, no. 10, pp. 2515 – 2526, 2010.

[42] R. K. Verma, T. Kuwabara, K. Chung, and A. Haldar, "Experimental evaluation and constitutive modeling of non-proportional deformation for asymmetric steels," *International Journal of Plasticity*, vol. 27, no. 1, pp. 82 – 101, 2011.

[43] F. Barlat, J. J. Gracio, M.-G. Lee, E. F. Rauch, and G. Vincze, "An alternative to kinematic hardening in classical plasticity," *International Journal of Plasticity*, vol. 27, no. 9, pp. 1309 – 1327, 2011.

[44] F. Barlat, J. Ha, J. J. Grácio, M.-G. Lee, E. F. Rauch, and G. Vincze, "Extension of homogeneous anisotropic hardening model to cross-loading with latent effects," *International Journal of Plasticity*, vol. 46, pp. 130 – 142, 2013.

[45] F. Barlat, G. Vincze, J. Grácio, M.-G. Lee, E. Rauch, and C. Tomé, "Enhancements of homogenous anisotropic hardening model and application to mild and dual-phase steels," *International Journal of Plasticity*, vol. 58, pp. 201 – 218, 2014. In Honor of Kwansoo Chung.

[46] N. Manopulo, F. Barlat, and P. Hora, "Isotropic to distortional hardening transition in metal plasticity," *International Journal of Solids and Structures*, vol. 56-57, pp. 11 – 19, 2015.

[47] L. Noels, L. Stainier, and J.-P. Ponthot, "Combined implicit/explicit time-integration algorithms for the numerical simulation of sheet metal forming," *Journal of Computational and Applied Mathematics*, vol. 168, no. 1, pp. 331 –

339, 2004. Selected Papers from the Second International Conference on Advanced Computational Methods in Engineering (ACOMEN 2002).

[48] L. Noels, L. Stainier, and J. Ponthot, "Self-adapting time integration management in crash-worthiness and sheet metal forming computations," *International Journal of Vehicle Design*, vol. 30, pp. 1–44, 2002.

[49] M. Finn, P. Galbraith, L. Wu, J. Hallquist, L. Lum, and T.-L. Lin, "Use of a coupled explicit—implicit solver for calculating spring-back in automotive body panels," *Journal of Materials Processing Technology*, vol. 50, no. 1, pp. 395 – 409, 1995.

[50] M. Bussler and A. Ramesh, "Eight-node hexahedral element in fea of part designs," *Foundry Management and Technology*, vol. 121, pp. 26–28, 1993.

[51] M. Raupach, S. Kreissl, L. Vuaille, T. Möller, H. Friebe, and W. Volk, "Mesh refinement study and experimental validation for stretch bending of sheet metals," *Journal of Physics: Conference Series*, vol. 896, no. 1, p. 012071, 2017.

[52] D. Kitting, M. Koplenig, A. Ofenheimer, H. Pauli, and E. T. Till, "Application of a concave-side rule approach for assessing formability of stretch-bent steel sheets," *International Journal of Material Forming*, vol. 2, p. 427, Dec 2009.

[53] K. Osakada, K. Mori, T. Altan, and P. Groche, "Mechanical servo press technology for metal forming," *CIRP Annals*, vol. 60, no. 2, pp. 651 – 672, 2011.

[54] D. Yadav, S. Kaya, and G. Groseclose, *Electromechanical Servo Drive Presses*, pp. 161–178. Ohio: ASM International, 2012.

[55] K. Wegener, *Forming Presses (Hydraulic, Mechanical, Servo)*, pp. 547–553. Berlin, Heidelberg: Springer Berlin Heidelberg, 2014.

[56] J.-Y. Lee, J.-W. Lee, M.-G. Lee, and F. Barlat, "An application of homogeneous anisotropic hardening to springback prediction in pre-strained u-draw/bending," *International Journal of Solids and Structures*, vol. 49, no. 25, pp. 3562 – 3572, 2012.

[57] R. H. Wagoner, H. Lim, and M.-G. Lee, "Advanced issues in springback," *International Journal of Plasticity*, vol. 45, pp. 3 – 20, 2013. In Honor of Rob Wagoner.

[58] E. Billur, B. Çetin, R. O. Uğuz, K. Davut, and E. Arslan, "Advanced material characterization of twip steels," in *Proc. New Developments in Sheet Metal Forming/Hydroforming, May 10-11, Stuttgart, Germany*, pp. 303–317, 2016.

CURRICULUM VITAE

PERSONAL INFORMATION

Surname, Name: Çetin, Barış

Nationality: Turkish (TC)

Date and Place of Birth: 06.02.1981, Bursa

Marital Status: Married

Phone: 0 312 4974619

Fax: 0 312 4974300

EDUCATION

Degree	Institution	Year of Graduation
B.S.	METU Department of Mechanical Engineering	2003
High School	İhsan Çizakça Lisesi, Bursa	1998

PROFESSIONAL EXPERIENCE

Enrollment	Place	Year
Senior Lead Engineer	FNSS Defense Systems Co. Inc., Engineering and Research Department, Ankara	2015-Present
Senior Manufacturing Engineer	FNSS Defense Systems Co. Inc., Manufacturing Services Department	2013-2015
Fixture Design Engineer	Oyak-Renault Oto. Fab. AŞ, R&D Department, Bursa	2010-2013
Method Engineer	Oyak-Renault Oto. Fab. AŞ, Engineering Department, Bursa	2005-2010
Method Engineer	Kerem Pres ve Kaplama San. Tic. AŞ, Bursa	2003-2005

PUBLICATIONS (PEER-REVIEWED)

1. A Potential Solution to Mystical Materials in Indentation Test, Procedia Engineering, Vol.207, 2017, pp.1952-1957

2. Multiscale Microstructural Analysis of Austempered Ductile Iron Castings, Microscopy and Microanalysis, Vol.23(S1), pp.350-351

3. Design of a Specific Image Processing Code in MatLab to Perform Advanced Nodularity Analysis of Austempered Ductile Iron Castings, Microscopy and Microanalysis, Vol.23(S1), pp.232-233

4. A Material Perspective on Consequence of Deformation Heating During Stamping of DP Steels, Journal of Physics: Conference Series, 896, 2017, 012059

5. Wear Performance of Boron Nitride (BN) Coatings on End Milling Cutters,

International Journal of Mechatronics and Manufacturing Systems (IJMMS), Vol.10 (3), 2017, pp.206-220

6. Gelistirilmis Yuksek Mukavemetli Celiklerin Servo Pres Kullanilarak Bukulmesi, Makina Tasarim ve Imalat Dergisi (MATIM), Vol.14 (2), 2016, pp.69-76

7. Microstructural Analysis of Austempered Ductile Iron Castings, Hittite Journal of Science and Engineering (HJSE), Vol.3 (1), 2016, pp.29-34

8. Gomulu Sistemlerin Ucus Oncesi Testlerdeki Kullanimi, Makina Tasarim ve Imalat Dergisi (MATIM), Vol.14 (1), 2016 pp.41-45

9. Investigation of the Hydrogen Content in Welding of Armor Steels by Raman Spectroscopy, Muhendis ve Makina, Vol.57 (674), 2016 pp.50-56 (Invited for republication)

10. Tool Wear Measurement by High Resolution Optical Scanning: First Results, International Journal of Scientific and Technological Research, Vol.2 (2), 2016, pp.6-12

11. New Generation Advanced High Strength Steels: Events, Trends, Constraints, International Journal of Scientific and Technological Research, Vol.2 (1), 2016, pp.50-62

12. Design of A Specific MatLab Code for Processing of Tensile Test Data for Sheet Metal Forming Simulations, Hittite Journal of Science and Engineering (HJSE), Vol.2 (2), 2015, pp.151-157

13. A New Generation Promising Engineering Mat erial: Cubic Boron Nitride (c-BN), Hittite Journal of Science and Engineering (HJSE), Vol.2 (1), 2015, pp.85-90

PUBLICATIONS (CONFERENCE PAPERS)

1. Isi Kaynagi Iceren Isi Iletimi Problemleri icin Alternatif Yaklasimlar, 21. Ulusal Isi Bilimi ve Teknigi Kongresi, 13-16/09/2017, Corum

2. A Material Perspective on Consequences of Deformation Heating During Stamping of DP590 Steel, 36th IDDRG Congress, 02-05/07/2017, Munich, Germany,

3. Design and Development of Hyperspectral Metallurgical Analysis System, 6th International Iron and Steel Symposium, (6. EFRS), 25-26/05/2017, Izmir, Turkey

4. The Potential and Constraints of Austempered Ductile Iron Castings in Defense Industry, 2nd International Defense Industry Symposium, (IDEFIS-2017), 06-08/04/2017, Kirikkale, Turkey

5. New Generation Ultra-High Strength Steels for Cold Forming, 18th International Metallurgy and Materials Congress (IMMC-2016), 29/09-01/10/2016, Istanbul, Turkey,

6. Mapping the Spatial Distribution of Nodular Properties in Spheroidal Graphite Cast Iron, 18th International Metallurgy and Materials Congress (IMMC-2016), 29/09-01/10/2016, Istanbul, Turkey,

7. Nodularity and Nodule Count Analysis of Austempered Ductile Iron Castings, 18th International Metallurgy and Materials Congress (IMMC-2016), 29/09-01/10/2016, Istanbul, Turkey,

8. Thermal Modelling of Heat Affected Zone of a Low Carbon Steel in Gas Metal Arc and Laser Welding, 17th International Conference on Machine Design and

Production (UMTIK-2016), 12-15/07/2016, Bursa, Turkey,

9. Design of Active Disturbance Rejection Based Controller for a Assembly Positioner, 17th International Conference on Machine Design and Production (UMTIK-2016), 12-15/07/2016, Bursa, Turkey,

10. Investigation of the Effect of Servo-Press Forming in Spring-Back and Minimum Bending Radii of Ultra High Strength Steels, 17th International Conference on Machine Design and Production (UMTIK-2016), 12-15/07/2016, Bursa, Turkey,

11. Advanced Material Characterization of TWIP Steels, International Conference on New Developments in Sheet Metal Forming (NEBU-2016), 10-11/05/2016, Stuttgart, Germany

12. Investigation of the Hydrogen Content in Welding of Armor Steels by Raman Spectroscopy, 9th National Conference and Exhibition on Welding Technologies (KayKon-2015), 20-21/11/2015, Ankara, Turkey,

13. Forming of New Generation AHSS Using Servo Presses, 5th International Conference Accuracy in Forming Technology (ICAFT-2015), 10-11/11/2015, Chemnitz, Germany,

14. Tool Life Improvements of End Mill Cutters with BN Coating by PVD Method, 8th International Conference and Exhibition on Design and Production of Machines and Dies/Molds, 18-21/06/2015, Aydin, Turkey

15. A New Approach to Measure the Wear on Cutting Tools with Elliptical Geometries: High Resolution 3D Optical Scanning , 7th National Applied Measurement Conference, 17-19/10/2014, Corum, Turkey

16. An Experimental Set-up Study for The Measurement of Tool and Workpiece Temperature in End Milling, 7th National Applied Measurement Conference, 17-19/10/2014, Corum, Turkey

SEMINARS & INVITED TALKS

1. Technical Constraints and Economical Aspects of Material Characterization, Metal Forming Technology Day (MEFTECH-2017), Divan Hotel, Bursa, 12/05/2017
2. Investigation of the Hydrogen Content in Welding of High Strength Steels by Raman Spectroscopy, Hitit University, Faculty of Engineering, 18/12/2015
3. c-BN Coatings, Hitit University, Faculty of Engineering, 21/05/2015
4. Joining Technologies in Automotive Body Engineering, Atilim University, Automotive Engineering Department, 26/03/2015
5. New Generation Steels in Automotive and Defense Industry, Bilkent University, Mechanical Engineering Department, 25/02/2015

INVITED REFEREE

1. Anadolu University Journal of Science and Technology-A
2. Society of Manufacturing Engineers, North American Manufacturing Research Conference (SME NARMC44)